INFORMATION TO USERS

This reproduction was made from a copy of a manuscript sent to us for publication and microfilming. While the most advanced technology has been used to photograph and reproduce this manuscript, the quality of the reproduction is heavily dependent upon the quality of the material submitted. Pages in any manuscript may have indistinct print. In all cases the best available copy has been filmed.

The following explanation of techniques is provided to help clarify notations which may appear on this reproduction.

1. Manuscripts may not always be complete. When it is not possible to obtain missing pages, a note appears to indicate this.

2. When copyrighted materials are removed from the manuscript, a note appears to indicate this.

3. Oversize materials (maps, drawings, and charts) are photographed by sectioning the original, beginning at the upper left hand corner and continuing from left to right in equal sections with small overlaps. Each oversize page is also filmed as one exposure and is available, for an additional charge, as a standard 35mm slide or in black and white paper format.*

4. Most photographs reproduce acceptably on positive microfilm or microfiche but lack clarity on xerographic copies made from the microfilm. For an additional charge, all photographs are available in black and white standard 35mm slide format.*

***For more information about black and white slides or enlarged paper reproductions, please contact the Dissertations Customer Services Department.**

U·M·I Dissertation Information Service

University Microfilms International
A Bell & Howell Information Company
300 N. Zeeb Road, Ann Arbor, Michigan 48106

Frantziskonis, George Nikolaos

PROGRESSIVE DAMAGE AND CONSTITUTIVE BEHAVIOR OF GEOMATERIALS INCLUDING ANALYSIS AND IMPLEMENTATION

The University of Arizona PH.D. 1986

PLEASE NOTE:

In all cases this material has been filmed in the best possible way from the available copy. Problems encountered with this document have been identified here with a check mark __✓__.

1. Glossy photographs or pages _____
2. Colored illustrations, paper or print _____
3. Photographs with dark background _____
4. Illustrations are poor copy _____
5. Pages with black marks, not original copy _____
6. Print shows through as there is text on both sides of page _____
7. Indistinct, broken or small print on several pages _____
8. Print exceeds margin requirements _____
9. Tightly bound copy with print lost in spine _____
10. Computer printout pages with indistinct print _____
11. Page(s) _____ lacking when material received, and not available from school or author.
12. Page(s) _____ seem to be missing in numbering only as text follows.
13. Two pages numbered 68 & 73. Text follows.
14. Curling and wrinkled pages _____
15. Dissertation contains pages with print at a slant, filmed as received ✓
16. Other _____

_____

_____

University
Microfilms
International

PROGRESSIVE DAMAGE AND CONSTITUTIVE BEHAVIOR OF GEOMATERIALS INCLUDING ANALYSIS AND IMPLEMENTATION

by

George Frantziskonis

A Dissertation Submitted to the Faculty of the

DEPARTMENT OF CIVIL ENGINEERING AND ENGINEERING MECHANICS

In Partial Fulfillment of the Requirements
For the Degree of

DOCTOR OF PHILOSOPHY
WITH A MAJOR IN ENGINEERING MECHANICS

In the Graduate College

THE UNIVERSITY OF ARIZONA

1 9 8 6

THE UNIVERSITY OF ARIZONA
GRADUATE COLLEGE

As members of the Final Examination Committee, we certify that we have read the dissertation prepared by G. Frantziskonis

entitled Progressive Damage and Constitutive Behavior of Geological Materials Including Analysis and Implementation

and recommend that it be accepted as fulfilling the dissertation requirement for the Degree of Doctor of Philosophy.

	6-11-86 Date
	6-11-86 Date
	6-11-86 Date
	6-11-86 Date
	Date

Final approval and acceptance of this dissertation is contingent upon the candidate's submission of the final copy of the dissertation to the Graduate College.

I hereby certify that I have read this dissertation prepared under my direction and recommend that it be accepted as fulfilling the dissertation requirement.

Dissertation Director	6-13-86 Date

STATEMENT BY AUTHOR

This dissertation has been submitted in partial fulfillment of requirements for an advanced degree at The University of Arizona and is deposited in the University Library to be made available to borrowers under rules of the Library.

Brief quotations from this dissertation are allowable without special permission, provided that accurate acknowledgment of source is made. Requests for permission for extended quotation from or reproduction of this manuscript in whole or in part may be granted by the head of the major department or the Dean of the Graduate College when in his or her judgment the proposed use of the material is in the interests of scholarship. In all other instances, however, permission must be obtained from the author.

SIGNED: 

ACKNOWLEDGMENTS

I wish to thank my advisor, Dr. C. S. Desai, for his encouragement, suggestions and consultations which helped toward successful completion of my research program.

I would like to thank members of my committee, Dr. I. Farmer, Dr. A. Varadarajan, Dr. D. DaDeppo and Dr. R. Richard.

This dissertation was typed by Mrs. Damon Marshall for whose patience and diligence I am eternally grateful.

The research performed herein was supported through Grant No. CEE 8215344 from the National Science Foundation (NSF), Washington, D. C. and Grant No. AFOSR-83-0256 from the Air Force Office of Scientific Research (AFOSR).

Finally, I take this opportunity to thank Becky for being cheerfully patient and understanding.

TABLE OF CONTENTS

TABLE OF CONTENTS--Continued

LIST OF ILLUSTRATIONS

LIST OF ILLUSTRATIONS--Continued

LIST OF ILLUSTRATIONS--Continued

ABSTRACT

In this dissertation, first the experimental and theoretical observations on the deformational characteristics of brittle geomaterials are reviewed and discussed. A basic conclusion is that special features such as strain softening can not be considered as true material (continuum) properties. These conclusions created a renewed emphasis on the constitutive modelling of such materials.

A model that accounts for structural changes is developed. Such changes are incorporated in the theory through a tensor form of a damage variable. It is shown subsequently that formation of damage is responsible for the degradation in strength (softening) observed in experiments, for the degradation of the elastic shear modulus and for mechanical, damage induced anisotropy. A generalized plasticity model is incorporated for the so-called topical or continuum part of the behavior, whereas the damage part is represented by the so-called stress-relieved behavior.

The question of uniqueness in the strain-softening regime is examined. It is shown that the constitutive equations lead to a unique solution for the case of rate dependent as well as rate independent formulation. Its implementation in finite element analysis shows mesh size insensitivity in the hardening and softening regimes.

The general theory of bifurcation of differential equations is employed in order to study the effect of damage accumulation on formation of narrow, so-called shear bands. It is shown that as the damage accumulates, the material approaches localization of deformation.

The theory of mixtures is employed for further theoretical establishment of the proposed model. Energy considerations show the equivalence of the two-component damage body to an elastoplastic body containing cracks; the equivalence is considered in the Griffith sense. The mechanisms of failure are considered and discussed with respect to multiaxial stress paths. An explanation of failure, at the micro level, is given.

The material constants involved in the theory are identified and determined from available experimental data. The model is then verified by back-predicting the observed behavior.

CHAPTER 1

INTRODUCTION AND SCOPE

1.1 General

Modelling for stress-deformation behavior of (engineering) materials plays an important role in providing meaningful and reliable results from solution procedures. The importance of material modelling has increased with the development of more sophisticated analysis tools, in particular computer-based numerical schemes. Often the applied loading on structures induces complex responses such as high inelastic strains, volume changes, cracking and fracturing. The influence of inelastic response becomes more prominent in the case of materials that are influenced by factors such as microcrack initiation, microcrack propagation, microcrack joining, induced anisotropy, friction and cohesion.

In the context of continuum mechanics, material modelling is termed constitutive modelling or constitutive laws. In general terms, a constitutive law is a mathematical model that describes material behavior.

The general principles of continuum mechanics such as conservation of mass, conservation of momenta, and the laws of thermodynamics are applicable to all materials, irrespective of their constitution. These principles are not sufficient in providing a solution procedure

for the response of a body under external loading. Additional mathematical equations that connect the static (e.g., force, stress) and the kinematic (e.g., displacement, strain) variables are needed. The constitutive model provides these additional equations.

The simplest constitutive laws used in engineering are linear elastic such as Hooke's law. A theory of this type describes a limited class of materials since most engineering systems are nonlinear and inelastic. For this reason, more complex groups of constitutive laws have been developed. The requirements that a model must satisfy can be categorized as follows:

1. Consistency with material test data
2. Consistency with the laws of mechanics
3. Mathematical proper posedness.

The final goal is prediction of the material behavior represented through test data. This goal though must be achieved in such a way that requirements 2 and 3 are not violated. If 2 and 3 are violated, then the material model is meaningless!

The primary objective of this study is to develop a basic and simplified realistic material model such that it can capture some important features of the behavior of geomaterials. One of these features is strain softening which can be defined as degradation of strength under increasing straining after a peak strength has been reached. This dissertation concentrates mainly on the theory for strain softening, including its analysis and implementation.

1.2 Objective of Investigation

In general terms, the objective of this investigation is to study the behavior of geomaterials under general three-dimensional loading conditions. Problems related with the "post peak" or softening part of the behavior are addressed and correlated to structural changes in the material. Both experimental and theoretical viewpoints are considered.

The objectives of the present work can be summarized as follows:

i) To review the existing theoretical and experimental literature. Experimental observations give light to some special features of material behavior in the softening regime. Models based on elasticity, plasticity, damage and other existing theories are also reviewed.

ii) To develop a general, basic and realistic model that can capture softening and effects of structural changes.

iii) To determine the material constants associated with the model using laboratory test data for typical engineering (geo) materials.

iv) To analyze the model with respect to criteria such as uniqueness and stability. The main focus is uniqueness in the softening regime and study of bifurcation points.

v) To implement the proposed constitutive model to numerical (finite element) procedures and study the stability of the procedure in the softening regime.

vi) To verify the proposed model with respect to laboratory test data. As mentioned previously, the constants associated with the model are determined from laboratory tests. These constants then are used in a numerical integration procedure to back-predict the observed response of the materials.

vii) To propose an extension of the approach to friction conditions such as interfaces and joints. Joint testing is given due consideration. The coupling of shear and normal behavior is analyzed.

1.3 Summaries of Various Chapters

Following the introduction and scope chapter, Chapter 2 reviews the existing literature. Here important experimental and theoretical viewpoints are considered. A large part of Chapter 2 is devoted to the review of recent literature, particularly damage-based models.

Chapter 3 describes, in detail, the proposed theory which includes modelling of strain softening behavior. The effect of damage accumulation and its consequences are described and discussed.

Elastoplasticity involved in the theory plays an important role in the formulation. The generalized plasticity-based hardening model used in this study is described in Chapter 4.

Chapter 5 outlines the procedure for determining the material constants. Damage-related and elastoplasticity-related constants are considered. The values of constants determined from tests on engineering materials are given.

Chapter 6 is devoted to the analysis of the proposed model. The question of uniqueness is examined for the rate dependent and the rate independent formulations of the model. It is shown that the proposed model leads to a unique solution in the hardening and softening regimes. Verification of the uniqueness attribute is considered with respect to a numerical implementation and subsequent solution of boundary value problems.

Chapter 7 considers the verification of the model with respect to laboratory test data. For this purpose, a numerical integration routine is used. Details of the materials considered for verification are given.

Chapter 8 proposes an extension of the damage model to friction conditions such as interfaces and joints. Damage and its consequences such as coupling of shear and normal behavior is considered. Importance of testing and testing procedures using a cyclic multi-degree-of-freedom device is an important part of this chapter.

Finally, a summary of the current work, conclusions, recommendations for extensions and modifications of the proposed model are presented in Chapter 9.

CHAPTER 2

REVIEW OF EXISTING LITERATURE

In this chapter, a short review of literature is given. The review is limited to literature related to the behavior of geomaterials with emphasis on the strain-softening. The physical bases of strain softening are explored and a review of proposed theories follows.

2.1 Experimental Observations

There are a number of materials such as concrete, rock and soils which exhibit a phenomenon termed as strain softening. Strain softening may be loosely defined as decrease in strength during progressive straining after peak strength value has been reached. Until recently, strain softening has been generally viewed as a true material (continuum) property and incorporated into constitutive models based on continuum theories.

A basic hypothesis in constitutive modelling is the concept of a continuum in which stress, strain, density, etc., are assumed to be defined at every point in the continuum. Under this assumption, material properties can be determined from tests on finite sized specimens undergoing homogeneous stress and strain. As the stress and strain deviate significantly from homogeneity, the observed behavior may no longer represent (continuum) material properties. Due to difficulties in identifying the influence of such nonhomogeneities, it is often

ignored, and the observed load-deformation relations of finite sized specimens are "translated" as stress-strain relations. However, influence of the nonhomogeneity can be very important in interpreting certain type of behavior such as strain softening. There is experimental evidence indicating that strain softening is not a material property of concrete, soil, or rock treated as continua, but rather the performance of a structure (e.g., of a finite size specimen) in which the individual components such as microcracks, joints and interfaces result in an overall loss of strength with progressive straining. The physical nature of strain softening in geomaterials has been examined in the literature from experimental studies.

Most strain softening data come from uniaxial (unconfined) compression and triaxial compression laboratory tests in which the axial strains are applied under displacement (strain) controlled loading. During the test, the axial force F varies with the controlled displacement u. The function F (u) is then translated to a "stress-strain" relation by means of

$$\sigma = F/A \tag{2.1}$$

$$\varepsilon = u/L \tag{2.2}$$

where σ and ε are the stress and strain, respectively, and A and L are the (undeformed) cross-sectional area and length of the specimen, respectively. Under this condition, curves such as that shown in Fig. (2.1) are obtained, where the following features are depicted:

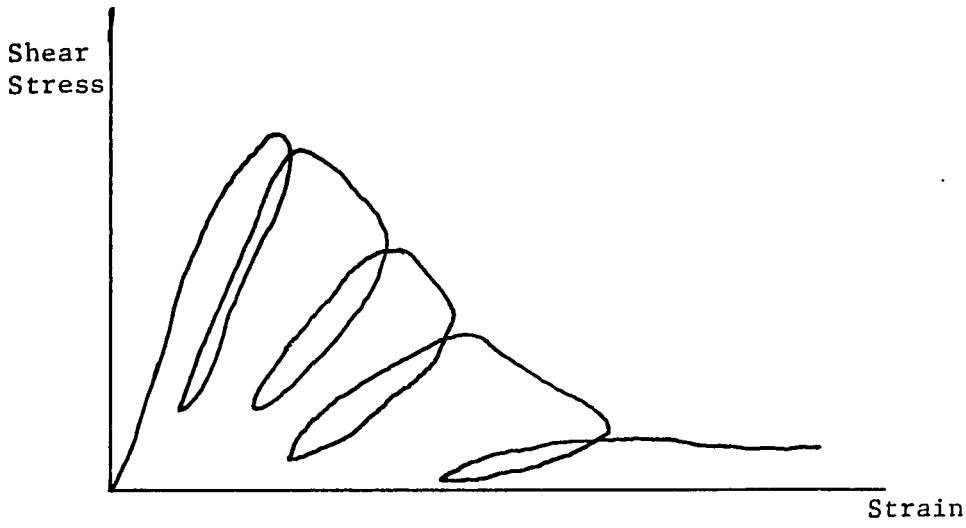

(a) Stress-Strain Behavior

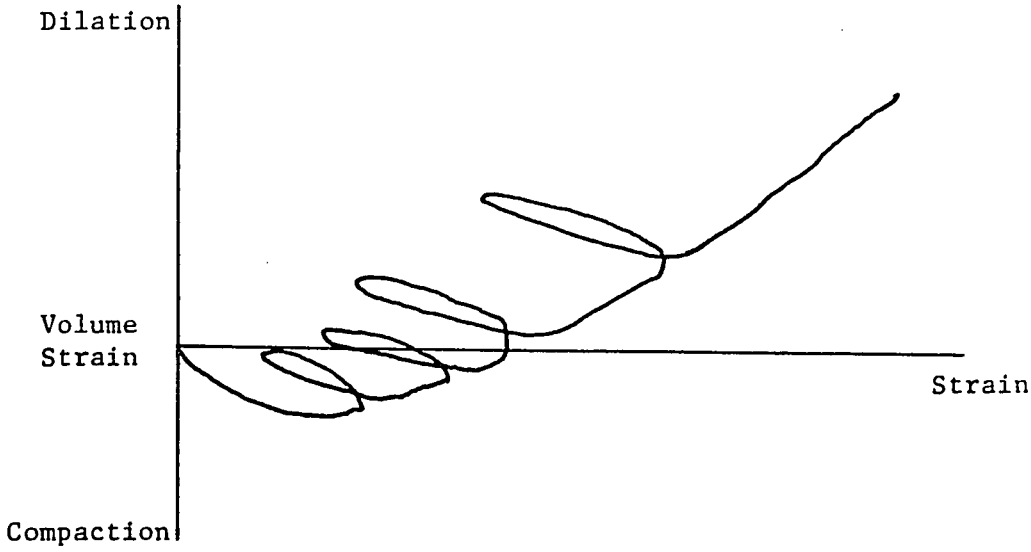

(b) Volumetric Behavior

Fig. 2.1 Schematic of Experimental Curves for Concrete

(1) softening under monotonic shear loading, (2) shear stiffness degradation under progressive loading and (3) strongly dilatant behavior.

The validity of using Eqs. (2.1) and (2.2) depends on the satisfaction of the following conditions: (1) the test specimen must be homogeneous, (2) a homogeneous state of stress must exist in the specimen during the test and (3) no significant changes in the geometry of the specimen occur during the test. If any of these conditions are not met, the force-displacement relation can not be transformed to stress-strain relation by means of Eqs. (2.1) and (2.2).

Several experiments which consider these aspects in depth have been performed on different geomaterials. Read and Hegenier (1985) and Sandler (1985) have recently discussed and reviewed such issues. Hudson et al. (1971) performed unconfined compression tests on marble specimens. Cylindrical specimens of various sizes and length over diameter (L/D) ratios were tested. The testing strain rate was "slow" and constant for all specimens. They found that, in general, the portion of the apparent stress-strain curve up to the peak is generally unaffected by variations in specimen geometry and size, while the descending branches are strongly dependent upon them. Also, it was found that structural breakdown of the specimens and subsequent progressive failure began at about 50 percent of the peak strength. As a result of the inhomogeneity of the material at the microscopic level, local tensile stresses aligned with the loading axis are developed. These tensile stresses produce microcracks that grow parallel to the major loading axis. As the loading continuously increases, the microcracks align in

the vertical direction which results in slabbing of the material from the specimen's lateral surfaces, as illustrated schematically in Fig. (2.2). In general, the density of the axial cracks is higher at the center of the specimen's length. This is because the restraints at the specimen ends, due to friction, inhibit crack growth near the specimen ends where the effect of interface between the loading platens and the specimen ends are predominant; this is particularly true for long specimens. In the short specimens, microcracks appear to be uniformly distributed over the entire specimen length. The slabbing (also called bursting) of part of the specimen reduces the cross-sectional area of the intact (healthy) material. Thus, the stress distribution in a cross section is not uniform. In the load-bearing cross-sectional area of the specimen, denoted by A in Fig. (2.2), the stress is relatively high, while the stress in the slabbed area is diminished. For specimens with small L/D ratios where D = diameter of the specimen, the slabbing of material from the lateral surface does not significantly reduce the effective load-bearing area, and in this case $a \cong A$. For long specimens, the true cross-sectional area is reduced significantly during the test. The effect of this drastic reduction is strain softening in the overall response of the specimen.

Hallbauer et al. (1973) performed a series of triaxial compression tests on a quartzite. The specimens used were cylindrical with L/D = 3 and they were jacketed in thin copper tubes so that lateral expansion was resisted significantly by the increasing confinement. The

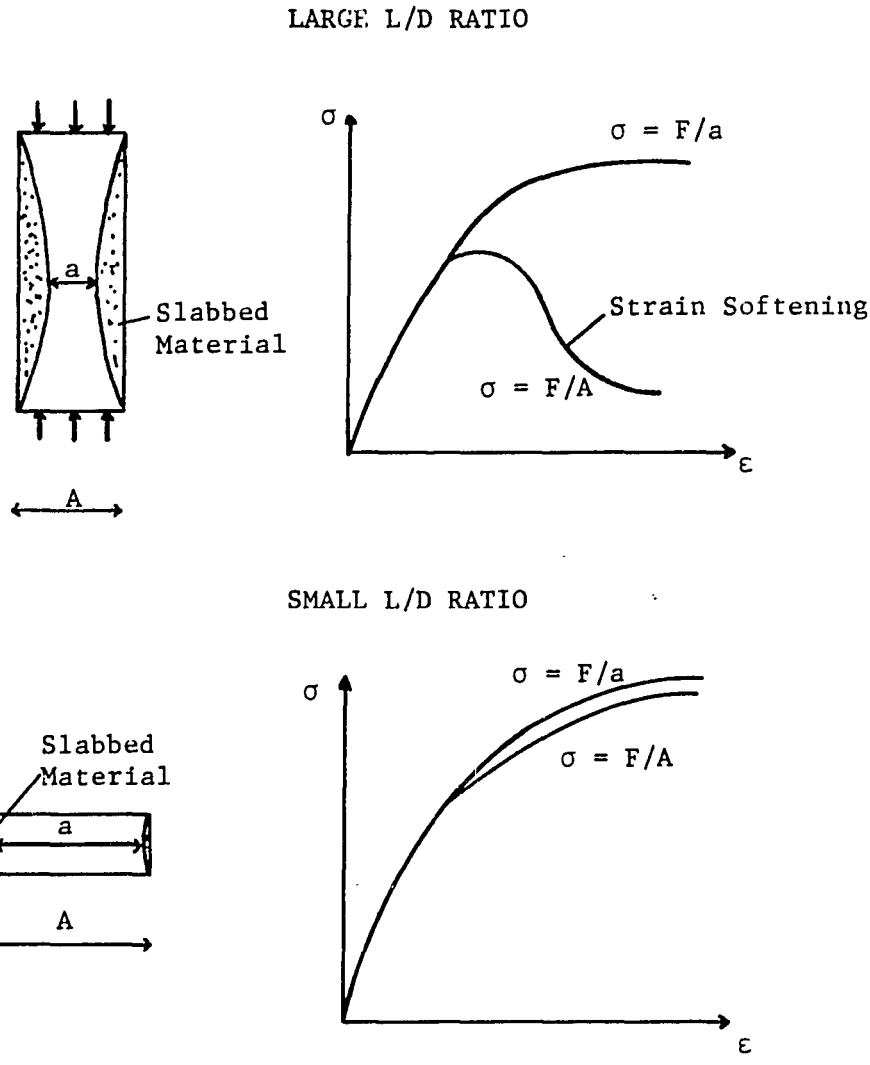

Fig. 2.2 Effect of Slabbing and Specimen Geometry on Stress-Strain Curves (After Sandler, 1984)

purpose was to determine the changes in the structure of the material that took place progressively as the rock was compressed to failure. Special consideration was given to the zone in the vicinity of the peak of the load-displacement curve. This was accomplished by stopping the tests at several points along the strain path. After unloading, the specimens were removed and sectioned for microstructural examination and progressive failure diagnosis. The results obtained can be summarized as follows: Little damage occurs until the stress reaches about 80 percent of its peak value. After increasing the stress from 80 to 90 percent of the peak and thereafter, a rapid extension of microcracks occurred. The degradation of the load carrying capacity was attributed to the failure of existing partially fractured material. On the basis of this evidence, it may be concluded that the softening part of the stress-strain curve is the result of the propagation of fracture planes and subsequent formation of a macroscopic fracture plane through the entire specimen. After the peak, the specimens were in the process of splitting (bursting) and, therefore, were not homogeneous continua.

Studies relating the shape of the stress-strain curve of plain concrete to the type and extent of internal microcracking were performed by Hsu et al. (1963), Shah and Slate (1965), Maher and Darwin (1982) and Van Mier (1984). They investigated the consequences of progressively increasing macroscopic fracture and material sliding in the overall stress-strain curves for plain concrete. Hsu et al. investigated plain concrete cylinders axially compressed over a range of strains from 0.0 to 0.003. Frictional effects between platens and specimen were

minimized since the cylinders were greased. The crack observations in the deformed specimens were achieved by two methods. In the first method, the specimen was cut, the cracks were filled with colored dye, and the cracked specimen was examined under a microscope. In the second method, a thin slice was cut and removed from the deformed cross section and then examined by using X rays. For both the above methods, the shape of the stress-strain curve was correlated to the internal microcracking morphology. For concrete, microcracks can, in general, be categorized as: (1) interface cracks between aggregate and mortar, termed bond cracks, (2) cracks through the mortar and (3) cracks through the aggregate. Due to shrinkage, band cracks exist before any load is applied to plain concrete. Mortar cracks initiate and propagate when increasing load is applied. At all stages of straining, the total extent of mortar cracking is considerably less than that of bond cracking (Hsu et al. 1963) and at about 70 percent of the ultimate (peak) load, the stress-strain curve begins to curve more sharply towards the horizontal, indicating the beginning of internal breakdown. On the descending branch of the stress-strain curve, the specimen is extensively cracked, the amount of cracking being greater with increasing slope of the curve. As Shah and Slate (1968) concluded, "... when a continuous crack pattern has developed extensively, the carrying capacity of concrete decreases and the stress-strain curve begins to descend." It appears that increase in straining increases the disintegration of the material and the inhomogeneity of deformation.

Additional noteworthy experimental results are that of Brady et al. (1973), Hettler and Vardoulakis (1984), Drescher and Vardoulakis (1982). Brady et al. conducted an interesting study of the unconfined compression behavior of several rocks. Each specimen was loaded to a preselected position along the post peak branch of the curve, then unloaded and cast in hydrostone. After that, it was "sliced" at half-inch slices normal to the main loading axis, and the resulting disks were smoothed. The disks were impregnated with fluorescent dye to reveal the cracked portions of the cross sections. The assumption that the load was carried essentially by the uncracked cross section was made. Under this assumption, the true stress-strain curve under uniaxial compression was determined and it was found that: (1) there is a maximum true stress that the intact material can sustain without extensive inelastic deformation, and (2) the maximum true stress does not change with axial strain.

Most information on strain softening of soils comes from conventional triaxial compression tests on dense specimens. As pointed out by Hettler and Vardoulakis (1984), experiments with "perfect" homogeneous material cannot insure, in general, homogeneous deformation since various modes of nonhomogeneous modes do develop. The modes of nonhomogeneous deformation considered by Hettler and Vardoulakis (1984) are shown in Fig. 2.3.

Studies by Drescher and Vardoulakis (1982) clearly establish that when sand is deformed homogeneously in triaxial compression, very

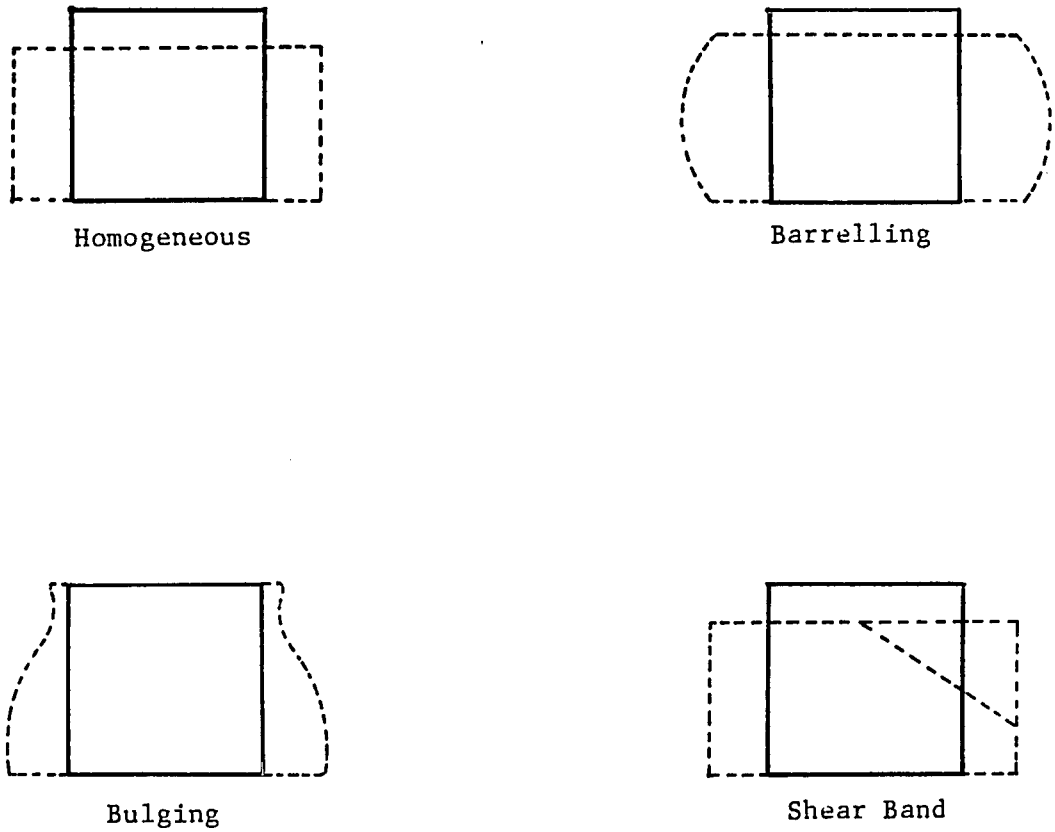

Fig. 2.3 Homogeneous and Nonhomogeneous Modes of Deformation (After Hettler and Vardoulakis, 1984)

little or no softening occurs for axial strains of at least 10 percent. For larger strains, instability (bifurcation) develops, producing subsequent nonhomogeneous deformation accompanied with strain softening.

The above-mentioned experimental observations conclude that strain softening may not be a material property of concrete, rock or soil treated as continua, but rather the performance of a structure (finite sized specimen) composed of microcracks, joints and interfaces that result in an overall loss of strength.

In the above, part of experimental observations regarding the strain softening in geomaterials were surveyed. Noteworthy experimental works related to the subject of microcracking and fracture are briefly discussed subsequently.

Progressive failure of brittle soft rock in triaxial compressive tests were considered by Sture and Ko (1978). Multiple stick-slips were found in the strain softening branch. Also, it was concluded that strain softening is confined to the joint developed (shear band) and its immediate vicinity, while the rock masses between the joints continue to behave in an elastic manner.

Test results obtained by Carrasquiblo et al. (1981 a, b) show a delayed crack-formation process for high-strength concrete when compared to low-strength concrete. It was found that at failure, a large amount of microcracks run through the aggregate particles. The delayed crack propagation is also shown by the nearly straight pre-peak stress-strain curve of the high-strength concrete. Experiments based on acoustic

emission were performed by Spooner et al. (1975, 1976). It was indicated that the fracture process of the specimens is progressive. It was argued that concrete behaves similar to an ideal material in which two specified energy dissipating processes are active.

Crack detection techniques that use X rays were reported by Slate and Olsefski (1963). Fluorescent dye for crack detection was used by Diaz and Hilsdorf (1973) and Stroeven (1979).

Before closing this section, definitions of the different size levels should be given so that structural effects can be considered with respect to the scales (Wittmann, 1982). Each scale is associated with a so-called characteristic length. Such a length is associated with properties that can be studied at this scale.

1. Gross Scale: Here the characteristic length is that of 1.0 inch (2.5cm). Strength of materials considers this as its appropriate scale.
2. Macroscopic Scale: The characteristic length is of the order of 0.1 inch (0.25cm). The structure of the material at this scale is of interest to crack-formation and fracture mechanics. The average stress and strain and the nonlinearity of the mechanical properties at the gross level will be influenced by phenomena occurring at this level.
3. Microscopic Scale: The characteristic length is of the order of 0.001 inch (0.0025cm). Metallurgists and material scientists are interested in this scale. Also,

here we may assume that the behavior at this lower level will be affected by mechanisms typical at this level. What is mainly active at this level are physical and chemical processes.

4. Atomic Level: The Angstrom (10^{-8}cm) is the characteristic length. Physicists are interested at this level.

NOTE: Different definitions of the various scales have been reported in the literature. For instance, some authors refer to the gross scale defined here as the macroscopic level and the macroscopic as the microscopic one.

2.2 Elasticity and Plasticity Models

In the preceding section, it was concluded that strain softening does not appear to be a true material property of geomaterials. This conclusion was based on what is accepted today as accurate and credible experimental evidence. The objective of this section is twofold. First, the elasticity and plasticity-based models for strain softening are reviewed briefly. Second, we examine the consequences of the assumption that strain softening is a true material property, theoretically and numerically.

2.2.1 Existing Literature

Despite the experimental evidence for the occurrence of strain softening, there has been little work done in developing consistent

analytical models. In the absence of a proper formulation for strain softening behavior, most analyses are performed with a simplified stress-strain curve which assumes either elastic or elastoplastic response.

The field of elasticity-based models is quite broad and can be divided into various sub-categories based on the state of stress (uniaxial, biaxial and triaxial) and the form of the constitutive relations such as incremental and total stress-strain models. The majority of the models are of the nonlinear elastic type and are used for representation of material behavior under monotonic or proportional loading only.

In the total stress-strain models, it is assumed that a unique state of stress can be determined as a function of strain or vice versa. In general,

$$\sigma_{ij} = F_{ij} (\varepsilon_{k\ell}) \tag{2.3}$$

where F_{ij} represents the tensorial material response function. One limitation is that the behavior is path independent, which is, in general, not true for geologic materials. Further limitations arise when stress histories including unloading and reloading histories are involved. In spite of these shortcomings, these types of models have been used in describing behavior of geomaterial, mainly because of their simplicity. In general, most of the models are based on a simple extension of the linear elastic and isotropic stress-strain relations by

substituting secant shear and bulk moduli which are assumed to be functions of stress, strain or both.

The incremental type of elasticity models can, in general, be expressed as a hypoelastic "type" stress-strain relation. The incremental stress-strain relation is expressed as

$$d\sigma_{ij} = C_{ijk\ell}\, d\varepsilon_{k\ell} \tag{2.4}$$

where d denotes increment and $C_{ijk\ell}$ is the (tangent) material stiffness tensor that generally depends on the stress and strain tensor. Because of the path-dependent behavior characteristics, these models provide a more realistic description of behavior of geomaterials under general loading conditions than the total stress-strain models. However, under general stress histories involving unloading, a loading criterion needs to be introduced which may cause problems related to or near neutral loading (Bathe and Ramaswamy, 1979; Nelson et al., 1971).

Uniaxial elasticity-based models have been developed mainly for concrete structures in which the concrete can be represented as being in a state of uniaxial stress. Interesting works in this area are that of Kowson and Jirsa (1969), Sinha et al. (1964). A review on the subject is also provided in these papers.

Desai (1974) proposed a hypothesis for strain softening behavior for overconsolidated soils (and interfaces) in which the material response is decomposed in two or more components: one due to basic, normally consolidated part that is continuously hardening and the other due to overconsolidation that contributes to progressive loss of

strength leading to strain softening. The resulting model modifies the initial constitutive matrix through a function that allows for strain softening with accumulation of deformation. The function is expressed in terms of various physical factors such as peak and residual stress and strain, area under the curve and initial moduli, in which the progress of softening is expressed in terms of the relative values of stresses and strains between the peak and the residual states; similar terms are used for description of the damage evolution proposed in this study. However, the model proposed in this study contains a number of novel and distinguishing features such as generalization of damage concept proposed by Kachanov (1958).

The above model was introduced in a nonlinear (elastic) finite element procedure involving a special incremental iterative scheme. The finite element predictions were verified with respect to softening behavior of soil specimen under triaxial conditions and load displacement behavior of a pile influenced by softening at the pile-soil interface.

The majority of the biaxial and triaxial elasticity models make use of isotropic total stress representations (Kotsovos and Newman, 1978; Ottosen, 1979; Cedolin et al., 1977; Palaniswamy and Shah, 1974; Phillips and Zienkiewicz, 1976). These models are based on either stress or strain invariants. Material properties are represented by the bulk and shear moduli in either the total form or the incremental form.

Experimental results for geomaterials indicate that the deformation process of these materials is basically inelastic and nonlinear.

Upon unloading, only a portion of the total strain is recovered (e.g., Fig. 2.1). Some of the elasticity-based models for geomaterials have been summarized and discussed previously. Plasticity-based models have been used extensively in order to describe the hardening and the softening behavior of concrete rock and soils. They are basically based on extensions of incremental rate independent plasticity theory.

In the classical theory of plasticity, uniqueness and stability are normally discussed in the context of the postulate formulated by Drucker (1959), where a distinction is made between materials which exhibit hardening and softening. Since, during loading, the incremental work done by a softening material is negative, such behavior is considered to be unstable. Drucker's postulate has far-reaching implications in the foundations of plasticity theory and completely dictates the structure of the stress-strain relations. For geological materials though, these postulates are considered to be far too restrictive, and more general postulates and formulations are required to model the complex observed material behaviors.

The incorporation of strain softening within a plasticity model follows the same procedure as for hardening rules. General hardening plasticity-based rules are described in detail in many textbooks (Hill, 1950; Kachanov, 1971; Mendelson, 1968; Desai and Siriwardane, 1983). In this dissertation, the general formulation of plasticity theory is described in a subsequent chapter. For completeness of this

section, plasticity-based models for strain softening are discussed herein. The procedure followed by Nayak and Zienkiewicz (1972), Hoeg (1972), Sture (1979) and Prevost and Hoeg (1975) is described subsequently. In these models, the distinguishing difference between hardening and softening is in the hardening rule. For the simple scheme of isotropic strain hardening/softening, the hardening rule is such that for hardening materials, the yield surface continuously expands. For softening materials, the yield surface contracts. Details on the above concepts are given in a subsequent chapter.

Motivated by the recent developments in the area of continuum mechanics, efforts have been focused on the attempt to develop a continuous model for elastic-plastic behavior which may not require the existence of a yield condition and thus is free from the cumbersome hardening/softening rules. Among many attempts, the endochronic theory has received much attention. It was originated by Valanis (1971) for the description of mechanical behavior of metals. Valanis showed that by employing a pseudo-time scale, the intrinsic time, a constitutive equation in integral or differential form can successfully be used to describe material behavior including cyclic loading. Using Valanis's concept, Bazant and co-workers have extended the theory to describe behaviors of rock, sand, plain concrete and reinforced concrete under various conditions (Bazant, 1978, and its references).

2.2.2 Implications of Strain Softening

In this section, we will assume that strain softening is a true material property and investigate the consequences of such an

assumption. In order to keep the discussion relatively simple, one-dimensional problems are considered and discussed. Both rate dependent (viscous) and rate independent materials are considered. Concepts of applied mathematics, in particular the method of characteristics, will be used in this section. Let σ and ε denote the stress and strain (compression positive) of one-dimensional motion of a semi-infinite material which strain softens after some critical strain level is reached. The equations of momentum balance and continuity for small strains have the form

$$\frac{\partial \sigma}{\partial x} + \rho_o \frac{\partial v}{\partial t} = 0 \tag{2.4}$$

$$\frac{\partial v}{\partial x} + \frac{\partial \varepsilon}{\partial t} = 0 \tag{2.5}$$

where ρ_o is the initial density, v is the velocity and x is the one-dimensional coordinate. In order that the formulation is complete, the constitutive equation for the material must supplement Eqs. (2.4) and (2.5). In the following, we consider two cases (Valanis, 1985; Read and Hegemier, 1984):

CASE 1: Simple rate-independent model

Consider a simple, rate independent constitutive model with strain softening

$$\sigma = F(\varepsilon) \tag{2.6}$$

where F has continuous derivative with respect to ε. At peak stress value let ε_o denote the corresponding strain. Then

$$F'(\varepsilon) \geq 0 \text{ for } 0 < \varepsilon \leq \varepsilon_o$$
$$F'(\varepsilon) < 0 \text{ for } \varepsilon > \varepsilon_o \tag{2.7}$$

and the superprime denotes differentiation with respect to ε. From (2.4) through (2.6), the following system of quasilinear first order partial differential equations result:

$$F'(\varepsilon)\frac{\partial \varepsilon}{\partial x} + \rho_o \frac{\partial v}{\partial t} = 0$$
$$\frac{\partial v}{\partial x} + \frac{\partial \varepsilon}{\partial t} = 0 \tag{2.8}$$

which have the characteristic determinant (Valanis, 1985)

$$\det \begin{vmatrix} F'(\varepsilon) & 0 & 0 & \rho_o \\ 0 & 1 & 1 & 0 \\ dx & dt & 0 & 0 \\ 0 & 0 & dx & dt \end{vmatrix} = 0 \tag{2.9}$$

From Eq. (2.9), the characteristics are given by

$$\frac{dx}{dt} = \pm \sqrt{F'(\varepsilon)/\rho_o} \tag{2.10}$$

when $F'(\varepsilon) > 0$, which corresponds to the hardening range of behavior, the characteristics are real and distinct as indicated in Eq. (2.10). In this case, the system of partial differential equations (2.8) is

hyperbolic and the solution to the initial value problem is unique. When $F'(\varepsilon) < 0$, which corresponds to the strain softening regime, the characteristics are not real (complex) and the system is ill-posed as an initial value problem (Valanis, 1985). Lack of well-posedness caused due to the existence of complex characteristics implies growth of disturbances of all the deformation fields and leads to instabilities when these equations are treated by numerical techniques such as the finite element method.

CASE II: Simple rate-dependent model

One of the simplest one-dimensional models which exhibits rate-sensitivity and strain softening is given by

$$\sigma = F(\varepsilon) + M \frac{\partial \varepsilon}{\partial t} \tag{2.11}$$

where $F(\varepsilon)$ has the properties of Eq. (2.7) and M is a material constant. From Eqs. (2.4, (2.5) and (2.11), the following system of partial differential equations is obtained:

$$\begin{aligned} &\frac{\partial \sigma}{\partial x} + \rho_o \frac{\partial v}{\partial t} = 0 \\ &M \frac{\partial v}{\partial x} = F(\varepsilon) - \sigma \end{aligned} \tag{2.12}$$

The characteristic determinant is given by (Valanis, 1985)

$$\det \begin{vmatrix} 1 & 0 & 0 & -\rho_o \\ 0 & 0 & M & 0 \\ dx & dt & 0 & 0 \\ 0 & 0 & dx & dt \end{vmatrix} = 0 \qquad (2.13)$$

Note that $F'(\varepsilon)$ does not appear in Eq. (2.13). Thus, the system remains parabolic regardless of the specific form of $F(\varepsilon)$. Therefore, one can conclude that no unusual mathematical or numerical difficulties will arise when such a model is used, even in the strain softening regime.

Two example problems were considered. It was shown that when the material is rate-independent, the governing equations lead to a unique solution as long as the material is hardening; when softening occurs, however, the equations become ill-posed. The ill-posedness leads to analytical and numerical difficulties. On the other hand, in the case of rate-dependent material, unique solution can be obtained independently of hardening or softening of the loading curve.

The one-dimensional initial value problem mentioned above was considered further by Wu and Freund (1984). Actually, they considered a somewhat different physical problem; namely, shear wave propagation in a half space of strain softening material. Despite the physical differences, the mathematical formulation of both systems leads to identical system of equations. What was concluded in this study can be summarized as

- The initial value problem is improperly posed for all times greater than that at which the material at the

boundary x = 0 first reaches the peak of the stress-strain curve, say t^*. Meaningful analytic or numerical solutions can not be obtained for $t > t^*$.

- At initiation of softening, the vanishing tangent modulus $F'(\varepsilon)$ leads to the concept of "deformation trapping" in general, and shear bonding for the particular problem considered by Wu and Freund (1984).

2.2.3. Numerical Solutions

In this section, numerical difficulties that arise when a problem is solved involving rate-independent strain softening material are studied. For this purpose, we consider a numerical study by Wright and Sandler (1983) in which the numerical aspects of such a problem were considered with a standard one-dimensional finite-difference method.

Wright and Sandler (1983) considered a rate-independent strain softening material whose limiting stress-strain curve for loading is of the form

$$\sigma = F(\varepsilon) \tag{2.14}$$

and

$$F(\varepsilon) = E_o \, \varepsilon \exp(-\varepsilon/\varepsilon_o) \tag{2.15}$$

and E_o, ε_o are material constants. The small strain assumption was adopted. Compressive unloading and reloading beneath the limiting loading curve were taken to occur reversibly and parallel to the initial

slope E_o, as illustrated in Fig. 2.4(a). The velocity boundary condition at x = 0 was prescribed as follows:

$$v(t) = \begin{cases} \frac{1}{2} V_o \left[1-\cos\left(\pi t/t_o\right)\right] & \text{for } t \leq t_o \\ V_o & \text{for } t > t_o \end{cases} \qquad (2.16)$$

where t_o = 0.2 msec; the variation of V with time according to Eq. (2.16) is illustrated in Fig. 2.4(b). At t = 0, the material was assumed to be stress free. The following values of the material parameters were adopted which are typical of plain concrete:

E_o = 20.684 GPa (3×10^6 psi)

ε_o = 0.002

ρ_o = 2403 kg/m^3 (150 lb/ft^3)

Numerical solutions of the initial value problem described above were obtained for two different, but very close, values of the peak boundary velocity, V_o. In one case, the value V_o = 3.225 m/sec (1.27 in/sec) was selected so that the material was driven very near to, but not over, the peak of the stress-strain curve. For this case, the tangent modulus, $F'(\varepsilon)$, is always positive. In the other case, the value V_o = 3.252 m/sec (128 in/sec) was used, which was just large enough to drive the material into the strain softening regime. As noted previously, the problem becomes ill-posed as soon as the material begins to strain soften and, as demonstrated by Wright and Sandler (1983), the corresponding numerical solution develops peculiar features when this occurs.

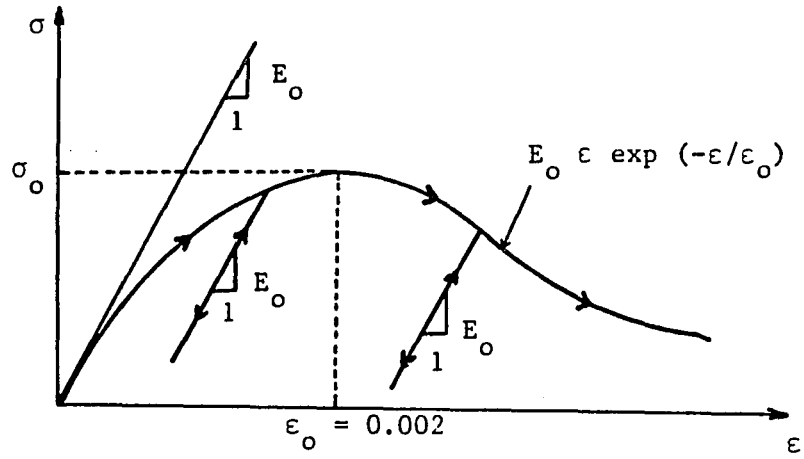

(a) Softening Stress-Strain Model

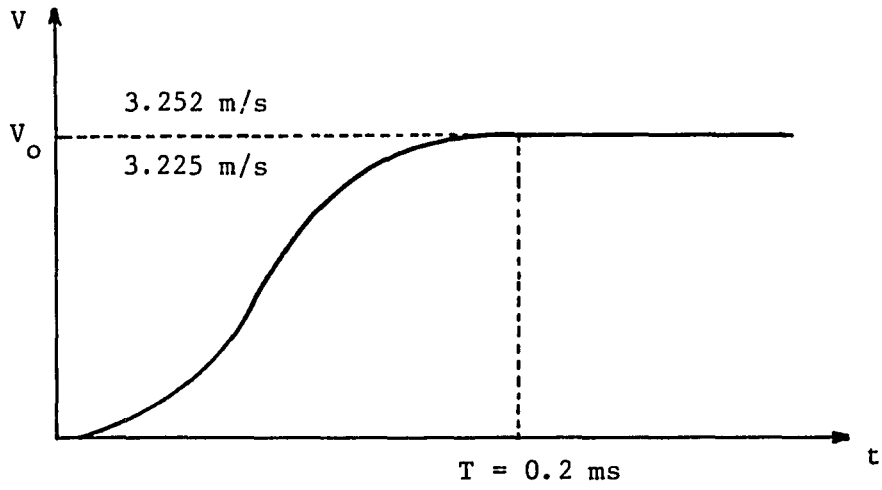

(b) Input Velocity

Fig. 2.4 Features of the One-Dimensional Problem Considered Numerically by Sandler (1984)

Figure 2.5(a) shows the numerical results obtained for the case V_o = 3.225 m/sec (127 in/sec). Here, the calculated velocity histories at a depth of 0.3048 m (12 inches) for two different zone sites are shown. As this figure reveals, such zoning was adequate, as evidenced by the fact that the two calculated histories essentially overlay one another.

The numerical results for the case V_o = 3.252 m/sec (128 in/sec) are given in Fig. 2.5(b). Here, calculated velocity vs. time histories at x = 0.3048 m (12 inches) for three different zone sizes are shown. The prescribed boundary velocity drives the material into the softening region and, when this occurs, the problem becomes ill-posed; this is reflected in the numerical results in several ways: (1) strain softening was confined, in all cases studied, to the zone adjacent to the boundary. Therefore, the amount of material that strain softens is actually decided by the numerical solution procedure (zone size) and not the physics. As a result, as the zone size approaches zero, the amount of material that actually softens can be reduced to zero, (2) the calculated velocity profiles depicted in Fig. 2.5(b) show a high sensitivity to zone size that was not present in Fig. 2.5(a), (3) the strain in the first zone grows very rapidly after the material begins to soften and quickly invalidates the assumption of small strains. The calculated strain-time history for the case Δx = 0.0254 m (1 inch), shown in Fig. 2.6, illustrates the point.

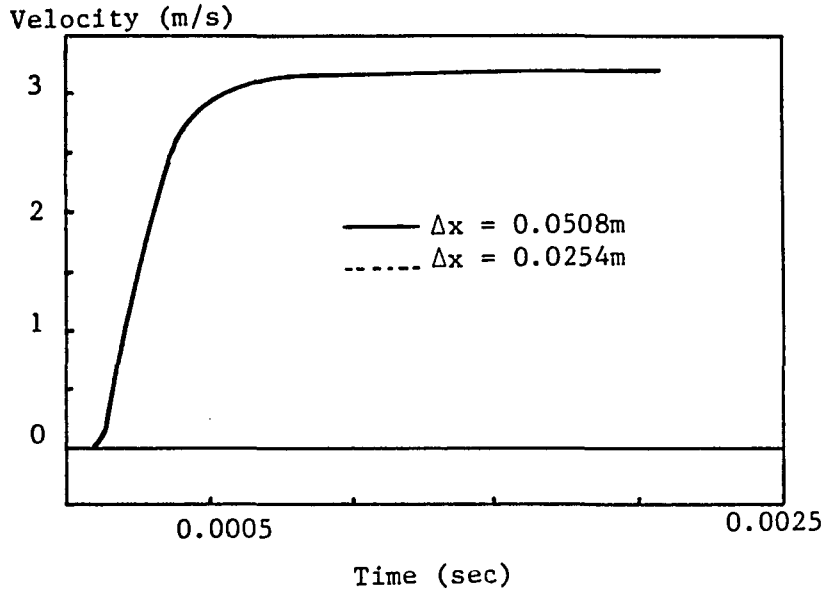

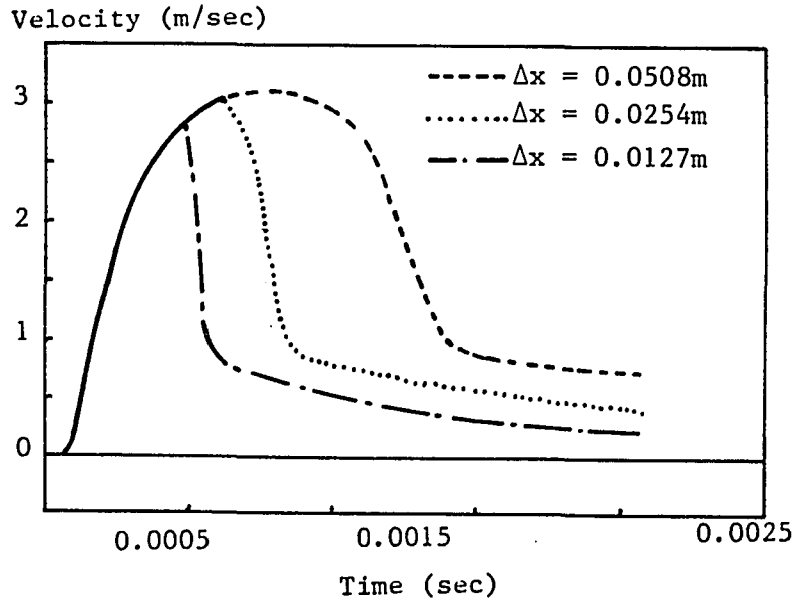

Fig. 2.5 Velocity Profiles for Various Grid Sites (a) V_o = 3.225 m/sec, (b) V_o = 3.252 m/sec (After Sandler, 1984)

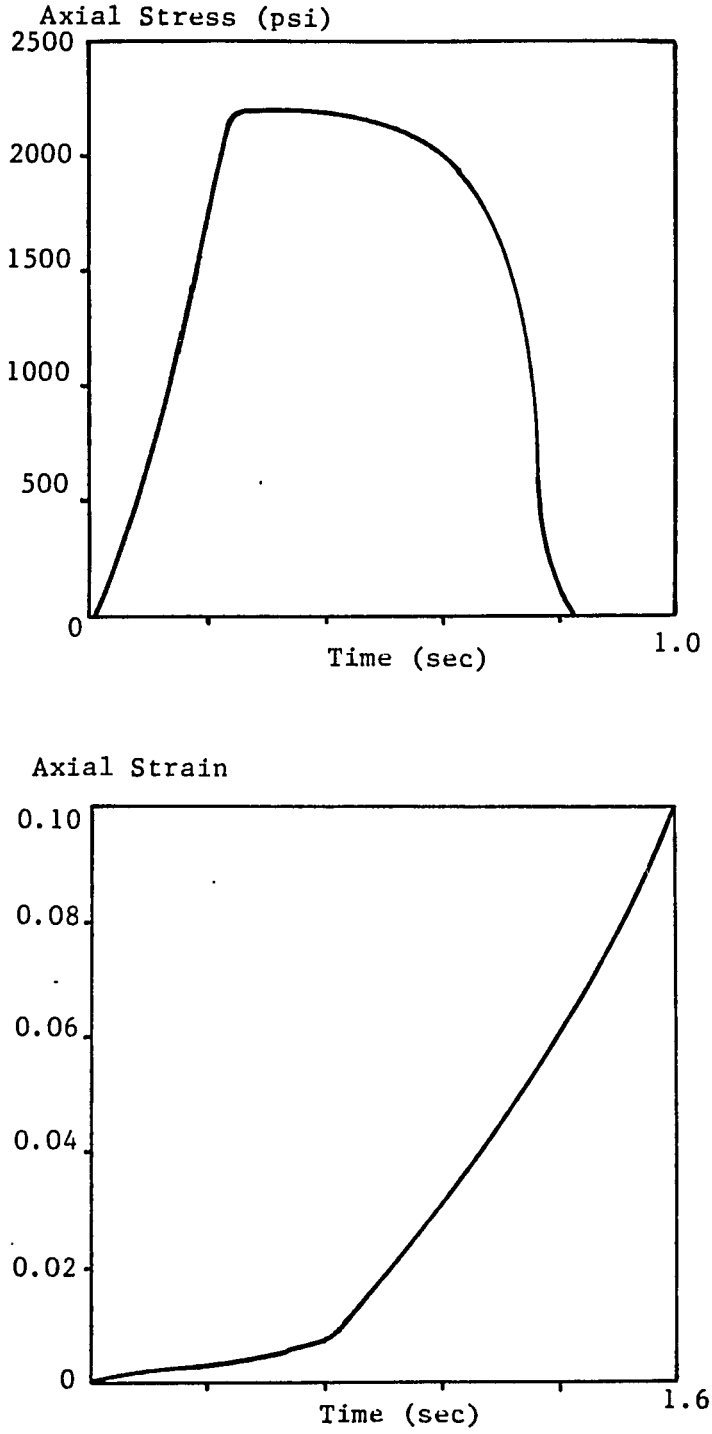

Fig. 2.6 Histories of Stress and Strain at Boundary for V_o = 3.252 m/sec (After Reed and Hegemier, 1985)

The wave propagation problems considered above illustrate the difficulties that arise in the numerical analysis of such problems when the material exhibits strain softening. Difficulties of a different type have been reported in numerical studies of the quasi-static loading of strain softening materials (Nayak and Zienkiewicz, 1972; Prevost and Hoeg, 1975; and Lo and Lee, 1973). It was found, for example, that if standard numerical approaches are used, the numerical solutions suffer from instability and mesh size sensitivity as soon as the material enters the strain softening range.

A special finite element approach was proposed by Pietruszczak and Mroz (1981) for numerically analyzing the behavior of materials which soften through shear bonding. In this approach, a shear band of specified thickness and orientation is introduced into those finite elements which reach a prescribed shear band initiation criterion. The characteristic thickness of the shear band is supposed to be determinable from compression test data. The incremental stiffness matrix of the elements is accordingly modified to reflect the effect of the shear bands. To illustrate the advantages of the proposed approach, the authors considered the plane strain response of a strain softening material that was compressed between two rigid parallel plates. The material was assumed to be bonded to the plates of their common interfaces (sticking friction conditions). The material was loaded by applying specified increments of vertical displacements. Figure 2.7 shows the problem geometry and the three finite element meshes considered. The thickness of the shear bond was held fixed as the mesh

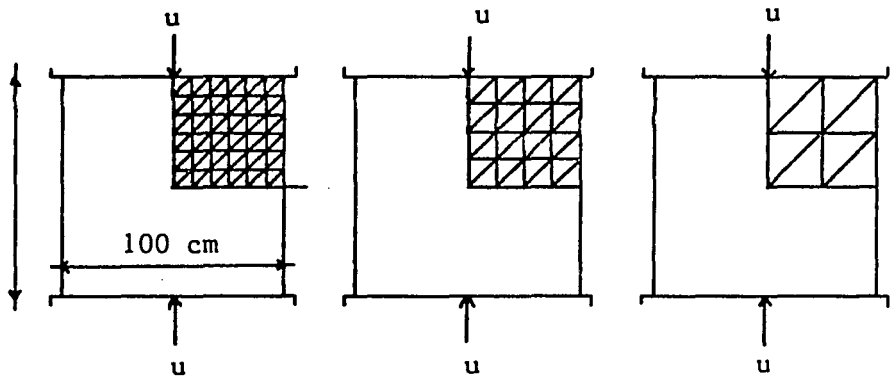

(a) Geometry of the Problem

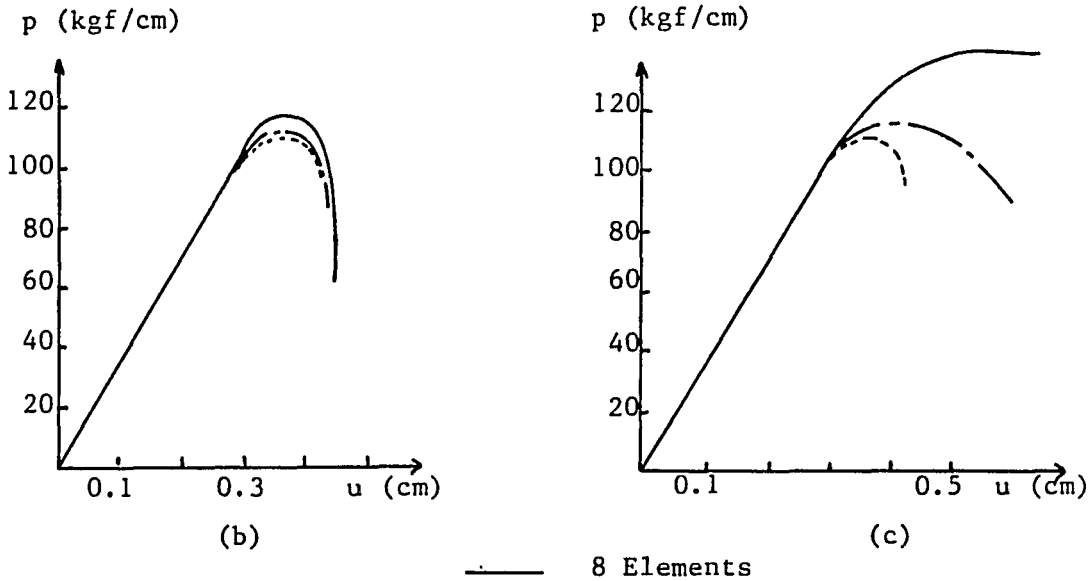

Fig. 2.7 Plain Strain Compression Problems Considered by Pietruszczak and Mrox (1981)

size changed. The load-displacement relationship calculated by the proposed approach is shown in Fig. 2.7(b). Here, it is seen that the results are nearly insensitive to the mesh size. In contrast, Fig. 2.7(c) shows the corresponding load-displacement relationship calculated with the conventional finite element approach. It is seen that the resulting curves are very sensitive to the element mesh size.

The above approach appears to be potentially useful in treating materials for which softening is known a priori to occur through shear bonding. On the other hand, as Read and Hegemier (1983) mentioned, for brittle materials such as rocks and concrete which deform and macroscopically soften through microcracking, the usefulness of the above method is doubtful.

2.3 Damage Based and Other Models

Here, models that consider measure(s) of damage are reviewed. The majority of the literature considers uniaxial stress conditions and damage is defined in such a manner that the effects of voids, microcracks, etc., are taken into account. Pioneers in this area are Kachanov (1959) and Rabotnov (1969). In their approach, under uniaxial conditions, a scalar is defined such that it represents a measure of the voids in a cross section of a specimen subjected to uniaxial stress. The approach proposed by Kachanov considers the effect of voids and flaws in metals. A scalar is defined as the quotient between intent cross-sectional area and total macroscopic cross-sectional area. The theory was implemented for prediction of the creep behavior of metals

and it did not include strain softening since softening is not, in general, a characteristic of metals. Here, instead of giving complete details of the Kachanov-Rabotnov approach, we consider a uniaxial example. The example is general enough to give an understanding of the approach. For generality and consistency with the present work, the example considers strain softening response.

Let a cylindrical specimen be subjected to uniaxial stress conditions. The total cross-sectional area of the specimen is denoted as A. At a cross section, we assume the existence of voids and flaws with a total area A_o. The intact area is denoted as A_t such that $A = A_t + A_o$. Let F be the force applied. The mean stress is defined as $\sigma = F/A$ while the true stress acting on A_t is $\sigma_t = F/A_t$. Thus

$$\sigma = \frac{F}{A} = \frac{\sigma_t A_t}{A} = \sigma_t \left(1 - \frac{A_o}{A}\right) \tag{2.17}$$

Now, define $r = \frac{A_o}{A}$. Then, Eq. (2.17) is written as

$$\sigma = (1-r)\, \sigma_t \tag{2.18}$$

For illustration purposes, let us assume that the stress-strain behavior of the intact part is linear, as shown in Fig. 2.8(a). The overall behavior though is like that of Fig. 2.8(b). It will be shown that growth of voids and flaws is responsible for the descending branch of the overall stress-strain curve. Since the intact (topical) part is linear, we have

$$\sigma_t = E\, \epsilon \tag{2.19}$$

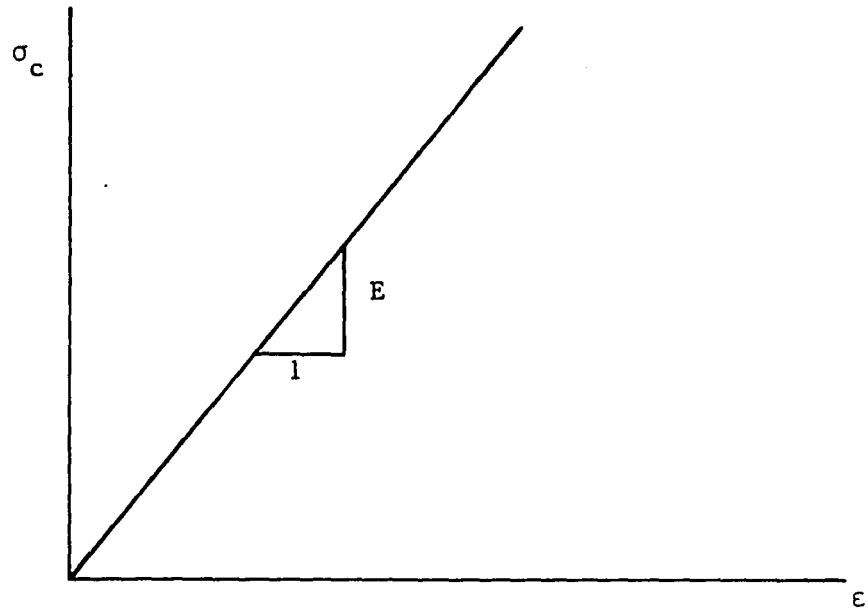

(a) Undamaged

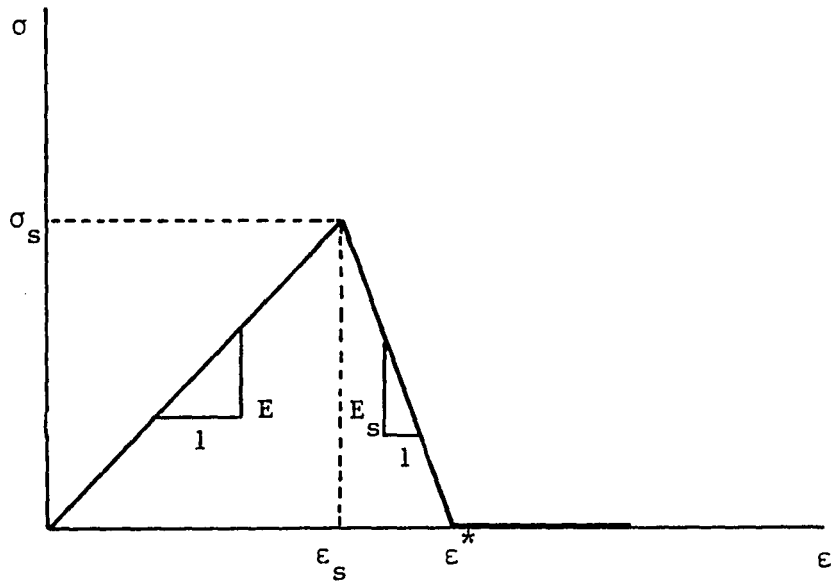

(b) Average

Fig. 2.8 Stress-Strain Curves for Example Problem

and E is the corresponding modulus. From Eqs. (2.18) and (2.19), we obtain

$$\sigma = (1-r)\, E\, \varepsilon \tag{2.20}$$

which holds for all ranges of ε. After the peak is reached, the stress-strain relation can be written (Fig. 2.8(b)).

$$\sigma = \sigma_s + E_s\, (\varepsilon - \varepsilon_s) \text{ for } \varepsilon^* \geq \varepsilon \geq \varepsilon_s \tag{2.21}$$

where σ_s, ε_s are the stress and strain at the peak and E_s is the modulus in the descending part of the stress-strain curve. From Eqs. (2.20) and (2.21), we obtain

$$\sigma_s + E_s\, (\varepsilon - \varepsilon_s) = E\, \varepsilon\, (1-r) \text{ for } \varepsilon^* \geq \varepsilon \geq \varepsilon_s \tag{2.22}$$

Equation (2.22) can be solved for r so that

$$r = 1 - \frac{\varepsilon_s}{\varepsilon} - \frac{E_s}{E}\left(1 - \frac{\varepsilon_s}{\varepsilon}\right) \text{ for } \varepsilon^* \geq \varepsilon \geq \varepsilon_s \tag{2.23}$$

The above equation represents the evolution or r in terms of strain ε and material constants. For such an evolution and linear stress-strain response for the intact part, the overall response is as of Fig. 2.8(b).

The above simple example illustrates the effect of defects such as void and flaw growth in the overall response of a material under uniaxial loading conditions. It is important to note that although the intact (topical) response is non-softening, the overall response may exhibit strain softening.

The above example may not be suitable for real materials. For example, when geomaterials like rock or concrete are subjected to uniaxial loading conditions, tensile stresses normal to the loading axis are developed. Thus, although the overall response is that of uniaxial loading, the response at a local (micro) level is that of biaxial or triaxial loading. These aspects are discussed in detail in a subsequent chapter.

Theoretical models based on characterization of damage will be briefly discussed subsequently. The majority of the models consider uniaxial loading conditions. Loland (1980) has worked out a model based on the Kachanov-Rabotnov approach for the behavior of concrete under uniaxial tension. The model does not take into account the stress-concentrations ahead of crack tips, but merely assumes that defects are initially present and start propagating under loading. Damage accumulation is considered to be caused by tensile strains. A similar model was proposed by Mazavs (1981).

The damage models used for tensile loading are usually considered to be applicable for compressive loading too. Similarities between the tensile and compressive stress-strain curves were observed by Hughes and Chapman (1966) for concrete. Also, the experimentally observed damage-function by Spooner and Dougill (1975) shows similarities.

Betten (1983) constructs constitutive equations by employing the damage tensor of rank two and a fourth order tensor characterizing the initial anisotropy or the anisotropy of the material in its

undamaged state. The theory is an extension of the uniaxial theory for creep developed by Kachanov and Rabotnov. Problems of creep damage have been investigated by many authors, for instance, by Martin and Leckie (1972), Hayhurst and Leckie (1973), Parman and Mellor (1980). Hayhurst et al. (1975) employed the finite element method to show how stresses, within a tension plate containing a circular hole, redistribute due to creep deformation. Constitutive and damage laws accounted for the growth of internal defects (or damage) during creep deformation.

Krajcinovic and Fonseka (1981) and Fonseka and Krajcinovic (1981) focused on the establishment of the damage law consistent with the adopted physical interpretation of the damage. The general theory of thermodynamics was employed for the development of the model. In addition, the model incorporates a mathematical description of the damage growth kinematics. Further, Krajcinovic and Silva (1982) addressed several fundamental aspects of a link connecting the damage theory and the existing statistical strength theories.

Fanella and Krajcinovic (1985) developed a nonlinear analytical model based on principles of damage representation for the stress-strain behavior of fiber-reinforced concrete subjected to monotonic compressive and tensile loading. Under uniaxial conditions, an equilibrium equation derived from a parallel bar arrangement of the composite material, coupled with the damage laws of the composite and the fibers, formed the basis of this model

Suaris and Shah (1984) developed a theory for the quasi-static and dynamic behavior of brittle materials. A multiaxial generalization of the damage theory is achieved by treating the damage as an internal state variable which affects the free energy of the material. It is postulated that a free energy function dependent on the coupled invariants of strain and damage exists. The theory predicts a decrease in the nonlinearity of the stress-strain curve as the strain rate is increased.

The aspect of both degradation of strength and stiffness was adopted by Dougill (1976) and Dougill and Rida (1980) in a theory of progressively fracturing solids. Underlying the progressively fracturing theory is an energy dissipation function J which takes essentially the shape of the energy requirement curve for stable crack propagation, as shown in Fig. 2.9. It was suggested by Dougill and Rida (1980) that the dissipation function J should be determined from the results of physical experiments rather than by deducing J from theoretical considerations.

The progressively fracturing theory provides for elastic unloading and reloading, as shown in Fig. 2.10. A plastic fracturing variant of the progressively fracturing solid was proposed by Bazant and Kim (1979) in order to accommodate this shortcoming. Incremental plasticity and fracturing material theory are combined to obtain a nonlinear triaxial constitutive relation. The theory combines the plastic stress decrements with the fracturing stress decrements to account for strain softening and degradation of elastic moduli due to microcracking.

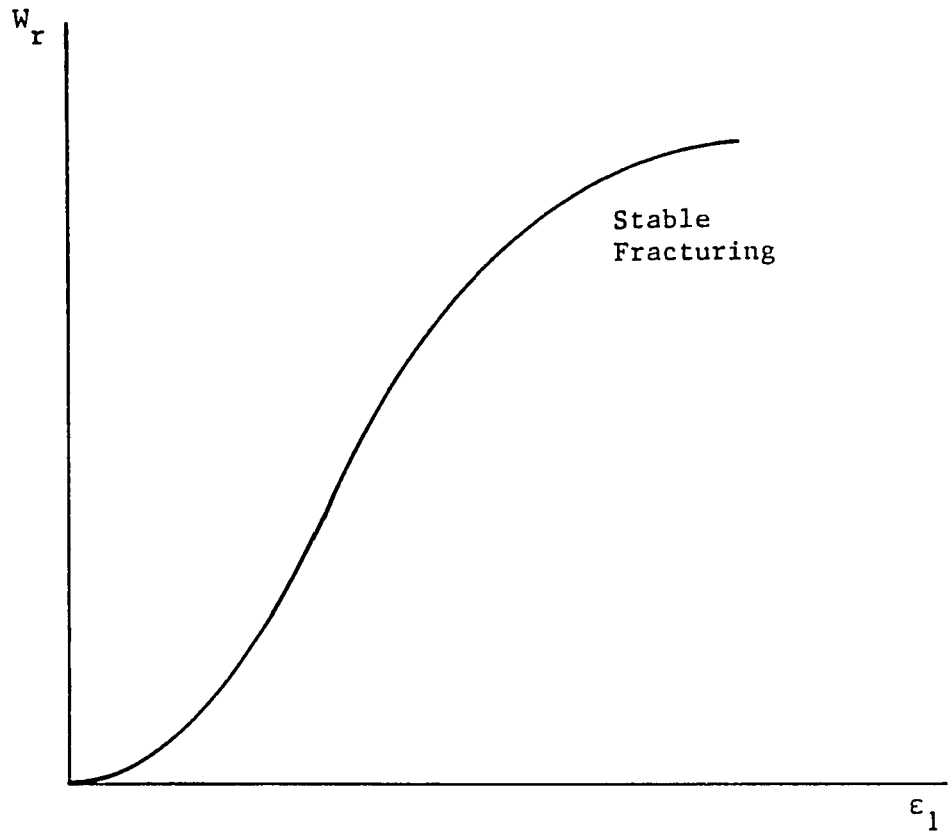

Fig. 2.9 Energy Requirement for Stable Crack Growth in Compression (After Van Mier, 1984)

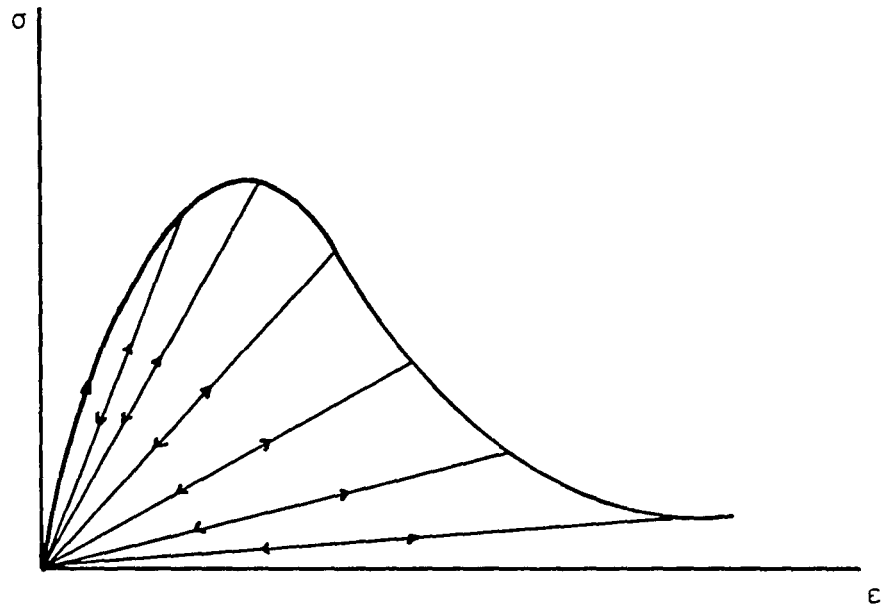

Fig. 2.10 Progressively Fracturing Solid
(After Dougill, 1976)

Further, work inequalities for stability of plastic strain increments and fracturing stress decrements are studied by Bazant (1980).

Similar results as those obtained with the theory of progressively fracturing solids may be obtained by adopting the self-consistent method of estimating the effective elastic properties of a cracked solid (Budiansky and O'Connell, 1976; O'Connell and Budiansky, 1974; Cleary, 1978; Cleary et al., 1980). The models predict the elastic properties of a material consisting of a homogeneous isotropic matrix in which flat elliptical cracks are dispersed. A crack-density parameter is defined which depends on the average size and number of microcracks. A solution for non-random crack distributions was reported by Hoenig (1978, 1979). Results were obtained for different cases of crack distribution.

Systems of periodically or randomly distributed inclusions have been considered by Nemat-Nasser and Taya (1981), Nemat-Nasser et al. (1981, 1982), and Horii and Nemat-Nasser (1983). These theories have characterized microcrack textures by controlling microcrack growth along selected directions. However, in order to obtain a "valid" representation of the process of damage, numerous such control directions need to be considered. Despite the strong theoretical appeal of this approach, the complexity of the analysis is such, particularly in three dimensions and in the presence of extended microcracking, that it is not yet clear how these theories may serve as a basis for devising material laws for concrete and rocks.

A second order tensorial representation has been used by Dragon and Mroz (1979). They defined damage as the dyadic product of the unit normal to the crack face and the displacement discontinuity at the crack surface. This formulation can account for crack growth in cleavage (Mode I) and slip (Mode II and III). In brittle materials such as rock and concrete, microcrack growth is assumed to result from tensile strains. Then, the microcracks can be defined by a vector oriented normal to the plane of the crack and having a magnitude equal to the surface area of the crack.

A rate independent model that considers concrete as a mixture of mortar and aggregates was considered by Ortiz (1985). Distributed damage was attributed to mortar and the application of mixture theories was employed for the composite nature of concrete. The model can account for elastic degradation, both in tension and compression.

A continuum model derived from the mechanics of tensile microcracking was presented by Costin and Holcomb (1983). The model employs the assumption that stress and time dependent microcrack growth are responsible for the inelastic deformation of brittle rock. The tensile part of the deviatoric stress tensor is considered as the cause of tensile microcracking. The resulting constitutive equations are essentially elastic, but account for behavior due to microcrack growth.

The models described above constitute only a part of the entire class of damage or other approach models. Research in this area is very active, especially in the area of concrete and rock mechanical behavior. Noteworthy related works are that of Barbee et al. (1972), Davison and

Stevens (1973), Shockey et al. (1974), Curran et al. (1977, 1983), Davison et al. (1977), Hart (1970), Whitman (1985), and Davis and Mroz (1985).

CHAPTER 3

PROPOSED MODEL INCLUDING STRAIN SOFTENING

3.1 General

As discussed previously, a basic hypothesis in constitutive modelling is the concept of a continuum in which stress, strain, density, etc., are assumed to be defined at every point in the continuum. Under this assumption, material properties can be determined from tests on finite size specimens undergoing homogeneous stress and strain. As the stress and strain deviate significantly from homogeneity, the observed behavior may no longer represent (continuum) material properties. Due to difficulties in identifying the influence of such nonhomogeneities, it is often ignored, and the observed load-deformation relations of finite sized specimens are "translated" as stress-strain relations. However, influence of the nonhomogeneity can be very important in interpreting certain type of behavior such as softening in geologic materials like rocks, concrete and soils. In Chapter 2 of this dissertation, it was pointed out that various limitations arise when strain softening is treated as a (continuum) material property with respect to solutions of boundary value and initial value problems. Also pointed out was the experimental evidence indicating that strain softening is not a true material property but rather the performance of a structure; e.g., a finite sized specimen in which the

individual components such as microcracks, joints and interfaces result in an overall loss of strength with progressive straining (Sandler, 1983); Brady et al., 1973; Drescher and Vardoulakis, 1982; Shah and Slate, 1965).

Clearly, development of a model that considers in detail all the structural changes such as microcrack propagation in concrete and rock-like materials is not easy. However, it is possible to model the average influence of the structural changes, and such an approach is followed in this paper. It is recognized that the total deformation in such materials is attributed to elastic deformation, plastic flow, and to formation of damage. The damage can be caused mainly due to pre-existing microfracture and microfracture planes that initiate and subsequently grow.

In the model proposed herein, behavior of an element (specimen) is decomposed in two parts. The first part, with volume V_t representing topical (continuum) behavior, is non-softening and obeys an elastoplastic constitutive law. In the second part, which refers to the damaged or fractured part with volume V_o, the behavior is such that its shear stiffness is assumed to be zero. At every finite material element the total volume is V; therefore, $V = V_t + V_o$. Details on this decomposition are given subsequently. It will be shown that the proposed model is relatively simple and that it can capture the essential features of the behavior of geomaterials undergoing general triaxial compressive

loading (Spooner and Dougill, 1975; Van Mier, 1984) such as: (1) strain softening under monotonic shear loading, (2) shear stiffness degradation under progressive loading, and (3) dilatant behavior under monotonic shear loading.

In terms of the decomposition and description of softening, the proposed model is similar to that proposed by Desai (1974). Also, the proposed model can be seen as being analogous to the uniaxial model proposed by Kachanov (1959) and Rabotnov (1969), described in Chapter 2. The distinguishing feature of the proposed model is that damage is represented through a second order tensor, which has a physical meaning. In order for such a multiaxial model to be rational, it should be capable of predicting damage induced anisotropy observed in brittle materials because microcracks follow preferred orientations. Here, it is appropriate to quote Drucker (1980) for his philosophic look ahead to the future when he emphasized importance of "renewed emphasis on failure and on response of heavily damaged structured and microstructures." The same author further concluded that "an almost limitless field of useful but difficult research lies ahead in the extension of the damage approach pioneered by Kachanov and Rabotnov."

3.2 Effect of Structural Changes

It is an experimental fact that microcrack propagation, microcrack initiation and joining of microcracks considerably affect the behavior of geomaterials. A crack may be defined as a discontinuity, of which the boundaries were in an initial parallel position when crack

formation occurs. Due to the inhomogeneity of the material at the microlevel, weak planes are developed leading to crack formation and subsequent propagation. For concrete, the microcracks are found to appear at the interface aggregate cement matrix and when loading is increased, the cracks tend to propagate along the aggregate surfaces (Shah and Chandra, 1970; Hsu et al., 1963). The bond between aggregate and cement matrix is, generally, considered as the "weakest link" in the concrete structure.

The laws that govern the above structural changes are not fully understood. A model should describe the structural changes effect in a qualitative manner. Following Van Mier (1984), we describe herein the effects of crack extension and crack joining in a qualitative manner. In the initial loading stage, fracture sites may be considered uniformly distributed. Qualitatively, the effect of an isolated fracture site is that a stress-relieved zone exists around it and a potential crack extension site at its edges, as shown schematically in Fig. 3.1. Under continued loading, stress-relieved zones increase (Fig. 3.1). Upon further increase in overall stress, isolated cracks join and finally continuous macrocracks are developed. At this stage, the volume of the stress-relieved zones is close to the total volume. In order to give a physical insight into the damage characterization defined subsequently, we note the volume of the stress-relieved zones as V_o and the total volume as V. Obviously, V_o increases during loading and at every stage $V_t = V - V_o$ where V_t is defined as the topical fraction of the total volume; the latter of the body is assumed to obey an elastic-plastic constitutive relation.

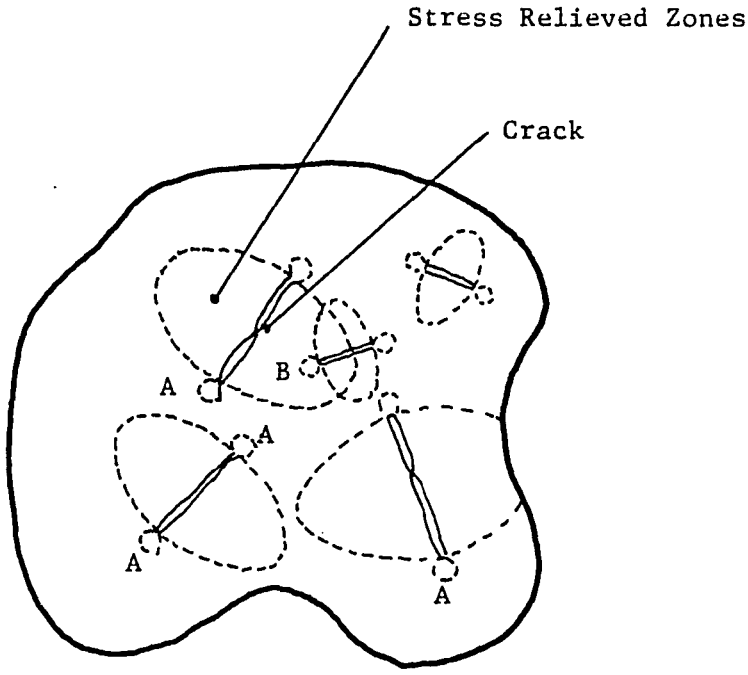

A - Potential Crack Extension Site
B - Unlikely Site for Crack Growth

Fig. 3.1 Schematic of Stress Relieved Zones and Crack Propagation Sites; (After Van Mier, 1984)

3.3 Basic Hypothesis

It was mentioned previously that in the proposed model the average material response is decomposed in two parts. Here, we describe this concept in more detail. It is assumed that topical material elements of volume V_t obey an elastoplastic constitutive relation (Fig. 3.2a) and the stress-relieved material elements of volume V_o, a law as depicted in Fig. 3.2b, as rigid, perfectly plastic with zero yield strength.

Let $r = V_o/V$, $(0 \leq r \leq 1)$ with the interpretation that before any load is applied, $r = 0$ and if under monotonic loading the residual stress level is reached, r reaches an ultimate value = r_u, which tends to 1. In this model, r is treated as continuum field variable over the entire body instead of at isolated parts of the body. Then for compatibility at the continuum level, strains in V_o should be equal to strains in V_t. Consequence of the decomposition is depicted in Fig. 3.3 where behavior corresponding to volumes V, V_t and V_o are schematically shown. The topical behavior for V_t, curve (b) in Fig. 3.3, plus the stress-relieved behavior for V_o, curve (c), result in the average behavior for the total volume V, curve (a). For monotonic loading, V_o continuously increases and V_t continuously decreases. By average behavior, we mean the gross behavior; for example, stress-strain results obtained from a (uniaxial) compression test, and it is typically represented by curve (a) in Fig. 3.3. We now explain the assumptions and approximations involved in the proposed model.

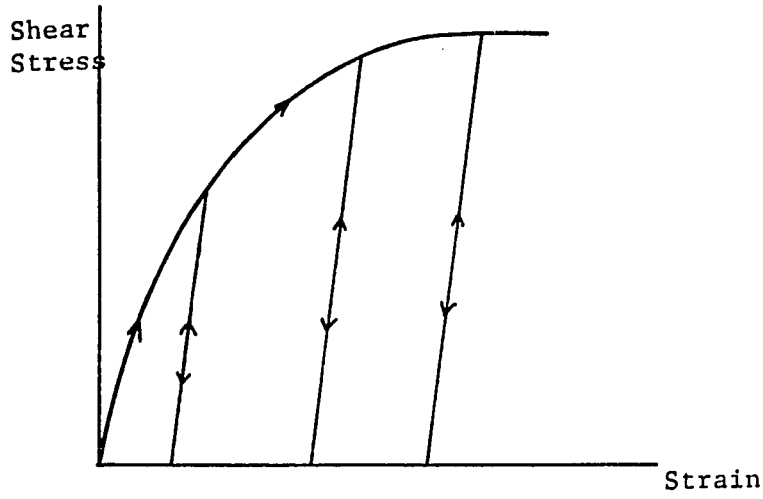

(a) Elastic-Plastic

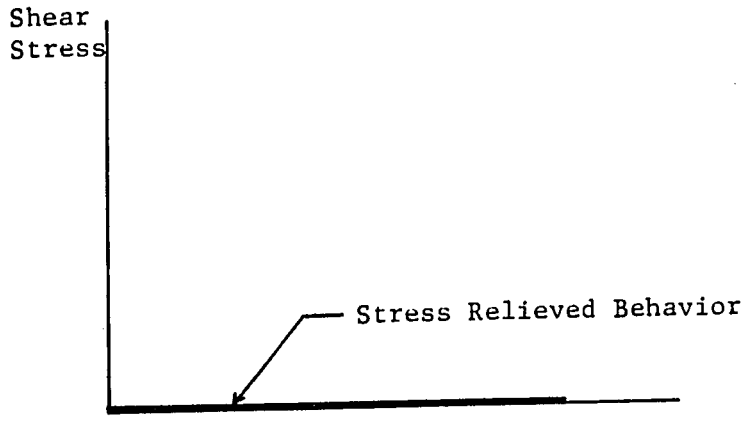

(b) Stress Relieved

Fig. 3.2 Components of Stress-Strain Response

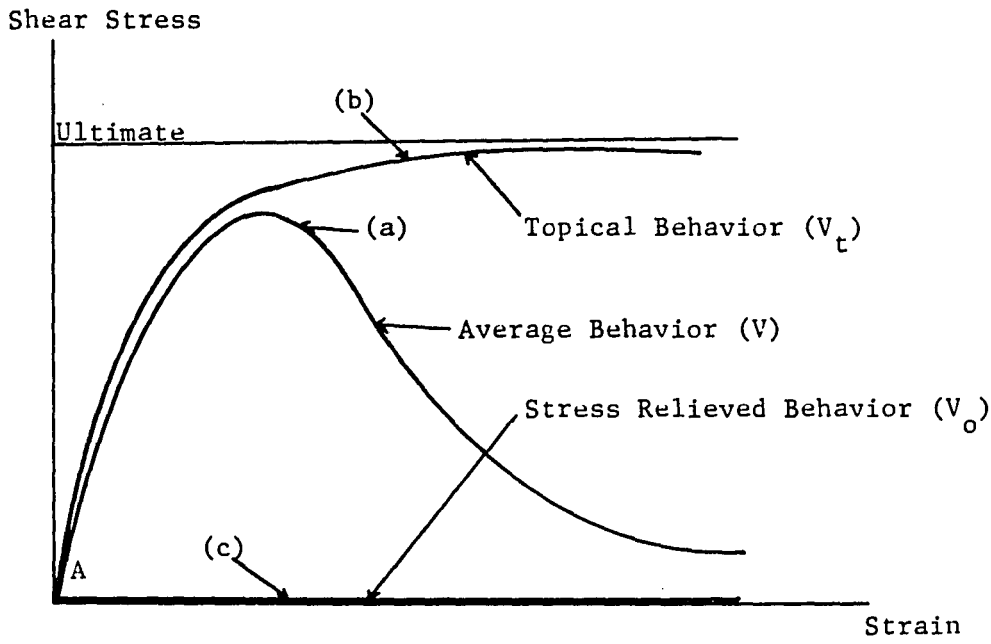

Fig. 3.3 Concept of Decomposition of Material Behavior

Let the topical stress tensor be denoted as σ^t_{ij} and the average stress tensor as σ_{ij}. From the above decomposition, and the fact that the strains in the decomposed volumes are equal, it is concluded that the average stress is related to the topical stress and the values of volumes V_o and V_t. The stress at the stress-relieved volume is not included in such a relation since it is zero (Fig. 3.3). In order to establish this relation, use of experimental observations is made. For hydrostatic compression loading, microcracks tend to close and thus no significant damage is recorded. This can imply that damage is caused from deviatoric components; thus, the topical and average stress lie on the same deviatoric plane, as shown in Fig. 3.4a. Now we consider a stress path such that, for example, two of the principal stresses of σ_{ij} are equal; that is, $\sigma_2 = \sigma_3$. Then the σ_{ij} tensor is positioned as shown in Fig. 3.4b. In this stress path, cylindrical symmetry exists and if the material is assumed as initially isotropic, this symmetry is maintained through the above stress path. Then this symmetry must be reflected in the topical stress tensor; thus, $\sigma^t_2 = \sigma^t_3$. Then the topical stress tensor σ^t_{ij} is positioned as shown in Fig. 3.4b. The above considerations let us come to the assumption that σ_{ij} and σ^t_{ij} lie on a line perpendicular to the hydrostatic axis, as shown in Fig. 3.4c. When there is no damage induced, $r = 0$ and $\sigma_{ij} = \sigma^t_{ij}$ or (AC) = (BC) in Fig. 3.4c. When the residual stress level is reached, damage is maximum and $r = r_u$. This implies that distance (AB) in Fig. 3.4c is small, representing the residual stress level. Based on these considerations, it is proposed that the distances (BC) and (AC) are connected through

(AB) = (AC) $(1-r)$,

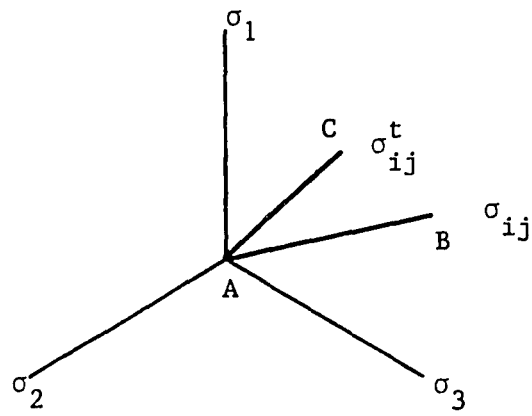

(a) In Deviatoric Plane ($\sigma^t_{kk} = \sigma_{kk}$)

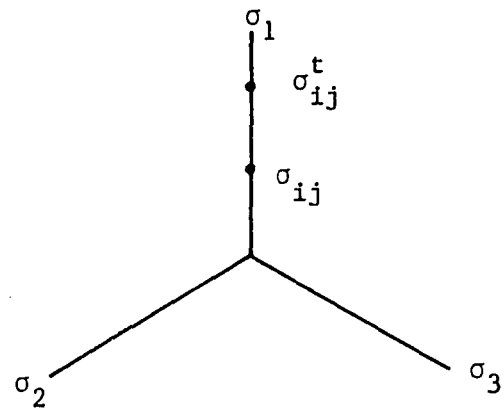

(b) In Deviatoric Plane ($\sigma_2 = \sigma_3$)

Fig. 3.4 Relative Position of σ^t_{ij} and σ_{ij}

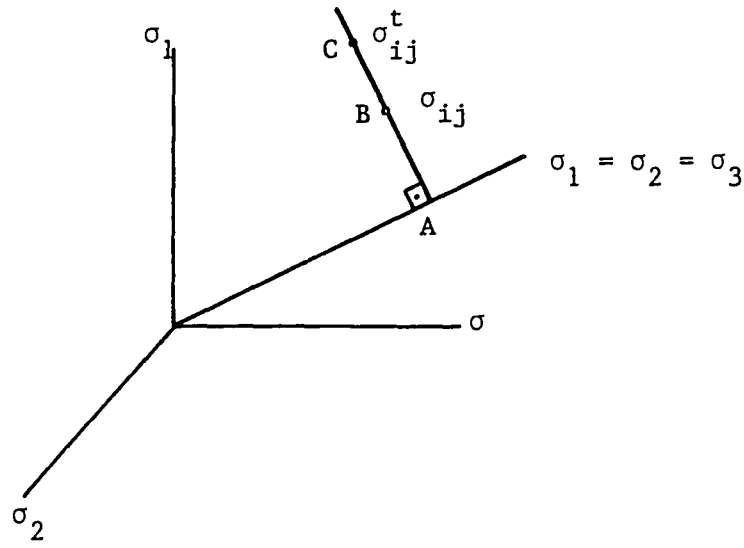

(c) In Principal Stress Space

Fig. 3.4 continued

$$\sqrt{J_{2D}} = \sqrt{J^t_{2D}}\ (1-r) \tag{3.1}$$

where $\sqrt{J_{2D}}$ is the stress intensity of σ_{ij} defined as $\sqrt{J_{2D}} = (\frac{1}{2} S_{ij} S_{ij})^{1/2}$ and S_{ij} is the deviatoric part of σ_{ij} such that $\sigma_{ij} = S_{ij} + \frac{1}{e} \sigma_{kk} \delta_{ij}$. Here summation notation is implied and δ_{ij} denotes the Kronecker delta. A similar definition holds for $\sqrt{J^t_{2D}}$. Through Eg. (3.1) and the fact that σ_{ij} and σ^t_{ij} lie on a line perpendicular to the hydrostatic axis, we obtain the tensorial equivalent of (3.1):

$$\sigma_{ij} = (1-r)\ \sigma^t_{ij} + \frac{r}{3} \sigma^t_{kk}\ \delta_{ij} \tag{3.2}$$

Relation (3.2) has the following desirable properties: (1) for r = 0, $\sigma_{ij} = \sigma^t_{ij}$, (2) when specialized to hydrostatic compression, it yields $\sigma_{kk} = \sigma^t_{kk}$ and (3) for $r = r_u \cong 1$, $S_{ij} = (1-r_u)\ S^t_{ij}$, and this implies that shear stresses are significantly reduced as happens at the residual stress level. It is shown subsequently that through relation (3.2) essential features of concrete or rock behavior can be modelled satisfactorily.

For tensile conditions, relation (3.2) is not valid since, for example, it would predict no damage progression for a hydrostatic tension stress path. It is our interpretation of experimental results that criteria for damage initiation and progression under tensile conditions are different than criteria for compressive states of stress. Thus, for tensile conditions, a relation between σ_{ij}, σ^t_{ij} and r can be assumed but such a relation would be different from Eq. (3.2).

As already mentioned, material behavior is decomposed in two parts. The topical part of the decomposed behavior obeys an elasto-plastic law given by

$$\dot{\sigma}^{t}_{ij} = C^{e-p}_{ijk\ell}\ \dot{\varepsilon}_{k\ell} \tag{3.3}$$

and for elastic unloading

$$\dot{\sigma}^{t}_{ij} = C^{e}_{ijk\ell}\ \dot{\varepsilon}_{k\ell} \tag{3.4}$$

Here, $\dot{\sigma}^{t}_{ij}$ denotes the time rate of the stress tensor σ^{t}_{ij}, $\dot{\varepsilon}_{k\ell}$ denotes time rate at the strain tensor, $C^{e-p}_{ijk\ell}$ is the elastoplastic constitutive tensor (Hill, 1950) involving a yield surface and hardening rule described subsequently, $C^{e}_{ijk\ell}$ is the elasticity tensor; elasticity in the present case is assumed linear and isotropic. The usual loading-unloading elastic-plastic criteria holds here (Hill, 1950).

3.3.1 Interacting Components

Total material behavior is assumed to consist of two components; namely, the topical and the damaged part. During the loading process, topical material is "transformed" to damaged one. The reason for such a transformation is that deformation is increasing. The above suggests use of the theory of mixtures or theory of interacting continua. In our case, the interacting components are the topical and damaged material. In order to define static and kinematic variables in the topical and damaged part, we consider an area element A, as shown in Fig. 3.5. The

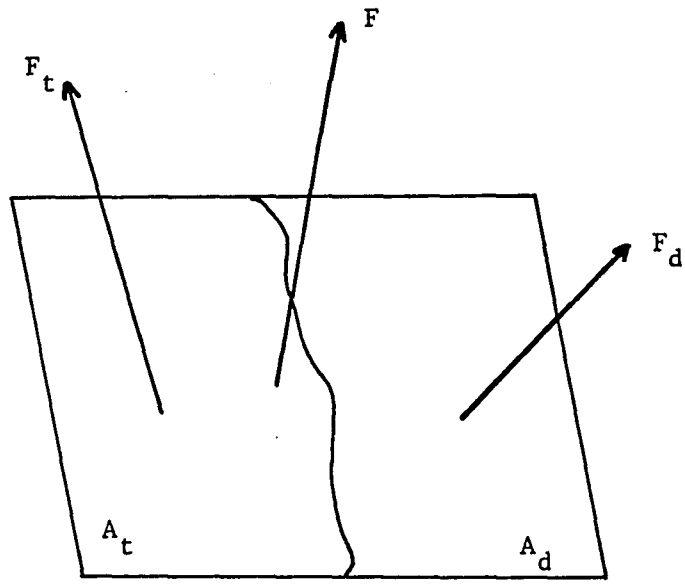

Fig. 3.5 Schematic of Component Areas and Forces

internal forces acting on A are $\underset{\sim}{F}^t$ acting on the total topical area A^t and $\underset{\sim}{F}^o$ acting on the total damaged area A^o. The total force is $\underset{\sim}{F}$ such that $\underset{\sim}{F} = \underset{\sim}{F}^t + \underset{\sim}{F}^o$, and it is acting on the total area A. The following stress tensors are defined. The topical stress tensor σ^t_{ij} such that $F^t_i = \sigma^t_{ij}\, n_j$ where n_j is the unit vector normal to the area A. Similarly, the damaged σ^o_{ij} and average σ_{ij} stress tensors are defined such that $F^o_i = \alpha^o_{ij}\, n_j$ and $F_i = \sigma_{ij}\, n_j$, respectively. Since $F_i = F^t_i + F^o_i$ and since from the definition of the damage variable r, $r = A^o/A$, it follows that

$$\sigma_{ij} = (1-r)\, \sigma^t_{ij} + r\, \sigma^o_{ij} \tag{3.5}$$

Relation (3.5) states that the average stress is the summation of the partial stresses defined on the two components (Green and Naghdi, 1965). It follows from the principle of angular momentum balance that the stress tensor σ_{ij} is symmetric (in the absence of body couples). This, however, does not necessarily imply that the stress σ^t_{ij} and σ^o_{ij} are symmetric. Although stress couples may be acting at the phases such couple stresses are applicable to some cases of fluid mixtures. For the present case herein, it is assumed that the stresses in the topical and damaged part are symmetric.

In the general theory of mixtures, factors such as diffusion between constituents, chemical reactions, etc., can be included (Bowen, 1969). The theory is considerably simplified if diffusion processes are

absent. Absence of diffusion implies that the strains in the two components are equal (Bowen, 1969). Thus, we can write

$$\varepsilon_{ij} = \varepsilon^{t}_{ij} = \varepsilon^{o}_{ij} \tag{3.6}$$

where ε_{ij} is the strain tensor, ε^{t}_{ij} and ε^{o}_{ij} are the strain tensors in the topical and damaged part, respectively.

As described subsequently, the damaged stress-strain response may be characterized as rigid perfectly plastic with the yield strength in shear reduced to zero. It is inherent of rigid perfectly plastic behavior that the strains are not uniquely determined when the stresses are specified (Hill, 1950). Thus, when the material behavior of a body or substance is rigid perfectly plastic the boundary conditions are to be employed for determination of the strain field from the stress field. In the case of the two-component material thought, Eq. (3.6) imposes an important restriction. It provides a condition such that the indeterminancy involved in the rigid perfectly plastic part is overcome. Thus, the topical part imposes restrictions in the deformation of the damaged part and vice versa.

Although the shear stress of the damaged part is assumed to be zero, this is not the case for the hydrostatic stress. In the present formulation, it is assumed that during the damage process a redistribution of shear stresses occurs, but the confining pressures remained unchanged in the two components. It follows from this assumption that Eq. (3.5) reduces to

$$\sigma_{ij} = (1-r)\ \sigma^{t}_{ij} + \frac{r}{3}\ \delta_{ij}\ \sigma^{t}_{kk} \tag{3.7}$$

which is identical to Eq. (3.2).

3.4 Degradation of Elastic Shear Modulus

Consider a loading stress path such that plastic deformation as well as damage have been induced. Then, $0 < r < r_u$. It is assumed here that no damage is induced under unloading. Then for unloading, $\dot{r} = 0$ and from Eq. (3.2) or (3.7), we have

$$\dot{\sigma}_{ij} = (1-r)\ \dot{\sigma}^{t}_{ij} + \frac{r}{3}\ \delta_{ij}\ \dot{\sigma}^{t}_{kk} \tag{3.8}$$

Since unloading is elastic, Eq. (3.4) holds and from Eqs. (3.4) and (3.8), we obtain

$$\dot{\sigma}_{ij} = (1-r)\ (2\mu\ \dot{\varepsilon}_{ij} + \lambda\ \dot{\varepsilon}_{kk}\ \delta_{ij}) + \frac{r}{3}\ (2\mu + 3\lambda)\ \varepsilon_{kk}\ \delta_{ij} \tag{3.9}$$

where λ, μ are the Lame's constants.

Specializing Eq. (3.7), we have

$$\dot{\sigma}_{12} = 2\mu\ (1-r)\ \dot{\varepsilon}_{12} \tag{3.10}$$

Equation (3.10) implies that unloading shear modulus depends on r where r = constant for unloading, and since r increases with loading, shear modulus degrades, as shown schematically in Fig. 3.6. This fact is well documented experimentally; e.g., Spooner and Dougill (1975), Van Mier

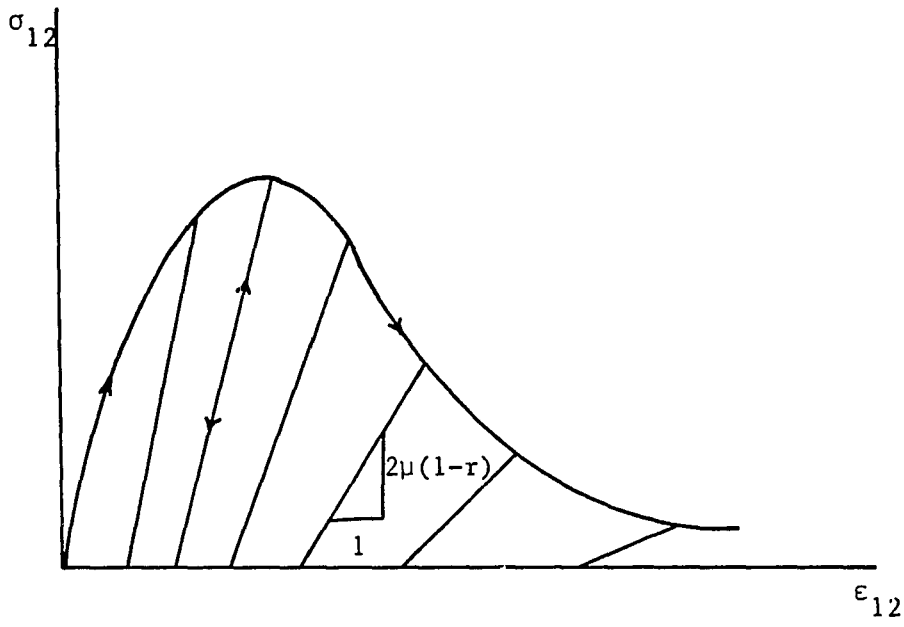

Fig. 3.6 Degradation of Elastic Shear Modulus

(1984), Wawersik and Fairhurst (1970). Theoretically, this is treated as a result of brittle-plastic behavior (Bazant and Kim, 1979; Dragon and Mroz, 1979) or as an elastic-plastic coupling problem (Hueckel, 1975; Maier, 1977; Dafalias, 1984; Young et al., 1985). It is also noted that when Eq. (3.9) is specialized for hydrostatic compression, we obtain

$$\dot{\sigma}_{kk} = (2\mu + 3\lambda)\ \dot{\varepsilon}_{kk} \tag{3.11}$$

and thus the bulk modulus is independent of r (constant). The degradation of shear modulus is further discussed and illustrated in a subsequent chapter where applications of the model are considered.

3.5 Induced Anisotropy

Here anisotropy in the stress-strain response of the material is considered. Let us consider a stress-strain relation of the form

$$f\ (\underset{\sim}{\sigma},\ \underset{\sim}{\varepsilon}) = 0 \tag{3.12}$$

where $\underset{\sim}{\sigma}$ and $\underset{\sim}{\varepsilon}$ denote the stress and strain tensors, respectively, and, in general, $\underset{\sim}{C}_i$ (i = 1, n) are tensors representing material properties involved in the stress-strain relation (3.12). In general, the tensors $\underset{\sim}{C}_i$ can be tensors of any order; e.g., 4th order, 2nd order, etc. In order that the stress-strain relation, Eq. (3.12), is isotropic, it is necessary and sufficient that

$$f\ (\underset{\sim}{\sigma}',\ \underset{\sim}{\varepsilon}') = 0 \tag{3.13}$$

$$(S^t_{ij})^{\cdot} \neq S^t_{ij} \tag{3.19}$$

This shows that the tensor $\dot{r}\, S^t_{ij}$ yields induced anisotropy in the macroscopic stress-strain relation.

Obviously, Eq. (3.17) does not hold for unloading where Eqs. (3.8) and (3.4) hold. This means that unloading is isotropic and loading anisotropic, and this is an assumed simplification of the reality.

3.6 Evolution of Damage

In the previous formulation, a variable, r, was introduced. Now we define an evolution law for r in order that the formulation is complete. We exclude the possibility of r being dependent on stress since r would be affected under unloading and this contradicts our initial assumption and experimental fact that no damage accumulation occurs during unloading. For the same reason, elastic strains are excluded. Then, generally, we can write

$$r = f\ (\varepsilon^p_{ij}) \tag{3.20}$$

where superscript p denoted plastic. Since no damage is accumulated for (initial) hydrostatic compression, volumetric plastic strains are excluded; thus, in general

$$r = f\ (e^p_{ij}) \tag{3.21}$$

and $e^p_{ij} = \varepsilon^p_{ij} - \frac{1}{3}\varepsilon^p_{kk}\,\delta_{ij}$. In order to include effects of history of deviatoric plastic strains, we write

$$r = f\,(\xi_D) \tag{3.21}$$

where

$$\dot{\xi}_D = (\dot{e}^p_{ij}\ \dot{e}^p_{ij})^{1/2} \tag{3.22}$$

In accordance with experiments (Van Mier, 1984) for low stress levels, no significant damage is induced. Thus, for continuity of the stress-strain curve at point A in Fig. 3.3, the slope of the r versus ξ_D curve at the origin should be zero (Fig. 3.7). Also, when residual stress level is reached, $r = r_u$ where $0 < r_u \leq 1$. Here we propose that r_u is reached asymptotically, as shown in Fig. 3.7. We note that the shape of the damage evolution curve in Fig. 3.7 is similar in shape to the energy dissipation curve shown in Fig. 2.9 (Spooner and Dougill, 1975).

The following function is proposed to define r:

$$r = r_u - r_u \exp\,(-\kappa\,\xi_D^R) \tag{3.23}$$

where r_u, κ and R are damage-related material constants.

The best way to determine the damage evolution parameters would be experimental techniques (such as X-ray and radiographic methods) in which the actual effects of crack propagation are measured. Since such

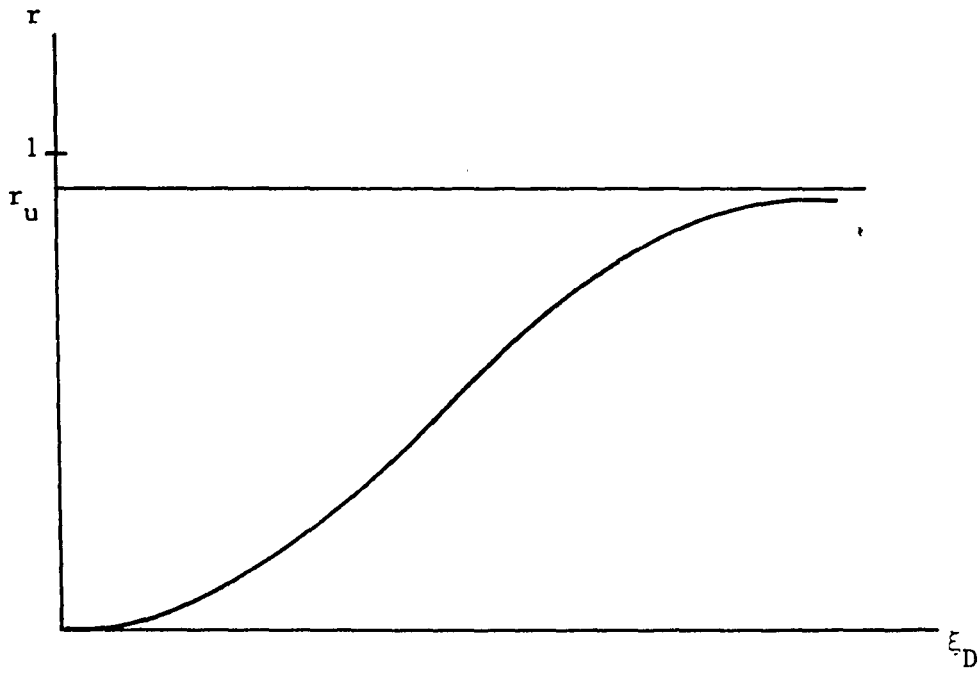

Fig. 3.7 Damage Evolution Law

techniques are not areadily available, parameters are indirectly evaluated from the observed stress-strain relations. An algorithm has been developed for this purpose and it is presented in Chapter 5 of this study.

CHAPTER 4

ELASTOPLASTIC MODEL FOR TOPICAL BEHAVIOR

Elastoplasticity theory is employed for the description of the stress-strain behavior of the topical part. In general, the theory of plasticity describes the rate independent, nonlinear, inealstic response of materials. In this chapter, details of the derivation of the elastic-plastic relations for the topical part are given.

4.1 Representation of the Yield Function and Plastic Potential

A procedure for finding appropriate yield and potential functions based on polynomial expansion in terms of the direct invariants (J_1, $J_2^{1/2}$, $J_3^{1/3}$) of the stress tensor was proposed by Desai (1980). It was shown subsequently (Baker and Desai, 1984; Desai and Faruque, 1983) that this procedure can be considered a special case of the concepts based on form invariance proposed previously (Rivlin and Ericksen, 1955; Green and Naghdi, 1965). Accordingly, the plastic potential function, Q, and the yield function, F, are expressed by using the same functional forms (Desai et al., 1985a; Desai et al., 1985b; Frantziskonis et al., 1986)

$$F = F\ (J_i^t,\ I_i^p,\ K_j,\ a_m) \tag{4.1}$$

points corresponding to asymptotic stress to stress-strain curves for different stress paths. For materials like concrete and rock, the yield surface may change shape during deformation; this can be incorporated by treating β as a function of J_1 (Salami, 1986). α is chosen as growth or hardening function of internal variables such as plastic strain trajectory

$$\xi = \int (\dot{\varepsilon}^p_{ij} \; \dot{\varepsilon}^p_{ij})^{1/2} \tag{4.5}$$

Details of definitions, determination and physical meaning of the constants are given later.

Typical plots of $F = 0$ in various stress spaces for a concrete (described later) are shown in Fig. 4.1. In order to allow for cohesive and tensile strengths, the origin, Fig. 4.1, is shifted along the negative J_1-axis by an amount $T = b\, P_a$ where b is dimensionless and P_a = atmospheric pressure (Salami, 1986; Desai and Salami, 1986).

The component function F_b in Eq. (4.3) represents continuous surfaces in the $J_1 - \sqrt{J^t_{2D}}$ space. For $S_r = 0$, the octahedral plane cross sections are circular. Here n acts as the shape parameter. If $n = 1$, the surface in $J^t_1 - \sqrt{J^t_{2D}}$ space is elliptical. The function F_s is termed as the shape function and modifies the circular shape in the principal stress space, Fig. 4.1c, to shapes appropriate for a given material (the topical behavior herein); here constants β and m define the shape. Thus, the function in Eq. (4.3) contains, as special cases, many of the yield functions proposed previously such as von Mises, Drucker-Prager,

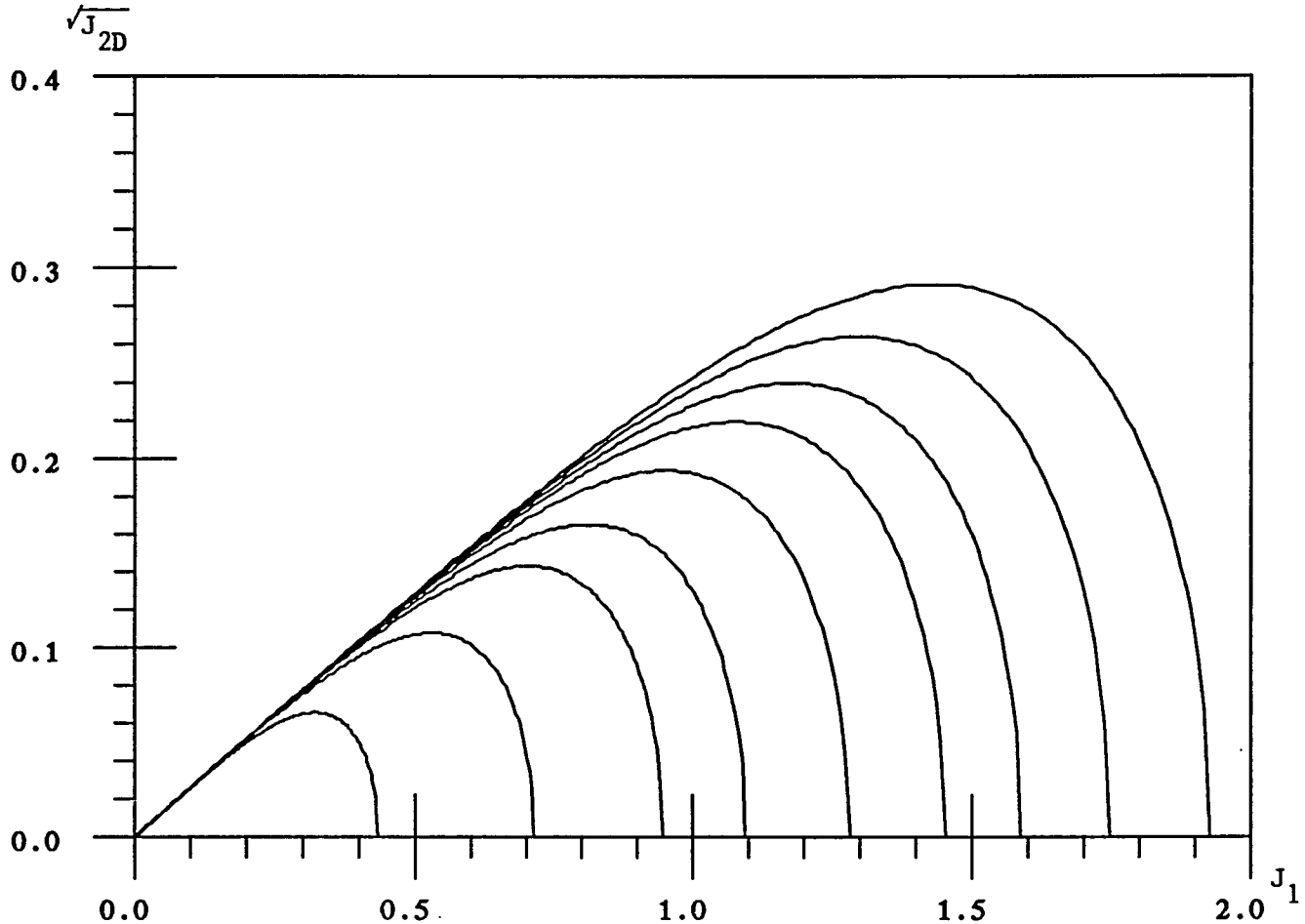

Fig. 4.1a Plots of f = 0 in $J_1 - \sqrt{J_{2D}}$ State (Concrete)

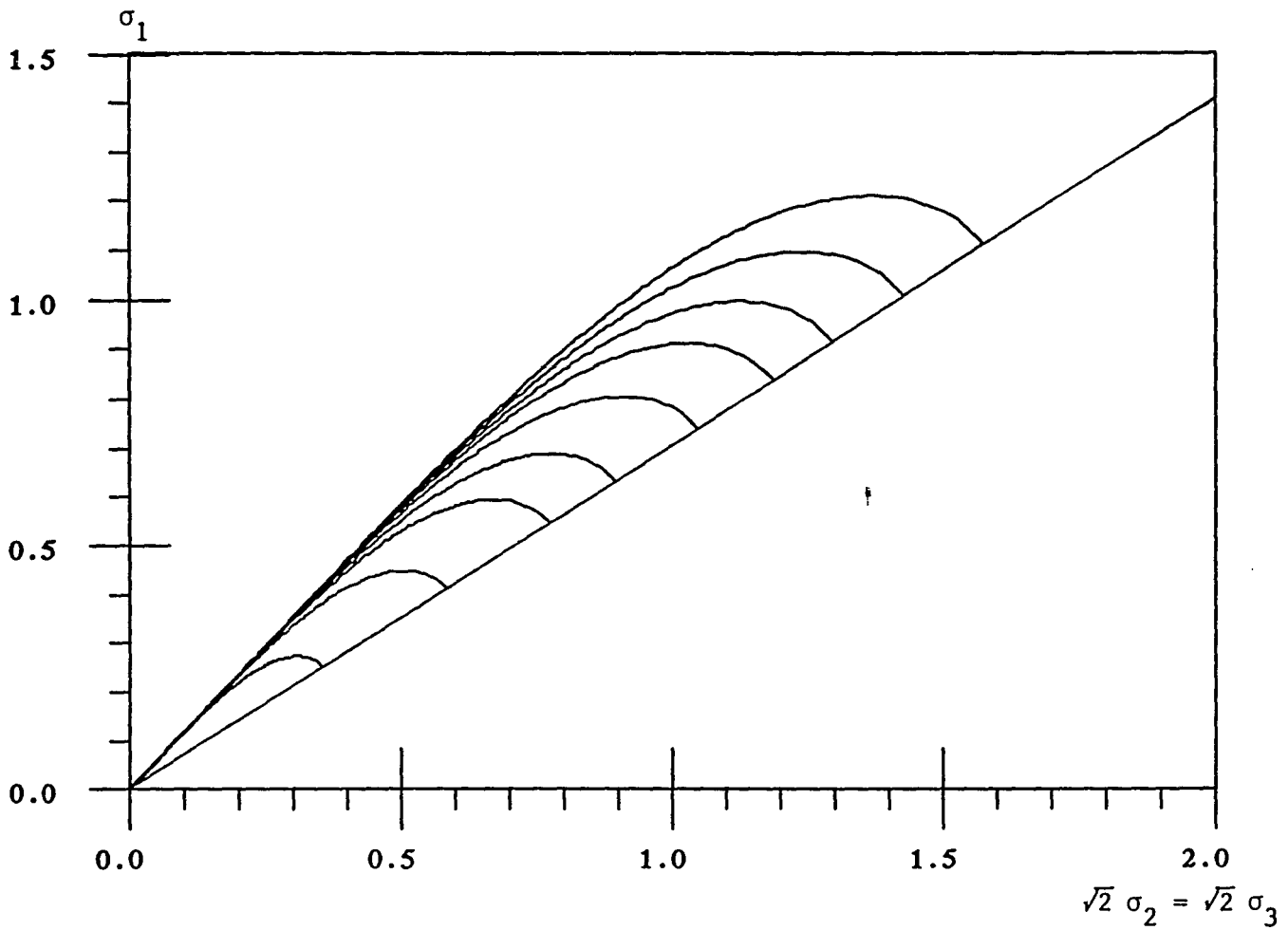

Fig. 4.1b Plots of f = 0 in Triaxial Plane (Concrete)

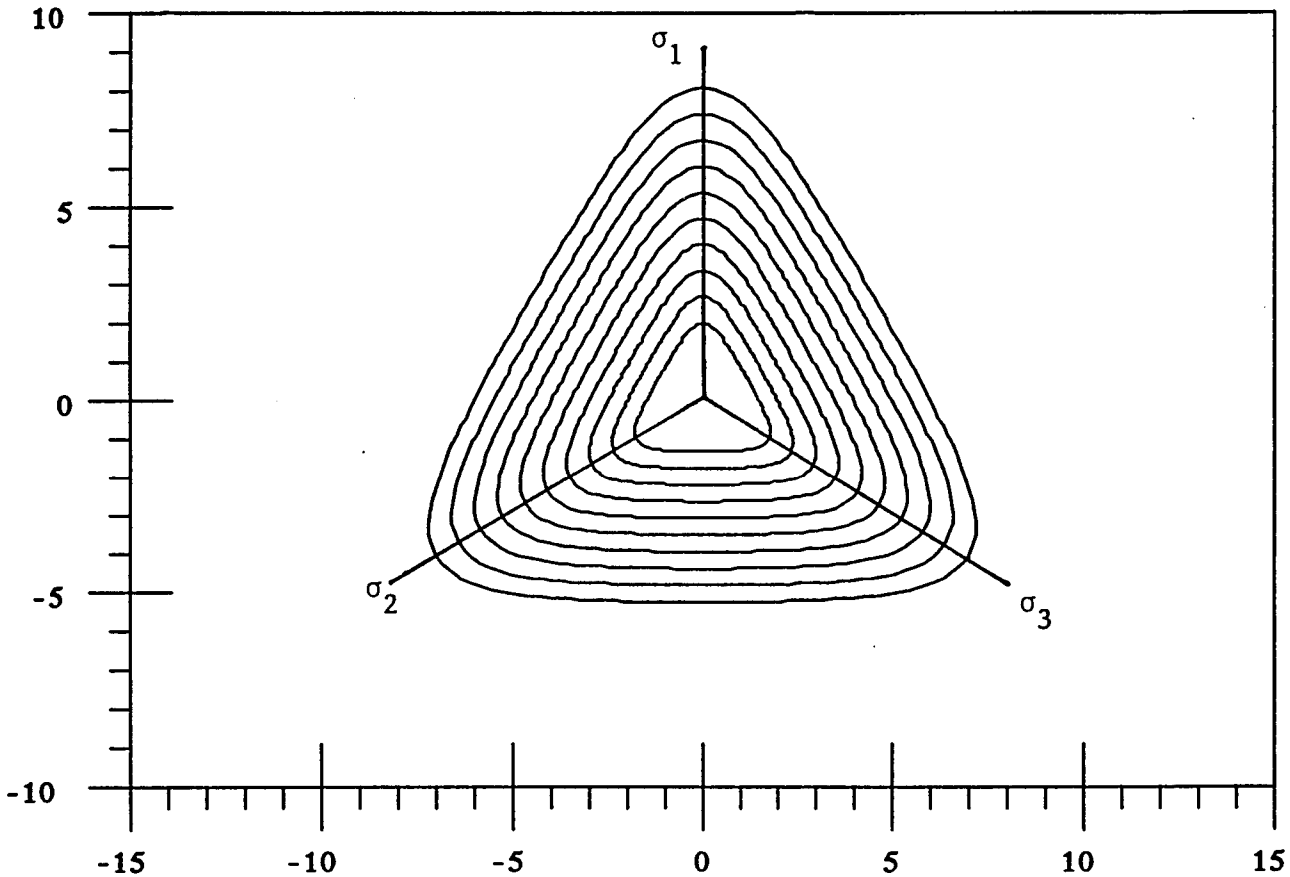

Fig. 4.1c Plots of F = 0 in Triaxial Plane

critical state (Schofield and Wroth, 1968), cap (DiMaggio and Sandler, 1971), Mroz et al. (1978), Wilde (1977), Van Eakelen (1980), Lade (1977), Vermeer (1978) and Matsuoka and Nakai (1974). A significant simplification of the proposed model is that it involves only a single continuous function for the entire range of the deformation history.

The response function α is chosen as growth function given by

$$\alpha = \alpha\ (\xi,\ \xi_v,\ \xi_D,\ r_v,\ r_D) \tag{4.6}$$

where ξ_v and ξ_D are the volumetric and deviatoric parts of ξ, respectively, and r_v and $r_D = \xi_v/\xi$ and ξ_D/ξ, respectively. A simple form of α is given by

$$\alpha = \frac{a_1}{\xi^{\eta_1}} \tag{4.7}$$

where a_1 and η_1 are two material constants for the hardening behavior of the topical part. If it is necessary, particularly if the influence of hydrostatic and proportional loadings is significant, it may be appropriate to express α as (Hashmi, 1986)

$$\alpha = b_1\ e^{-b_2\ \xi\ (1-A)} \tag{4.8}$$

where A and b_i (i = 1, 2) are hardening constants. Other forms of the growth function are possible and they are discussed by Desai and Faruque (1984a, b), Faruque and Desai (1985). For the topical response

of a number of materials, the simple form, Eq. (4.7), is found to provide satisfactory results; hence, it is discussed in detail herein.

The simplest model for the topical behavior of geomaterials results when the normal at a stress point to both Q and F coincide (Fig. 4.2). In this case, F ≡ Q, and only F is used as the yield function and plastic potential.

When the normals to Q and F do not coincide, Fig. 4.3, the nonassociative model is applicable. A concept in which the yield function F is corrected, constrained or controlled to a function $\overline{F}$ was proposed by Desai and Siriwardane (1980) and Desai and Faruque (1984). Accordingly, $\overline{F}$ can be expressed as

$$\overline{F} = F + h\ (J_i,\ \xi) \tag{4.9}$$

where h (J_i, ξ) is a correction function of the stress invariants J_i (i = 1, 2, 3) and ξ. This can lead to nonassociative flow rule where the plastic potential Q is given by $\overline{F}$. A simple approach is such that the plastic potential Q is obtained by correcting the growth function α in the yield surface F during plastic straining. Thus, Q is written as

$$Q = J_{2D}^t - (-\alpha_Q\ J_1^{t^n} + \gamma\ J_1^{t^2})\ F_s \tag{4.10}$$

Here the growth function α in Eq. (4.3) is replaced by α_Q and the two are related as follows (Frantziskonis et al., 1986):

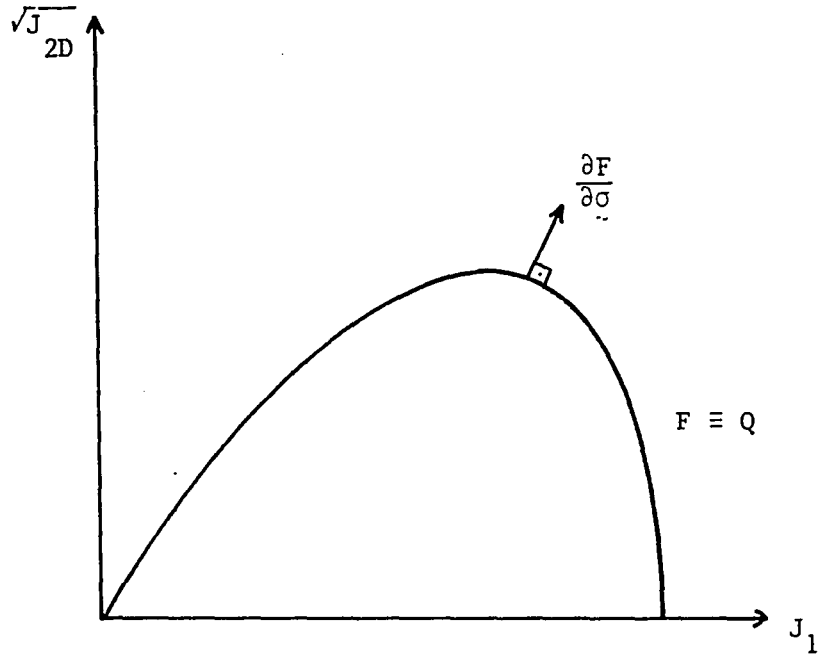

Fig. 4.2 Associative Behavior

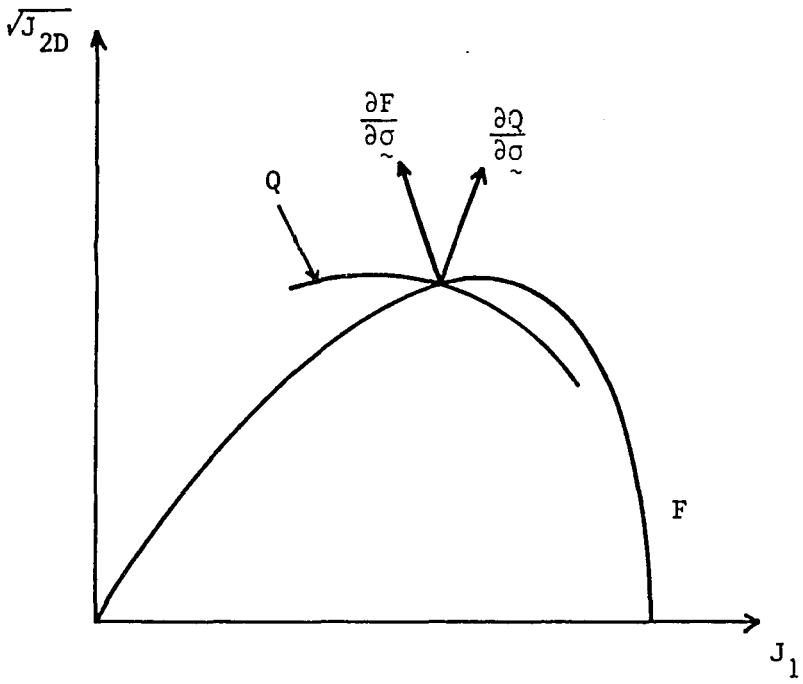

Fig. 4.3 Nonassociative Behavior

$$\alpha_Q = \alpha + k\ (\alpha_I - \alpha)\ (1-r_v) \tag{4.11}$$

where k is a material constand and α_I is the value of α at the initiation of nonassociativeness. If there is initial hydrostatic compression on an initially isotropic material, initiation of nonassociativeness may be assumed to occur after the hydrostatic compression, If not, α_I corresponds to the value of α at the initial yield surface demarcating the limit of the elastic zone. It is noted that for isotropic materials under hydrostatic compression, $r_v = 1$ and Eq. (4.11) yields $\alpha_Q = \alpha$. That is, nonassociativeness does not occur due to hydrostatic compression of an isotropic material. For $k = 0$, $\alpha_Q = \alpha$, from which it is observed that the associative model is a special case of the nonassociative one. The nonassociative model involves only one extra parameter; namely, k. The foregoing procedure for nonassociativeness constrains or controls the growth function involved in the yield surface. In most geomaterials, the associative flow rule usually overpredicts the volume changes as compared to the observed behavior. The nonassociative flow rule corrects that overprediction (Frantziskonis et al., 1986).

4.2 Elastoplastic Constitutive Relations

In this section, details of the derivation of the elastic-plastic relation for the topical part are given. The yield function and plastic potential involved were described previously. In general, we can write the incremental (rate) constitutive relation for the topical part as

$$\dot{\sigma}^{t}_{ij} = C^{e-p}_{ijk\ell}\ \dot{\varepsilon}_{k\ell} \tag{4.12}$$

In the above relation, $C^{e-p}_{ijk\ell}$ is termed as the elastoplastic constitutive tensor. In order to derive the expression for this tensor, the relations of elastic-plastic theory are used (Hill, 1950).

$$\dot{\varepsilon}_{ij} = \dot{\varepsilon}^{e}_{ij} + \dot{\varepsilon}^{p}_{ij} \tag{4.13}$$

that is, strain rate (increment) are decomposed into elastic $\dot{\varepsilon}^{e}_{ij}$ and plastic $\dot{\varepsilon}^{p}_{ij}$. Also,

$$\dot{\varepsilon}^{p}_{ij} = k\ \lambda\ \frac{\partial Q}{\partial \sigma^{t}_{ij}} \tag{4.14}$$

known as the flow rule such that

$$k = \begin{cases} 1 \text{ if } F = 0 \text{ and } \dfrac{\partial F}{\partial \sigma^{t}_{k\ell}}\ \dot{\sigma}^{t}_{k\ell} > 0 \\ \\ 0 \text{ otherwise} \end{cases} \tag{4.15}$$

For a hardening material (topical part) $\lambda \geq 0$ and in the present theory the topical behavior is hardening (non-softening); thus, always $\lambda \geq 0$. The elastic strain increments (rates) are related to stress rates

$$\dot{\sigma}^{t}_{ij} = C^{e}_{ijk\ell}\ \dot{\varepsilon}_{k\ell} \tag{4.16}$$

where $C^e_{ijk\ell}$ is the elasticity constitutive tensor. In the present case, elasticity is assumed linear and isotropic; thus,

$$C^e_{ijk\ell} = \frac{1}{2G}\,\delta_{ik}\,\delta_{\ell i} - \frac{K}{2G\,(2G + 3K)}\,\delta_{k\ell}\,\delta_{ij} \tag{4.17}$$

where G, K denote the initial elastic shear and bulk moduli, respectively. From Eqs. (4.13) and (4.16), we obtain

$$\dot{\sigma}^t_{ij} = C^e_{ijk\ell}\,(\dot{\varepsilon}_{k\ell} - \dot{\varepsilon}^p_{k\ell}) \tag{4.18}$$

From the definition of the plastic strain trajectory ξ, we obtain

$$\dot{\xi} = (\dot{\varepsilon}^p_{k\ell}\,\dot{\varepsilon}^p_{k\ell})^{1/2} \tag{4.19}$$

It follows from the flow rule, Eqs. (4.14) and (4.19), that

$$\dot{\xi} = \lambda\,\left(\frac{\partial Q}{\partial \sigma^t_{k\ell}}\,\frac{\partial Q}{\partial \sigma^t_{k\ell}}\right)^{1/2} \tag{4.20}$$

The consistency condition for the yield function F is expressed as

$$\dot{F} = \frac{\partial F}{\partial \sigma^t_{k\ell}}\,\dot{\sigma}^t_{k\ell} + \frac{\partial F}{\partial \xi}\,\dot{\xi} = 0 \tag{4.21}$$

Substituting Eqs. (4.18) and (4.19) into Eq. (4.21), we obtain

$$\lambda \left[\frac{\partial F}{\partial \sigma^t_{ij}} C^e_{ijk\ell} \frac{\partial Q}{\partial \sigma^t_{k\ell}} - \frac{\partial F}{\partial \xi} \left(\frac{\partial Q}{\partial \sigma^t_{k\ell}} \frac{\partial Q}{\partial \sigma^t_{k\ell}}\right)^{1/2}\right] = \frac{\partial F}{\partial \sigma^t_{k\ell}} C^e_{ijk\ell} \dot{\varepsilon}_{k\ell} \tag{4.22}$$

The above equation can be solved for λ so that Eqs. (4.14), (4.18) and (4.22) yield

$$\dot{\sigma}^t_{ij} = \left[C^e_{ijk\ell} - \frac{C^e_{ijpq} \frac{\partial Q}{\partial \sigma^t_{pq}} \frac{\partial F}{\partial \sigma^t_{mn}} C^e_{mnk\ell}}{\frac{\partial F}{\partial \sigma^t_{uv}} C^e_{uvrs} \frac{\partial Q}{\partial \sigma^t_{rs}} - \frac{\partial}{\partial \xi} \left(\frac{\partial Q}{\partial \sigma^t_{k\ell}} \frac{\partial Q}{\partial \sigma^t_{k\ell}}\right)^{1/2}}\right] \dot{\varepsilon}_{k\ell} \tag{4.23}$$

The above relation is the final elastoplastic relation for the topical part.

CHAPTER 5

DETERMINATION OF MATERIAL CONSTANTS

The proposed constitutive model involves a number of material constants. Determination of such constants for any material requires a comprehensive series of laboratory tests. Material constants are categorized as damage-related, plasticity-related and elasticity-related. Two different materials are considered here to obtain the material constants associated with the proposed constitutive model. They are: (i) a concrete, and (ii) a soil (sand). The test data for concrete are adopted from Van Mier (1984) and for the soil from Lee and Seed (1967) and Lade (1977). Details of the materials and devices used by Van Mier and Lee and Seed are given in a subsequent chapter.

5.1 Procedure

Each category of constants is considered here. As mentioned previously, elasticity, in the present formulation, is assumed as linear and isotropic; thus, for the elastic constants, we have

1. Elasticity constants:

   G, K or E, ν

   The plasticity constants involved are ultimate related and hardening related. The ultimate constants define the ultimate yield envelope in stress space while the hardening constants are involved in the growth function, thus

2. Plasticity constants:

   2.1 Ultimate:

   γ, β, m

   2.2 Hardening:

   a_1, n_1

   Finally, damage-related constants are involved in the model. These constants appear in the evolution law for the damage parameter r, Eq. (3.23).

3. Damage constants:

   r_u, κ, R

   The above constants are sufficient for the model. Note that if the nonassociative flow rule is to be used, one extra parameter; namely, κ, is needed. If the associative flow rule holds. the total number of parameters is nine; if the nonassociative flow rule is used, the total number of parameters is ten. In this study, only the associative flow rule is employed.

5.2 Damage Constants

The best way to determine the damage constants would be experimental techniques (such as X-ray and radiographic methods) in which the actual effects of crack propagation are measured. Since such techniques are not readily available, parameters are evaluated indirectly from the observed stress-strain behavior. Parameter r_u is determined from shear tests, and it is directly related to the ratio of $\sqrt{J_{2D}}$ at the residual stress level divided by the value of $\sqrt{J_{2D}}$ at the peak. Given a stress-strain curve, at the residual stress level, we have

$$1 - r_u = \frac{(\sqrt{J_{2D}})_{res}}{(\sqrt{J_{2D}})_{ult}} \tag{5.1}$$

which is the same as relation (3.1) and the subscript "res" indicates ultimate conditions. The ultimate condition is close to the peak and represents the asymptotic value to the extension of the prepeak curve. Thus,

$$r_u \cong 1 - \frac{(\sqrt{J_{2D}})_{res}}{(\sqrt{J_{2D}})_{peak}} \tag{5.2}$$

Relation (5.2) is used to find the value of r_u. When more than one test is available, the value of r_u is obtained from each test and then a weighted average value for r_u is calculated. After the value of r_u is known, constants κ and R are determined from back analysis of Eq. (3.1). The value of r at each point in the available stress-strain curve is given by

$$r \cong 1 - \frac{\sqrt{J_{2D}}}{(\sqrt{J_{2D}})_{peak}} \tag{5.3}$$

where J_{2D} corresponds to the point under consideration. At every point, the value of $\Delta\xi_D$ is calculated using the incremental deviatoric, principal plastic strains, Δe_i^p (i = 1, 2, 3) where

$$\Delta\xi_D = \{(\Delta e_1)^2 + (\Delta e_2)^2 + (\Delta e_3)^2\}^{1/2} \tag{5.4}$$

The total value of ξ_D at each point is calculated as

$$\xi_D^{\dot{J}} = \sum_{i=1}^{\dot{J}} \Delta\xi_D^i \tag{5.5}$$

where $\xi_D^{\dot{J}}$ is the value of ξ_D at the $\dot{J}$th point on the stress-strain curve. Note that for calculation of $\Delta\xi_D^i$, the values of plastic strains at point i are required. In the experiment though, only the total strains are measured; thus, plastic strains can not be evaluated directly. If unloading curves are given then, since unloading is assumed elastic, the elastic strains can be calculated at each point. Then the plastic strains are calculated from the known total strain and elastic strains ($\varepsilon_{ij}^p = \varepsilon_{ij} - \varepsilon_{ij}^e$). With the values of ξ_D and r known at every point on a stress-strain curve, Eq. (3.23) can be written as

$$\exp\ (-\kappa\ \xi_D^R) = \frac{r_u - r}{r_u} \tag{5.5}$$

$$-\kappa\ \xi_D^R = \ell n\ \left(\frac{r_u - r}{r_u}\right) \tag{5.6}$$

where ℓn denotes the natural logarithm. Further, Eq. (5.6) is written as

$$R\ell n\ (\xi_D) + \ell n\ (\kappa) = \ell n\ \{-\ell n\ \left(\frac{r_u - r}{r_u}\right)\} \tag{5.7}$$

At every point on the experimental stress-strain curve, Eq. (5.7) is valid. The unknowns involved in Eq. (5.7) are R and κ or ℓn (κ). A minimum of two points on the experimental curve are required for determination of R and κ. It is a good idea to use more than two points (usually 10 to 20 points) and employ a least-square fit for determination of R and κ from Eq. (5.7), (Fig. 5.1).

5.3 Elasticity and Plasticity Constants

5.3.1. Elasticity Constants

After the damage-related constants r_u, κ and R are known, the value of r at every point in the experimental stress-strain curve is known. This value of r is important in determining the elasticity parameters. There are two elastic constants for an isotropic material, Young's modulus, E, and Poisson's ratio, ν. Also, bulk modulus, K, and shear modulus, G, may be used as the two elastic constants. As mentioned earlier, unloading and reloading in the present study are elastic. Then the elasticity constants can be determined from the slopes of the unloading-reloading curves. In the damage model, the current value of the shear modulus is dependent on the current value of r. As shown in Chapter 3, Eq. (3.10), the shear modulus, modified for damage, is given by

$$G' = (1-r)\, G \tag{5.8}$$

This modified value of G, G' can be measured from the unloading-reloading curves of shear tests. It is an experimental fact that the

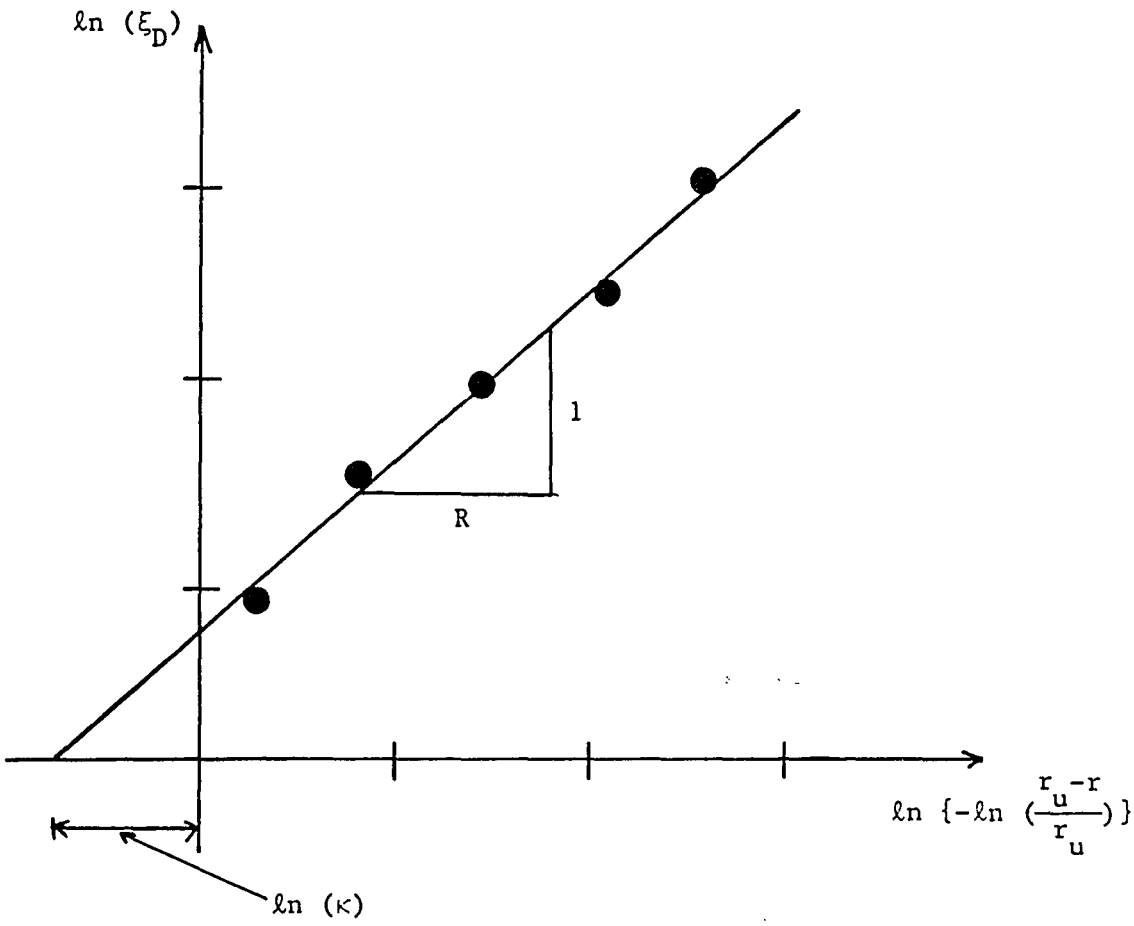

Fig. 5.1 Schematic for Determination of κ, R from Eq. 5.7

value of G' degrades with increasing deformation. The measured value of G' at a point together with the value of r at this point provide sufficient information for determination of G through Eq. (5.8). The value of G is determined at several points on the available stress-strain curves and then a weighted average of G is calculated.

The bulk modulus K, not dependent on damage, can be determined from unloading-reloading curves of hydrostatic compression tests.

A different but equally good procedure for determining the elastic constants is that of measuring Young's modulus and Poisson's ratio from the available unloading-reloading curves. For example, if unloading-reloading curves for a uniaxial compression test are available, then the slope of these curves in the major stress vs. major strain space is the modified value of E; namely, E' and the ratio of minor strain to major strain represents the modified Poisson's ratio ν'. The modified E' and ν' values are defined as

$$E' = \frac{9KG'}{3K + G'} \tag{5.9}$$

and

$$\nu' = \frac{1}{2}\frac{3K - 2G'}{3K + G'} \tag{5.10}$$

After E' and ν' are known, the values of G' and K can be determined by inverting Eqs. (5.9) and (5.10); thus, yielding

$$K = \frac{E'}{3\ (1-2\nu')} \tag{5.11}$$

and

$$G' = \frac{E'}{2\ (1+\nu')} \tag{5.12}$$

5.3.2. Plasticity Constants

After the damage parameters are known, the value of r is known at each stress σ_{ij}. Equation (3.2) can be rearranged to yield

$$\sigma^t_{ij} = \frac{\sigma_{ij}}{(1-r)} - \frac{r}{3\ (1-r)}\ \sigma_{kk}\ \delta_{ij} \tag{5.13}$$

Then the topical stress σ^t_{ij} and ε_{ij} are known at every point in the available experiments. Since σ^t_{ij} and ε_{ij} are related through Eq. (4.12), determination of plasticity parameters is as follows.

At the ultimate conditions (topical behavior), the value of α tends to zero; thus, the yield surface degenerates to an open surface intersecting the J^t_1 axis at infinity. Then, at the ultimate conditions

$$J^t_{2D} - \gamma\ (J^t_1)^2\ (1-\beta\ S_r)^{-1/2} = 0 \tag{5.14}$$

or

$$(1-\beta S_r)\ (J^t_{2D})^2 - \gamma^2\ (J^t_1)^4 = 0 \tag{5.15}$$

For each available shear test, the values of J_1^t, J_{2D}^t, S_r are known at the ultimate conditions. Then, by employing a least-square procedure on (5.15), β and γ are determined.

Two parameters define the ultimate yield envelope. Hence, results of at least two tests carried to the ultimate topical condition are required. It should be noted that as the topical stress approaches ultimate conditions, the mean stress approaches residual conditions.

The growth function, Eq. (4.7), can be written as

$$\eta_1 \ln (\xi) + \ln (\alpha) = \ln (a_1) \tag{5.16}$$

By setting F = 0 at distinct topical stress levels, α can be determined at these states. Also, ξ is known from the strain history and the present state of strain. For each test, a least-square fit performed on Eq. (5.16) yields the values of η_1 and a_1 (Frantziskonis et al., 1986) and Fig. 5.2.

The value of n can be determined at the state of stress (in the experiment) at which the volume change is zero. At this state, from Eq. (4.3),

$$\frac{J_{2D}^t}{(J_1^t)^2} = (-\alpha (J_1^t)^{n-2} + \gamma) F_s \tag{5.17}$$

Also, at zero volume change,

$$\frac{\partial F}{\partial J_1^t} = 0 \tag{5.18}$$

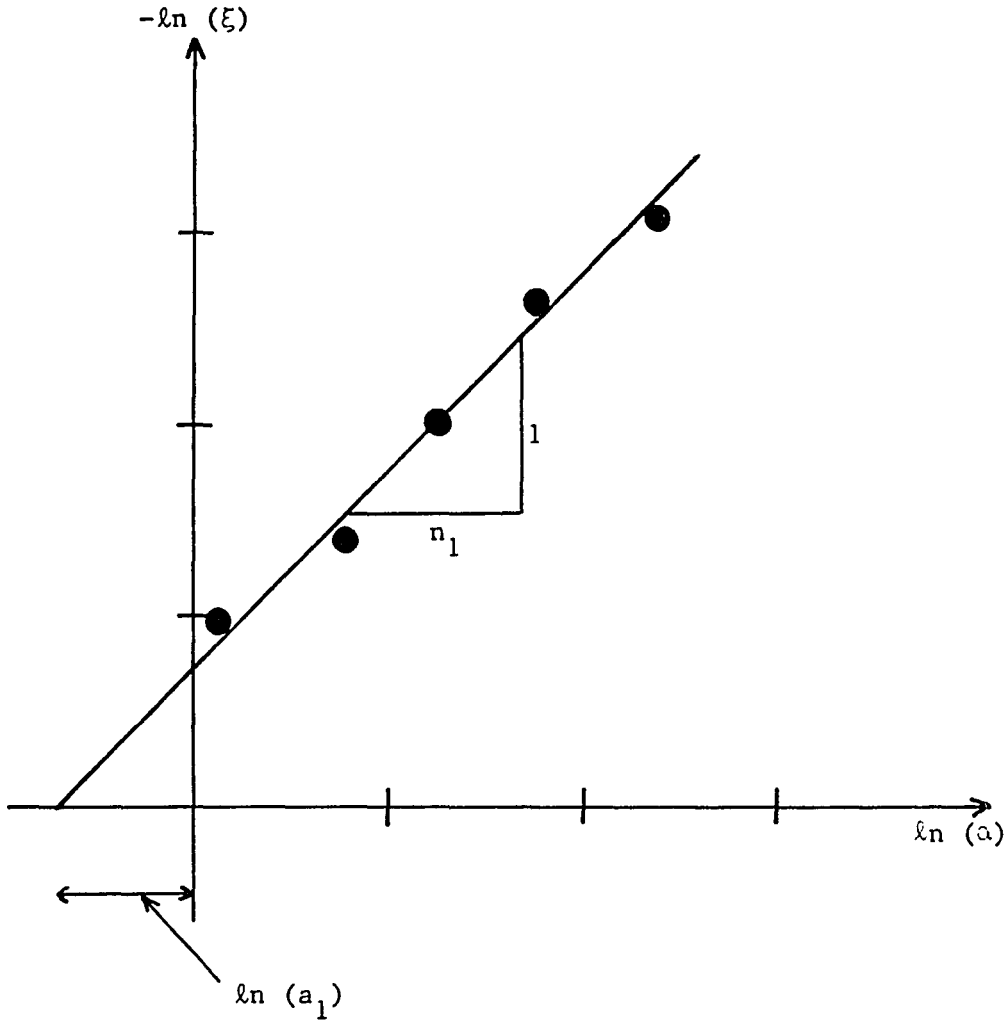

Fig. 5.2 Schematic for Determination of Hardening Constants a_1, n_1

or

$$- (-\alpha n \ (J_1^t)^{n-1} + 2\gamma \ J_1) \ F_s = 0 \tag{5.19}$$

or

$$J_1^t = \left(\frac{2\gamma}{\alpha n}\right)^{\frac{1}{n-2}} \tag{5.20}$$

From Eqs. (5.17) and (5.20), we obtain

$$1 - \frac{2}{n} = \frac{J_{2D}^t / J_1^t)^2}{F_s \ \gamma}$$

from which n is obtained. The value of n can be also determined from HC (hydrostatic compression) test. Specialization of Eqs. (4.3), (4.4) and (4.22) for HC, and then substitution of Eq. (4.22) in Eq. (4.14) and elimination of α through Eq. (4.22) leads to

$$J_1^t \ d\varepsilon_{kk} \ (J_1^t)^{n-2} = \sqrt{3} \ \gamma d \ J_1^t \ (n-2) \tag{5.22}$$

where "d" denotes increment of the quantity following it. At any state in the HC experiment, the total J_1^t, the increment of J_1^t, dJ_1^t and increment of volumetric strain $d\varepsilon_{kk}$ are known. Then n can be obtained from Eq. (5.22).

5.4 Constants for Materials Considered

Description of the concrete results used is given in the section titled "Available Laboratory Test Data" in Cahpter 7. Two test results were used for determination of the parameters associated with the model. The first test used is a uniaxial compression test in which the measured major and minor strains were available. The second test used for determination of parameters is a triaxial test such that the following relation between the stresses holds: $\sigma_1/\sigma_2 = \sigma_1/\sigma_3 = 1.0/0.1$. These test results are shown in Figs. 5.3 and 5.4, respectively.

First, the elastic constants (initial) were determined. Since no unloading is included in these tests, elastic parameters were determined from the initial slopes of the monotonic stress-strain curve. The average values determined from these two tests are

$$E = 5.4 \times 10^6 \text{ kPa (1 psi = 6.89 kPa)}$$

$$\nu = 0.25$$

The values of stress at the peak and residual stress levels were used for determination of the damage parameter, r_u. The values of $\sqrt{J_{2D}}$ at peak and residual stress were calculated and the following value of r_u was obtained:

$$r_u = 0.875$$

which is an average value obtained from the above two tests.

The values of stress and strain at a number of points on the stress-strain curves were used for determination of R and κ. The following values were found:

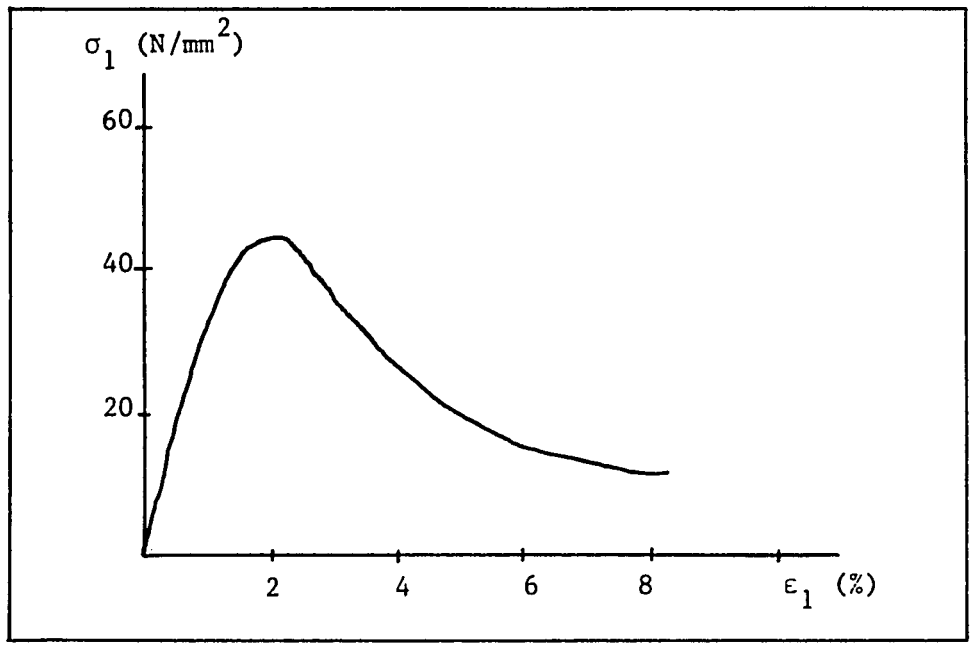

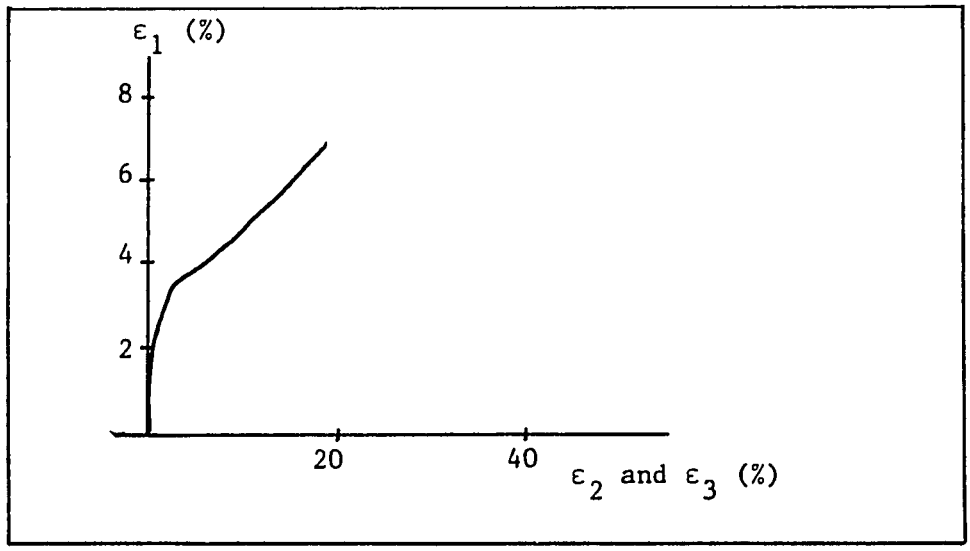

Fig. 5.2 Concrete Uniaxial Compression Test Results (After Van Mier, 1984)

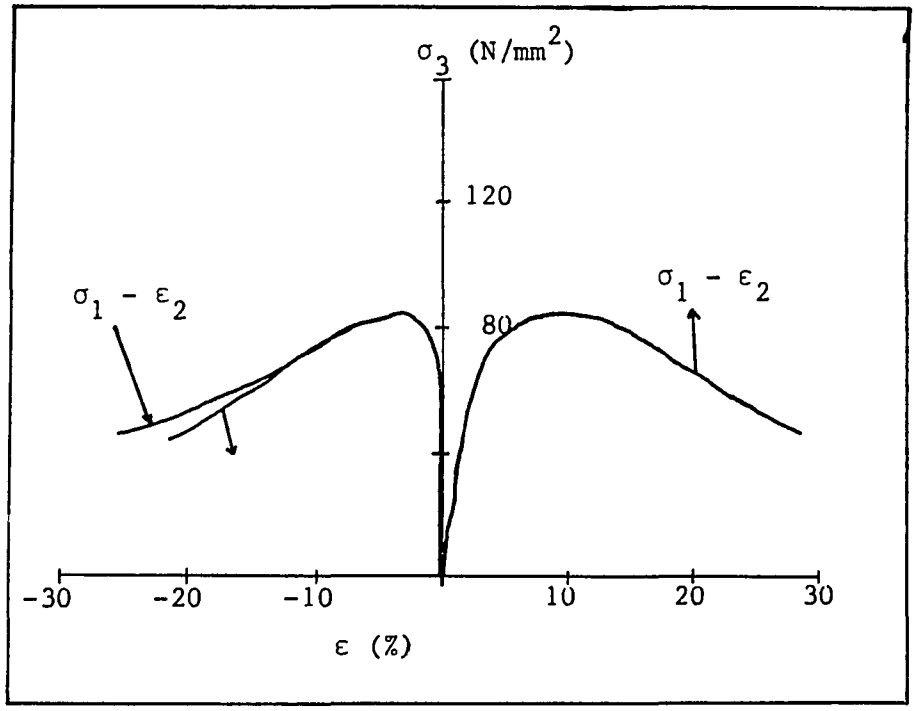

Fig. 5.4 Concrete Test Results
$\sigma_1/\sigma_2 = 10/1$, $\sigma_1/\sigma_3 = 10/1$
(After Van Mier, 1984)

$R = 1.502$

$\kappa = 668.00$

Plasticity-related constants are determined after the damage constants are known. The values of the plasticity constants are

$\gamma = 0.068$

$\beta = 1.038$

$n = 5.24$

$a_1 = 4.9 \times 10^{-6}$

$n_1 = 0.849$

5.4.1. Cohesionless Soil

Details on this soil are given in the section titled "Available Laboratory Test Data" in Chapter 7. The test results available were Conventional Triaxial Compression (CTC), in which the specimen is initially loaded hydrostatically and subsequently one of the stresses is increased while the other two stresses are kept constant. Five different initial confining pressures were available; namely, 1.0, 3.0, 6.0, 10.5 and 20.0 kg/cm^2. The confining pressures of 3.0 and 10.5 tests were chosen for determination of the constants. These test results are shown in Figs. 5.5 and 5.6. The following constants were obtained:

$E = 1600.0$ psi

$\nu = 0.25$

$r_u = 0.49718$

$R = 1.92705$

$\kappa = 31.932$

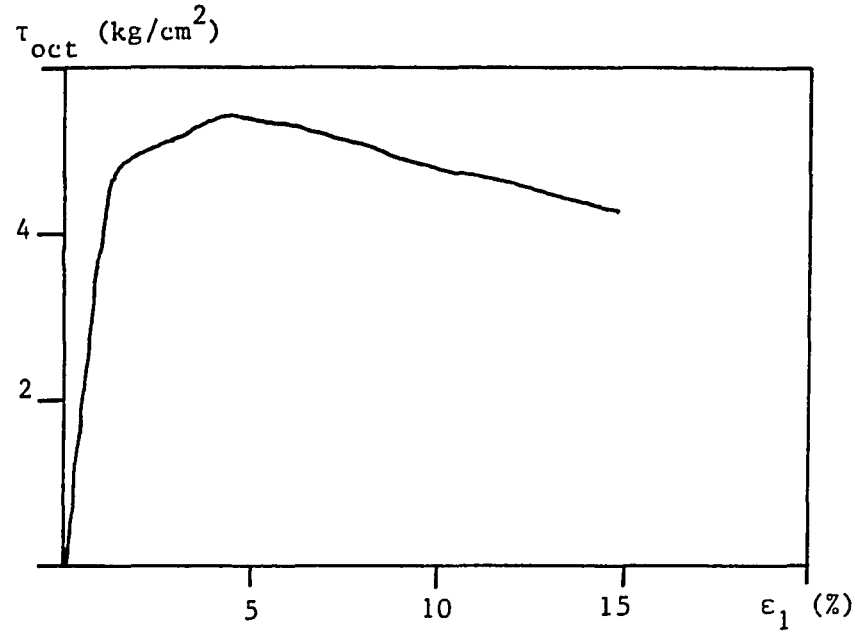

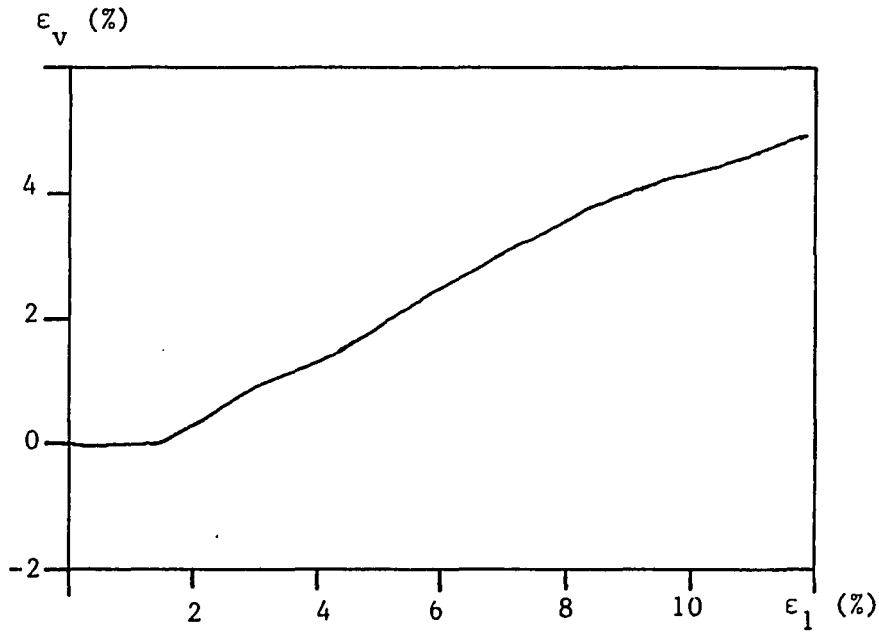

Fig. 5.5 Soil Test Results, σ_o = 3 kg/cm^2
(After Lee and Seed, 1967)

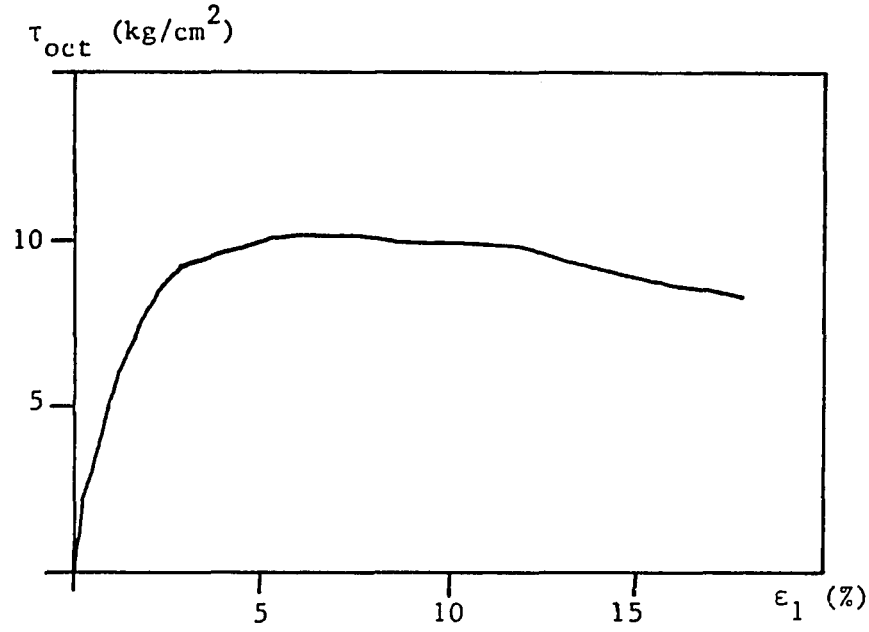

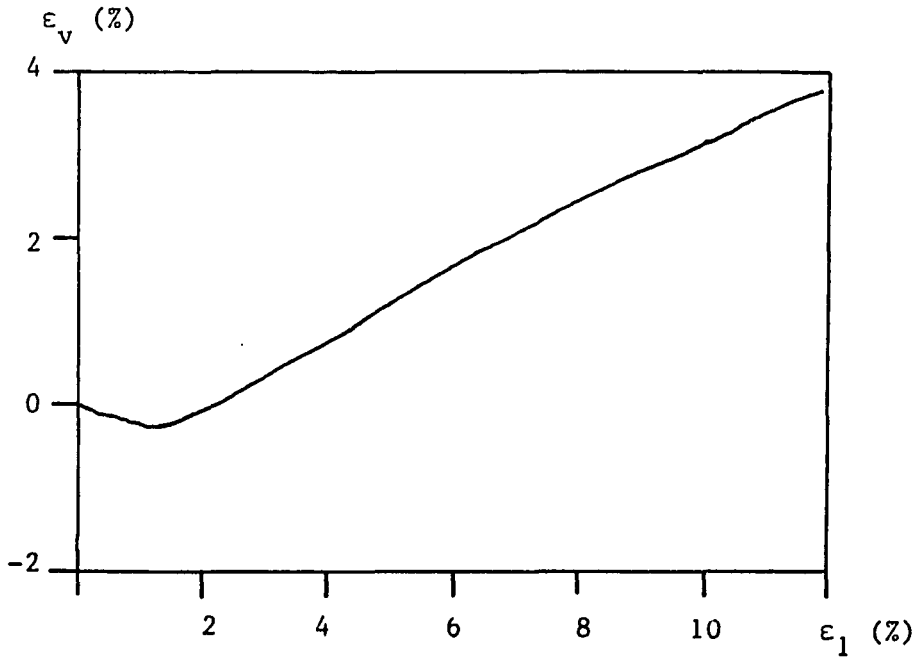

Fig. 5.6 Soil Test Results, σ_o = 6 kg/cm^2)
(After Lee and Seed, 1967)

γ = 0.2277

β = 0.0

n = 3.9616

a_1 = 7.2 E-5

n_1 = 0.3458

The following should be mentioned. The strain level at which softening occurred in these test results is high. In most of the tests, softening initiated at a strain level of 5% to 10%. At the residual stress level, the strains were between 20% and 25%. Clearly, a small strain theory is not strictly applicable for such high strain levels. Thus, determination of constants and back prediction of such test results involve the approximation and error involved from the small strain assumption.

5.4.2. Concrete-Concrete Interface

The subject of interfaces and joints is discussed in Chapter 8 where details on the material used and the parameters determined are given.

CHAPTER 6

ANALYSIS OF THE PROPOSED MODEL

In this chapter, first, the question of uniqueness of the proposed model is examined. It is shown that the proposed constitutive equations lead to a unique solution for the case of rate dependent as well as rate independent formulation and its implementation in finite element analysis shows mesh size insensitivity in the hardening and softening regimes. Conditions for formation of narrow shear bonds are developed and discussed. It is shown that as the damage accumulates, the material approaches localization of deformation. Finally energy considerations and failure criteria are analyzed and discussed.

6.1 Uniqueness

In a recent publication by Valanis (1985), the question of uniqueness of solution of initial value problems in softening materials is examined. An inequality is established which is true for all materials, irrespective of their constitution. It is shown that a number of constitutive equations that give rise to realistic softening behavior lead to a unique solution. Ordinarily, rate dependent models lead to a unique solution but rate independent ones either fail to lead to a unique solution or the question of uniqueness is difficult to analyze. Valanis addresses a simple uniaxial model (Eq. (6.6)) in the paper by Valanis (1985) which assures uniqueness only when the model is

formulated as rate dependent. It seems that formulation of a rate independent model that assures uniqueness in the softening regime is not trivial.

For convenient reference, we will provide here a brief outline of the results of Valanis. Let the solution be unique at time t, and let Δt be a vanishingly small nonzero time interval. Let two solutions exist at $t+\Delta t$. Let $\dot{\sigma}^1_{ij}$, $\dot{\varepsilon}^1_{ij}$; and $\dot{\sigma}^2_{ij}$, $\dot{\varepsilon}^2_{ij}$ be the stress and strain rate corresponding to the two solutions evaluated at t. If Δ denotes the difference between the two solutions; e.g., $\Delta\dot{\varepsilon}_{ij} = \dot{\varepsilon}^2_{ij} - \dot{\varepsilon}^1_{ij}$, then the solution is unique if

$$\Delta\dot{\sigma}_{ij}\ \Delta\dot{\varepsilon}_{ij} > 0 \tag{6.1}$$

Now, we examine the conditions under which the constitutive equations represented through Eqs. (3.17) and (3.18) provide a unique solution. Assuming two solutions, we obtain from Eq. (3.17)

$$(\dot{\sigma}^m_{ij})^2 = L_{ijk\ell}\ \dot{\varepsilon}^2_{k\ell} - \dot{r}^2\ S^t_{ij} \tag{6.2.1}$$

$$(\dot{\sigma}^m_{ij})^1 = L_{ijk\ell}\ \dot{\varepsilon}^1_{k\ell} - \dot{r}^1\ S^t_{ij} \tag{6.2.2}$$

where

$$L_{ijk\ell} = (1-r)\ C^{e-p}_{ijk\ell} + \frac{r}{3}\ C^{e-p}_{ppk\ell}\ \delta_{ij} \tag{6.3}$$

and the superscripts 1 and 2 denote the two solutions.

Now we consider two special cases of Eq. (3.21).

CASE 1

$$\dot{r} = \dot{r}\ (\xi_D) \tag{6.4}$$

CASE 2

$$\dot{r} = \dot{r}\ (\xi_D,\ \dot{\xi}_D) \tag{6.5}$$

such that Eq. (3.23) holds for Eq. (6.5). We note that Case 1 expressed by Eq. (6.4) brings a rate dependency in the formulation, while Case 2 expressed by Eq. (6.5) or Eq. (3.23) represents rate independent problem. If Eq. (3.29) is used, the formulation is rate independent. Here, the question of uniqueness for both cases is considered.

CASE 1

It follows from Eqs. (6.2) and (6.4) that

$$\Delta\dot{\sigma}_{ij}\ \Delta\dot{\varepsilon}_{ij} = \Delta\dot{\varepsilon}_{ij}\ L_{ijk\ell}\ \Delta\dot{\varepsilon}_{k\ell} \tag{6.6}$$

As already mentioned, $C^{e-p}_{ijk\ell}$ is always positive definite. Then since $0 \leq r \leq 1$, it follows from Eq. (6.3) that $L_{ijk\ell}$ is always positive definite. Then the right hand side of Eq. (6.6) is positive; thus, Eq. (6.1) is satisfied. Thus, we see that the rate dependent formulation satisfies the uniqueness criterion.

CASE 2

It follows from Eqs. (6.2) and (3.23) that

$$\Delta\dot{\sigma}_{ij}\ \Delta\dot{\varepsilon}_{ij} = \Delta\dot{\varepsilon}_{ij}\ L_{ijk\ell}\ \Delta\dot{\varepsilon}_{k\ell} - \Delta\dot{r}\Delta\dot{\varepsilon}_{ij}\ S^{t}_{ij} \tag{6.7}$$

where $\Delta\dot{r} = \dot{r}^{2} - \dot{r}^{1}$.

From Eq. (3.23), we obtain

$$\Delta\dot{r} = U\ \Delta\dot{\xi}_{D} \tag{6.8}$$

and from the definition of $\dot{\xi}_{D}$, we have

$$\Delta\dot{\xi}_{D} = \alpha_{ij}\ \Delta\dot{E}^{p}_{ij} \tag{6.9.1}$$

$$\alpha_{ij} = \dot{E}^{p}_{ij}\ (\dot{E}^{p}_{k\ell}\ \dot{E}^{p}_{k\ell})^{-1/2} \tag{6.9.2}$$

Since $\Delta\dot{E}^{p}_{ij} = \Delta\dot{\varepsilon}^{p}_{ij} - \frac{1}{3}\ \Delta\dot{\varepsilon}^{p}_{nn}\ \delta_{ij}$ and $\Delta\dot{\varepsilon}^{p}_{ij} = \Delta\dot{\varepsilon}_{ij} - \Delta\dot{\varepsilon}^{p}_{ij}$, we have

$$\Delta\dot{E}^{p}_{ij} = (\Delta\dot{\varepsilon}_{st} - \Delta\dot{\varepsilon}^{e}_{st})\ (\delta_{is}\ \delta_{jt} - \frac{1}{3}\ \delta_{st}\ \delta_{ij}) \tag{6.10}$$

where the superscript e denotes elastic.

The elastic strain rates are related to $\dot{\sigma}^{t}_{ij}$, so that

$$\dot{\varepsilon}^{e}_{st} = D^{e}_{stk\ell}\ \dot{\sigma}^{t}_{k\ell} \tag{6.11.1}$$

$$D^{e}_{stk\ell} = \frac{1}{2G}\ \delta_{sk}\ \delta_{\ell t} - \frac{K}{2G\ (2G + 3K)}\ \delta_{k\ell}\ \delta_{st} \tag{6.11.2}$$

where G, K denote the initial elastic shear and bulk moduli, respectively. It follows from Eqs. (3.3), (6.8), (6.9), (6.10) and (6.11) that

$$\dot{\Delta r} = U\, T_{pq}\, \dot{\Delta \varepsilon}_{pq} \tag{6.12.1}$$

where

$$T_{pq} = \dot{\alpha}_{pq} - \alpha_{st}\, D^{e}_{stk\ell}\, C^{e-p}_{k\ell pq} \tag{6.12.2}$$

Now the elastoplastic tensor $C^{e-p}_{ijk\ell}$ needs to be written explicitly. In here a generalized plasticity model is used where the associative flow rule was assumed. Following Mandel (1947) and Rudnicki and Rice (1975), $C^{e-p}_{ijk\ell}$ is written in terms of the internal friction coefficient, μ, and the dilatancy factor, β. If $\beta \neq \mu$, the nonassociative rule holds. Since here it is not required that $\beta = \mu$, the associative flow rule assumption is not necessary. The geometric interpretation of β and μ is shown schematically in Fig. 6.1. For clarity, in Appendix 1 of this chapter, β and μ are related to the generalized model used herein, and the strain rates are expressed in terms of the stress rates. If h denotes the plastic modulus and $\tau^{t} = (\frac{1}{2}\, S^{t}_{ij}\, S^{t}_{ij})^{1/2}$, the elastoplastic constitutive tensor is expressed as

$$C^{e-p}_{abpq} = G\,(\delta_{pa}\,\delta_{qb} + \delta_{bp}\,\delta_{aq}) + (K - \tfrac{2}{3}\,G)\,\delta_{ab}\,\delta_{pq} - \tag{6.13}$$

$$\frac{(\frac{G}{\tau^{t}}\, S^{t}_{ab} + \beta\, K\, \delta_{ab})\,(\frac{G}{\tau^{t}}\, S^{t}_{pq} + K\,\mu\,\delta_{pq})}{h + G + \mu\, k\, \beta}$$

which is the inverse relation of (A.6). Now from Eq. (3.1), we obtain that $S_{ij} = (1\text{-}4)\, S^{t}_{ij}$, thus

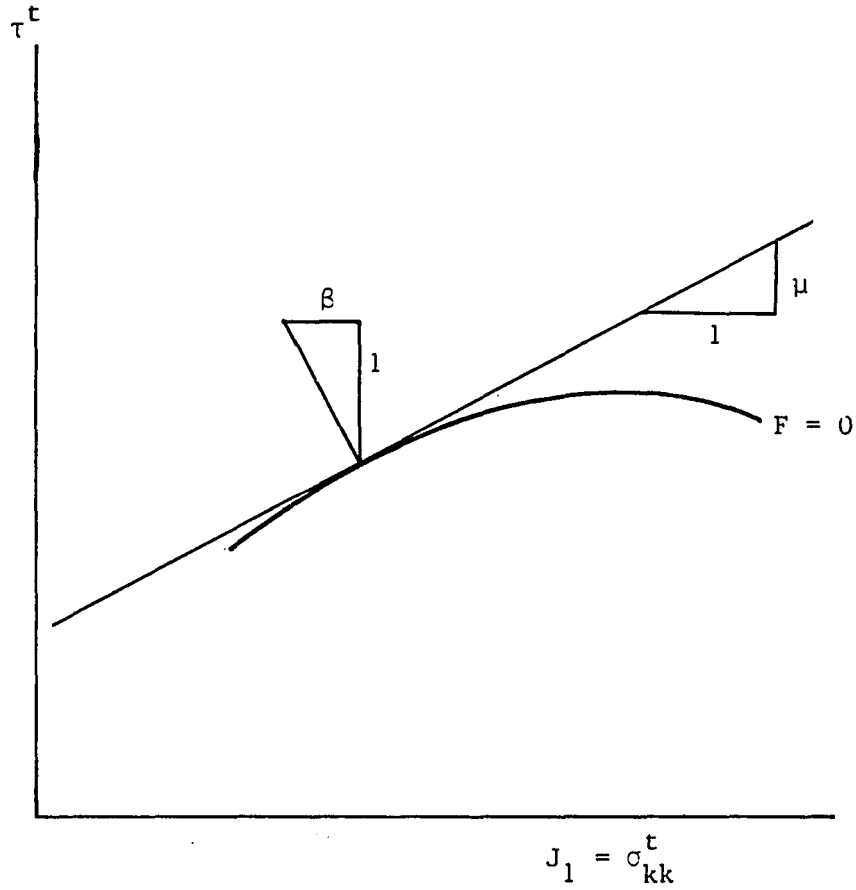

Fig. 6.1 Geometric Interpretation of μ and β

$$\frac{S_{ij}}{\tau} = \frac{S^t_{ij}}{\tau^t} \tag{6.14}$$

where $\tau = (\frac{1}{w} S_{ij} S_{ij})^{1/2}$. The topical stress in Eq. (6.13) can be eliminated by using Eq. (6.14); thus, from now on, the mean stress will appear in place of the topical stress in Eq. (6.13).

As it is seen from Eq. (6.9.2), α_{ij} is a unit vector in the direction of $\dot{E}^p_{ij}$ in the six-dimensional space. It is a property of the plasticity theory, and it can be seen from (A.6) that $\dot{E}^p_{ij}$ is dependent on S^t_{ij}. Then the following holds:

$$\alpha_{ij} = \frac{S^t_{ij}}{\tau^t \sqrt{2}} \tag{6.15}$$

and from Eq. (6.14)

$$\alpha_{ij} = \frac{S_{ij}}{\tau \sqrt{2}} \tag{6.16}$$

From Eqs. (6.12.2), (6.11.2), (6.13), (6.14) and (6.16), it follows that

$$T_{pq} = \frac{\frac{G}{\tau} S_{pq} + K \mu \delta_{pq}}{(h + G + \mu K \beta) \sqrt{2}} \tag{6.17}$$

From Eqs. (3.1), (3.22), (6.12.1) and (6.17), we obtain

$$\dot{\Delta r} \dot{\Delta \varepsilon}_{ij} S^t_{ij} = T_1 + T_2 \tag{6.18.1}$$

$$T_1 = \frac{U}{\sqrt{2}} \frac{\frac{G}{\tau} S_{k\ell}}{(h + G + \mu\, k\, \beta)} \frac{S_{ij}}{(1-r)} \Delta\dot{\varepsilon}_{ij}\, \Delta\dot{\varepsilon}_{k\ell} \tag{6.18.2}$$

$$T_2 = \frac{U}{\sqrt{2}} \frac{\frac{G}{\tau} S_{k\ell}}{(h + G + \mu\, K\, \beta)} \frac{S_{ij}}{(1-r)} \Delta\dot{\varepsilon}_{ij}\, \Delta\dot{\varepsilon}_{k\ell} \tag{6.18.3}$$

Equation (6.18.1) defines the second term on the right hand side of Eq. (6.7). Since $L_{ijk\ell}$ is always positive definite, the first term in Eq. (6.7) is always positive. In order that the solution be unique, it is sufficient to show that the absolute value of the second term in Eq. (6.7) is smaller than the first term. As shown subsequently, the absolute value of the second term is not only less but much smaller than the first term in Eq. (6.7). From Eqs. (6.3), (6.13) and (6.14), $L_{ijk\ell}$ is expressed as

$$\begin{aligned} L_{abpq} = {} & (1-r)\, G\, (\delta_{pa}\, \delta_{qb} + \delta_{bp}\, \delta_{aq}) + \\ & \left[K - \frac{2}{3}(1-r)\, G\right] \delta_{ab}\, \delta_{pq} - \\ & \frac{\left[\frac{(1-r)\, G}{\tau} S_{ab} + \beta\, K\, \delta_{ab}\right]}{(1-r)} \\ & \frac{\left[\frac{(1-r)\, G}{\tau} S_{pq} + K\, (1-r)\, \mu\, \delta_{pq}\right]}{(h + G + \mu\, K\, \beta)} \end{aligned} \tag{6.19}$$

We note that Eq. (6.19) may be obtained from Eq. (6.13) by making the following substitutions:

$$G \to G' = (1-r)\, G \tag{6.20.1}$$

$$\mu \to \mu' = (1-r) \tag{6.20.2}$$

$$h \to h' = (1-r)\, h \tag{6.20.3}$$

From Eq. (6.19), it follows that

$$\Delta\dot{\varepsilon}_{ij}\, \Delta\dot{\varepsilon}_{k\ell}\, L_{ijk\ell} = T_1' + T_3' \tag{6.21.1}$$

$$T_1' = (1-r)\, \frac{(\frac{G}{\tau})^2\, S_{k\ell}}{(h + G + \mu\, K\, \beta)}\, S_{ij}\, \Delta\dot{\varepsilon}_{k\ell}\, \Delta\dot{\varepsilon}_{k\ell} \tag{6.21.2}$$

$$T_2' = (1-r)\, \frac{\frac{G}{\tau}\, K\, \mu\, \delta_{k\ell}}{(h + G + \mu\, K\, \beta)}\, S_{ij}\, \Delta\dot{\varepsilon}_{ij}\, \Delta\dot{\varepsilon}_{k\ell} \tag{6.21.3}$$

$$T_3 = \Delta\dot{\varepsilon}_{ij}\, \Delta\dot{\varepsilon}_{k\ell}\, L_{ijk\ell} - T_1' - T_2' \tag{6.21.4}$$

From Eqs. (6.18) and (6.21), we obtain

$$\frac{T_1}{T_1'} = \frac{T_2}{T_2'} = \frac{U}{\sqrt{2}}\, \frac{\tau^t}{G'} \tag{6.22}$$

Relations, Eqs. (6.18), (6.21) and (6.22), imply that a sufficient condition for Eq. (6.1) to hold is

$$\frac{U}{\sqrt{2}}\, \frac{\tau^t}{G'} < 1 \tag{6.23}$$

From Eqs. (3.22) and (3.23), it follows that U is a dimensionless (positive) number representing the slope of the r vs. ξ_D curve. Its

value depends on the value of ξ_D and the constants associated with the damage evolution law. In order to estimate the order of its magnitude, the values of the constants estimated for a concrete described in the previous chapter are employed. The values of these constants will vary from material to material and it is reasonable to assume that the order of the values may not be much different for similar materials. Then, since ξ_D is of the order of deviatoric plastic strain and τ^t/G' is of the order of deviatoric elastic strains (much less than unity), the value of the left hand side of Eq. (6.23) is found to vary between zero and order of 10^{-2}; thus, Eq. (6.23) is satisfied. Hence, the rate independent formulation satisfies the uniqueness criterion. Next, the numerical implementation of the formulation is examined and discussed.

6.2 Numerical Implementation

As mentioned in the introduction, when strain softening of materials is treated as an elasticity or elastoplasticity problem, numerical analysis may suffer from instabilities and high sensitivity to mesh size. The subject is discussed in details by Sandler (1984) and Pietruszczak and Mroz (1981). Typical load-displacement relationships resulting from such analysis, termed as "standard" by Pietruszczak and Mroz, are shown in Fig. 6.2. As discussed by Valanis (1985), lack of uniqueness in the softening regime may be the reason for such mesh sensitivities when the standard procedures are employed.

The principle of virtual work leads to the following incremental equations in matrix notation, Desai and Abel (1972):

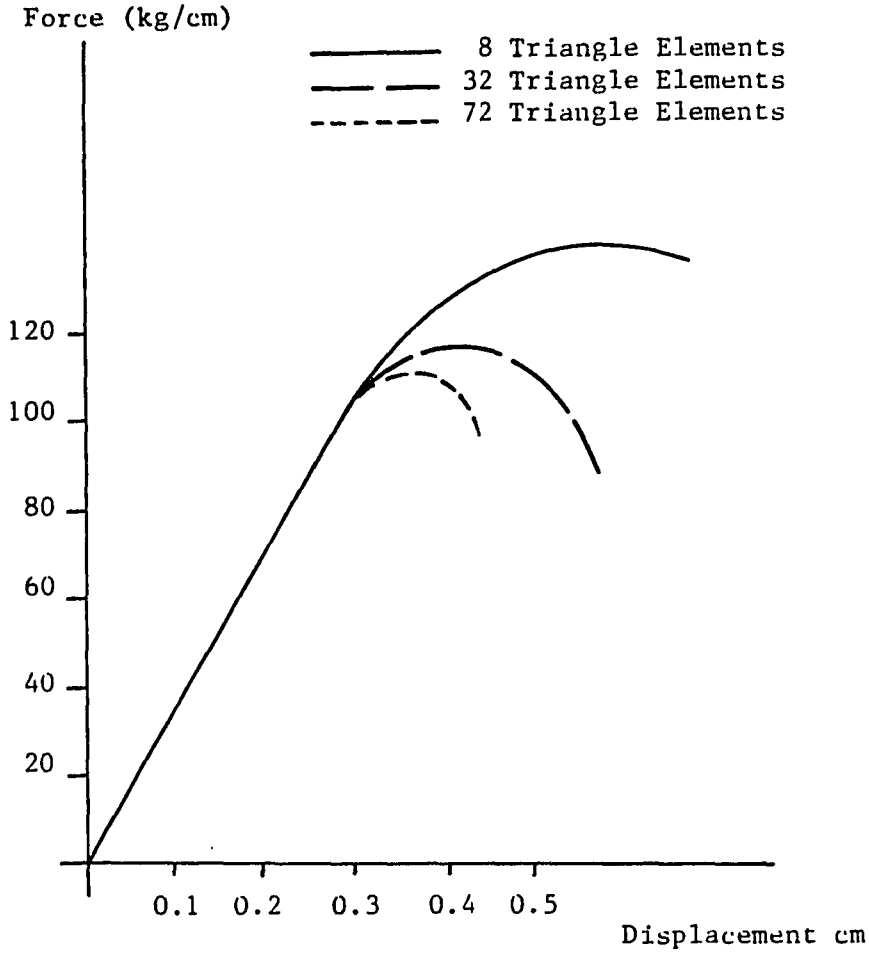

Fig. 6.2 Typical Load-Displacement Relationship Resulting from Analysis Termed as Standard (After Pietruszczak and Mroz, 1981)

$$\int_V \underset{\sim}{B}^T \, d\underset{\sim}{\sigma} \; dV = d\underset{\sim}{Q} \tag{6.24}$$

where $\underset{\sim}{B}$ is the strain-displacement transformation matrix, $d\underset{\sim}{\sigma}$ denotes increment in stress, $d\underset{\sim}{Q}$ is the increment in external force including surface and body forces, and superscript T denotes transpose. The incremental form of the stress-strain relation is written as Eq. (3.16)

$$d\underset{\sim}{\sigma} = \underset{\sim}{L} \, d\underset{\sim}{\varepsilon} - dr \, \underset{\sim}{S}^t \tag{6.25}$$

where the expression for $\underset{\sim}{L}$ is given in Eq. (6.3), dr denotes increment of r and $\underset{\sim}{S}^t$ is the topical stress vector. From Eqs. (6.24), (6.25) and the incremental strain-displacement relations, we obtain

$$\underset{\sim}{k} \, d\underset{\sim}{q} = d\underset{\sim}{Q} + d\underset{\sim}{Q}^r \tag{6.26.1}$$

where

$$\underset{\sim}{k} = \int_V \underset{\sim}{B}^T \, \underset{\sim}{L} \, \underset{\sim}{B} \, dV \tag{6.26.2}$$

and

$$\Delta\underset{\sim}{Q}^r = \int_V \underset{\sim}{B}^T \, dr \, \underset{\sim}{S}^t \, dV \tag{6.26.3}$$

In Eq. (6.26), $\underset{\sim}{k}$ is always positive definite since $\underset{\sim}{L}$ is always positive definite. Thus, $\underset{\sim}{k}$ in Eq. (6.26) is non-softening and problems related to negative modulus are avoided. Further, $\Delta\underset{\sim}{q}^r$, termed the "damage force," is responsible for the softening in the average constitutive

description. Thus, the formulation is such that the stiffness matrix always remains positive definite. The decomposition, depicted schematically in Fig. 3.2, and discussed previously, involves the damage force that modifies positive definite $\underset{\sim}{k}$, thus giving the capability of stable calculations in the softening regime.

6.3 Mesh Sensitivity

For illustration purposes, the following problem adopted from Pietruszczak and Mroz (1981) is considered. Figure 6.3 shows the dimensions and finite element mesh. Three different meshes were used with 1, 4 and 16 elements; the 8-noded isoparametric element is used, Zaman et al. (1983). The problem is idealized as two-dimensional and plain strain conditions are assumed.

Increments of vertical displacements were applied along the top and bottom surfaces while the horizontal displacements at the top and bottom were restrained; this represents a sticking friction end condition. An iterative (Newton-Raphson) procedure, Desai and Abel (1972), Nagaraj (1986), is employed for the incremental solution of the problem. The material parameters used were those given in the previous chapter.

Figure 6.4 shows the computed load-displacement curves obtained by using the model proposed herein. It is seen that the mesh-size sensitivity is insignificant as compared to the sensitivity depicted in Fig. 6.1 that was reported by Pietruszczak and Mroz (1981). The small differences can be due to normal finite element discretization errors.

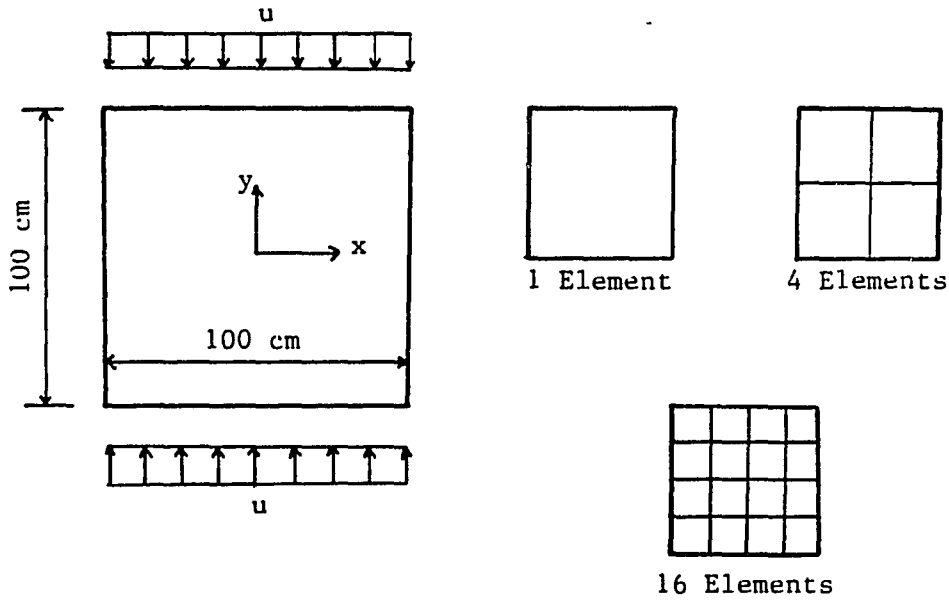

Fig. 6.3 Finite Element Discretization for Example Problem

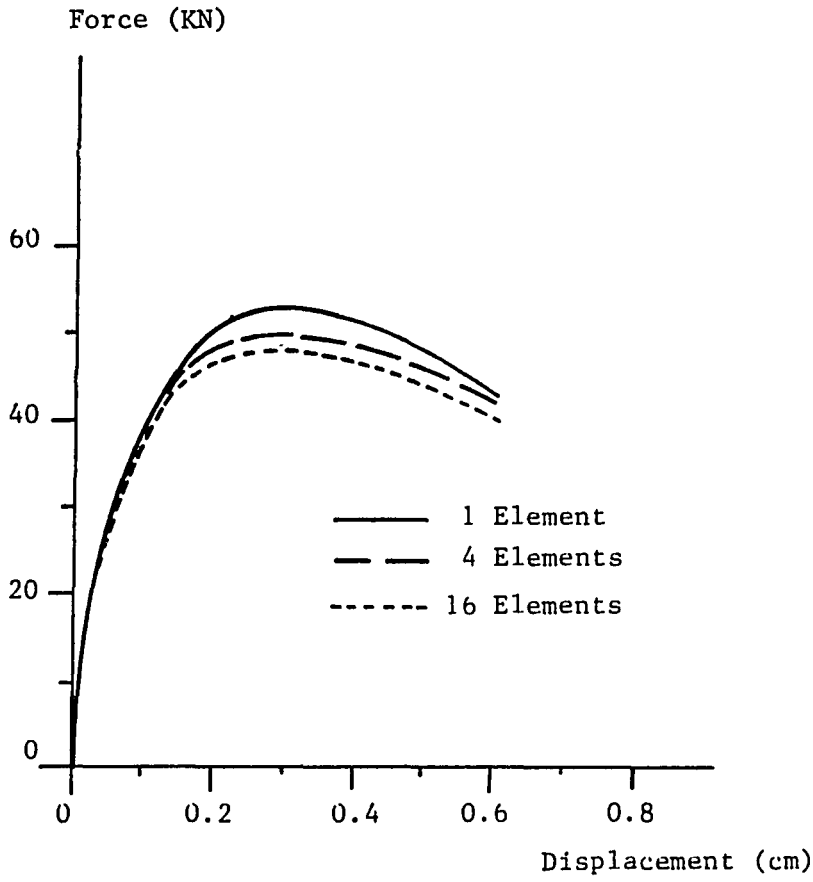

Fig. 6.4 Computed Load-Displacement Curves for 1, 4 and 16 Eight-Noded Quadrilateral Elements

6.4 Localization

Here, the possibility that the proposed damage model leads to a bifurcation point, at which nonuniform deformation can be incipient in a planar band, usually called "shear band," is examined. The condition for localization of the deformation into a shear band can be derived from the requirement that the internal and external stress vectors across a shear band boundary are in equilibrium. This type of analysis is usually called "shear band analysis" and has been explained in detail in various publications, Hill (1962), Mandel (1966, Hill and Hutchinson (1975); such analysis and results for geomaterials are given by Rudnicki and Rice (1975) and Vardoulakis (1980). A brief outline of shear band analysis based on the work of Rudnicki and Rice is presented here.

Let Δ denote the difference between the local field at a point in the band and the uniform field outside the band. Let the constitutive equations be written in the form

$$\overset{\nabla}{\sigma}_{ij} = E_{ijk\ell} D_{k\ell} \tag{6.27}$$

where $\overset{\nabla}{\sigma}_{ij}$ is the Jaumann (co-rotational) stress rate defined as

$$\overset{\nabla}{\sigma}_{ij} = \dot{\sigma}_{ij} - \sigma_{ip} W_{pj} - \sigma_{jp} W_{pi} \tag{6.28}$$

In Eqs. (6.27) and (6.28), D_{ij} is the symmetric part, and W_{ij} the antisymmetric part of the velocity gradient, $\partial v_j/\partial x_i$, and $E_{ijk\ell}$ in

Eq. (6.27) denotes the modulus tensor. Let X_i, i = 1, 2, 3, denote a coordinate system such that the direction X_2 is perpendicular to the shear band, Fig. 6.5. If, at the bifurcation of deformation rates, the values of $E_{ijk\ell}$ remain the same in and outside the band

$$\Delta \overset{\nabla}{\sigma}_{ij} = E_{ijk\ell}\, \Delta D_{k\ell} \tag{6.29}$$

Expressing the ΔW_{ij} and ΔD_{ij} in terms of $\Delta\,(\partial v_i/\partial x_j)$, the following condition for bifurcation results, Rudnicki and Rice (1975):

$$\det\left|E_{2jk2} - R_{jk}\right| = 0 \tag{6.30}$$

where R_{jk} denote stress terms resulting from the expression for ΔW. If a zero th order analysis is to be developed, the R_{jk} terms in Eq. (6.30) may be neglected, as compared to the $E_{ijk\ell}$ terms. Such an analysis amounts to retaining the first term in an expansion of the stress/elastic modulus ratio.

As shown previously, Eqs. (3.14), (6.3), the constitutive relations involve evolution of damage in the material. The purpose here is to examine how <u>damage</u> and its evolution <u>influence</u> the conditions for localization.

From Eqs. (3.14) and (6.3), the constitutive relations may be expressed as

$$\overset{\nabla}{\sigma}_{ij} = L_{ijk\ell}\, D_{k\ell} - \dot{r}\, S^t_{ij} \tag{6.31}$$

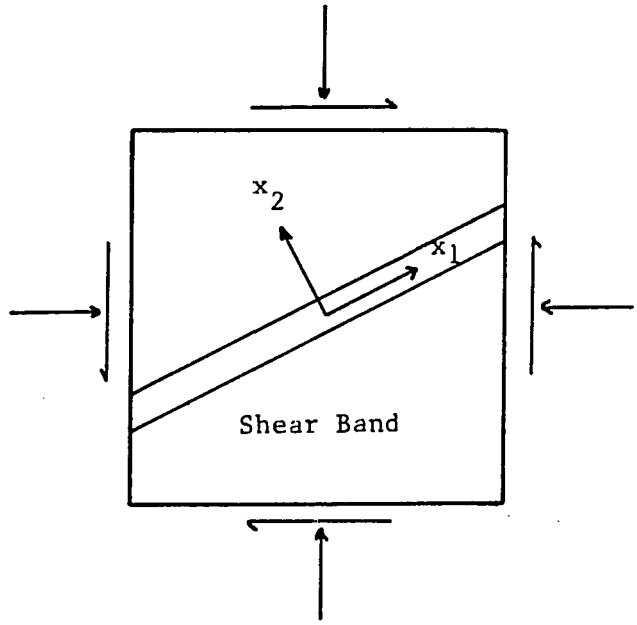

Fig. 6.5 Shear Band and Coordinate System

From Eq. (6.31), the following difference is formed:

$$\Delta\overset{\nabla}{\sigma}_{ij} = L_{ijk\ell}\,\Delta D_{k\ell} - \Delta\dot{r}\,S^{t}_{ij} \tag{6.32}$$

where Eq. (3.23) holds as an evolution of the damage parameter r. In this chapter, Δ has different physical meaning than the one assigned in the previous section. Mathematically though, the same operations can be performed on Δ. Thus, following the same steps as in Eqs. (6.8) through (6.12), a relation similar to Eq. (6.12) is obtained as

$$\Delta\dot{r} = U\,T_{k\ell}\,\Delta D_{k\ell} \tag{6.33}$$

and $T_{k\ell}$ is expressed as in Eq. (6.12.2). From Eqs. (6.32) and (6.33), the following condition for localization is obtained; here the zero th order analysis holds:

$$\det\left|L_{2jk2} - U\,T_{k2}\,S^{t}_{2j}\right| = 0 \tag{6.34}$$

Following the same steps as in the previous section (relations (6.13) through (6.23), it can be shown that the second terms in the left side of Eq. (6.34) are much smaller than the first terms as long as Eq. (6.23) holds. Then, they can be neglected. The tensor $L_{ijk\ell}$ is expressed analytically through Eq. (6.19), and the condition for localization reduces to $\det\left|L_{2jk2}\right| = 0$. As previously noted, the tensor $L_{ijk\ell}$ is obtained from $C^{e-p}_{ijk\ell}$ by making the substitutions, Eq. (6.20). Thus, the procedure employed for bifurcation analysis of elastoplastic

materials may be employed here if the following distinguishing points are considered: (1) substitutions as of Eq. (6.20) are made, (2) the plastic modulus h, referred to as the topical behavior, is always non-negative. Similar manipulations are described by Rudnicki and Rice (1975) and Vardoulakis (1980). For this reason, we present the results for the critical value of h and the angle of inclination of the shear band. At the localization conditions, the following holds:

$$\frac{h}{G} = \frac{[(1-r)\ X + \beta \frac{K}{G}]\ (X + \mu \frac{K}{G})}{\frac{4}{3}\ (1-r) + \frac{K}{G}} - XN - N^2 - X^2 - \mu \frac{K}{G} \beta \tag{6.35.1}$$

where

$$\frac{K}{G} = \frac{2\ (1+\nu)}{3\ (1-2\nu)}$$

and

$$X = \frac{[(1-r)\ \mu + \beta]\ (1+\nu)}{2\ (1+\nu) + (1-r)\ (1-2\nu)} - \frac{N\ [2\ (1-r)\ (1-2\nu) + (1+\nu)}{2\ (1+\nu) + (1-4)\ (1-2\nu)} \tag{6.35.2}$$

and ν is the Poisson's ratio, $N = S_{22}/\tau$. The angle θ_o, which maximizes h, and hence defines the plane of localization, is given by

$$\tan \theta_o = \left(\frac{X - N_1}{N_3 - X}\right)^{1/2} \tag{6.36}$$

where $N_1 = S_{11}/\tau$ and $N_3 = S_{33}/\tau$. Figure 6.6 shows the orientation of the shear band with respect to the principal stress coordinate system. The angle θ_o is the angle between the normal to the plane of localization and the σ_3 principal stress.

In order to interpret the expressions, Eqs. (6.35) and (6.36), the values of h/G and θ_o at localization are shown in Figs. 6.7, 6.8 and in Appendix 6.2 for different values of r. As mentioned before, h is always nonnegative. Then, negative values of h/G indicate that to the corresponding damage accumulation no critical value of h exists. During a monotonically increasing shear path, the value of h/G initially has a relatively large value and subsequently decreases. At the same time, r is initially zero and subsequently increases. At localization, the (h/G) or vs. r lies on the curve shown in Fig. 6.7; e.g., point A. As shown in Appendix 6.2 and Fig. 6.7, the value of r influences considerably the critical value of h/G. Specifically, the greater the accumulation of damage, the closer the material comes to a state where localization of deformation can occur. This is expected since accumulation of damage brings the material closer to an instability or collapse. A basic conclusion is that damaged material is more inclined to instability by localization of deformation than a material that is not damaged. The damage also affects the angle θ_o as shown in Appendix 6.2 and Fig. 6.8.

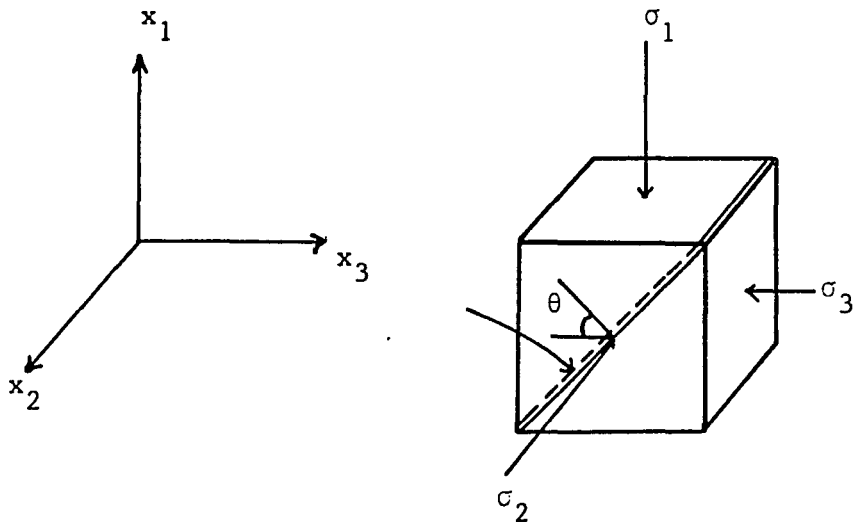

Fig. 6.6 Orientation of Shear Band in Principal Stress Space; $\sigma_1 \geq \sigma_2 \geq \sigma_3$

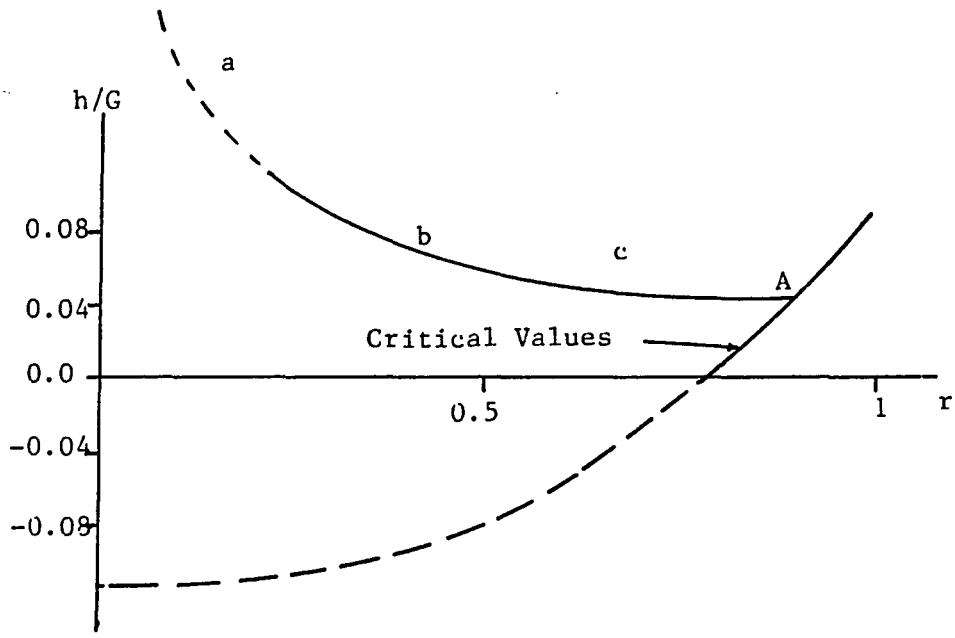

Fig. 6.7 Effect of Damage Accumulation on the Initiation of Localization. Plot Corresponds to Pure Shear Stress Conditions, N = 0, μ = 0.9, β = 0.6, ν = 0.3

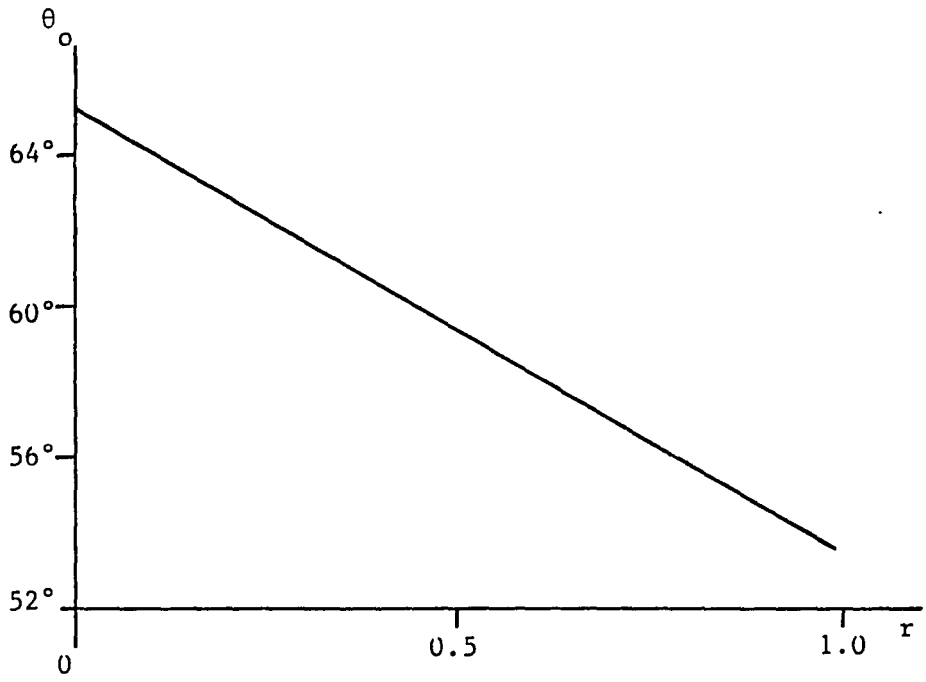

Fig. 6.8 Effect of Damage Accumulation on the Shear Band Inclination θ_o. Plot Corresponds to Pure Shear Stress Conditions (N = 0), $\mu = 0.9$, $\beta = 0.6$, $\nu = 0.3$

Experimental measurements of conditions at the initiation of localization is not an easy task. To our knowledge, precise measurements of such conditions are not available in the literature; hence, comparisons of the theoretical predictions with observations are difficult. However, the effect of damage accumulation on the conditions under which strain localization can initiate, leading to shear band formation, have been examined here.

6.4.1. Comment

From Eqs. (6.3) and (6.30), it is clear that damage accumulation as well as the elastoplasticity relations, expressed through $C^{e-p}_{ijk\ell}$, considerably affect the conditions for shear band formation; for instance, Molenkamp (1985) found that considerable variations in the predicted instant of initiation for different elastoplastic models occurred. In this study, however, the analysis is restricted to only one elastoplastic model.

As shown in the previous section, uniqueness was associated with the constitutive relations where the theory of Valanis (1985) was employed, and small deformations were considered. The localization analysis involves large deformation and shows that the formulation may allow nonuniqueness, especially at highly damaged states. The analysis suggests that initiation of localization depends on the parameters involved in the macroscopic description of damage.

6.5 Energy Considerations

As mentioned earlier, the proposed model accounts phenomenologically for directional properties induced by cracking; it is not intended for detailed identification of location and directional propagation of cracks. In this section, balance of energy of the two interacting components is considered. The damaged body is compared to an elastoplastic body with cracks. Equivalence between the damaged body and the cracked body is examined through rate of work considerations in the "Griffith Sense" (Griffith, 1920, 1921). A discussion of the concepts and results introduced herein follows subsequently.

6.5.1 Elastoplastic Cracked Body vs. the Two Component Damaged Body

6.5.1.1 Elastic-Plastic Cracked Body. Consider an elastic-plastic body that occupies a region R (Fig. 6.9). On part of its boundary, ∂R, surface fractions T_i are applied, while body forces F_i act on R. Also, traction-free propagating cracks are contained in the body with instantaneous total crack surface area equal to A (t) (Fig. 6.9). Balance of rate of global energy for the above requires that (Eftis and Liebowitz (1975), Lotsberg (1977))

$$- \left[\int_{\partial R} T_i \dot{u}_i \, dS + \int_R \rho f_k \dot{u}_k \, dV \right] = \int_R \dot{E} \, dV + \frac{1}{2} \int_R \rho \frac{d}{dt} \left(\dot{u}_i \dot{u}_i \, d_V + \dot{\Gamma} \right) \tag{6.37}$$

where the left hand side of Eq. (6.37) represents the rate of work by tractions and body forces, $\dot{E}$ is the internal energy density rate per

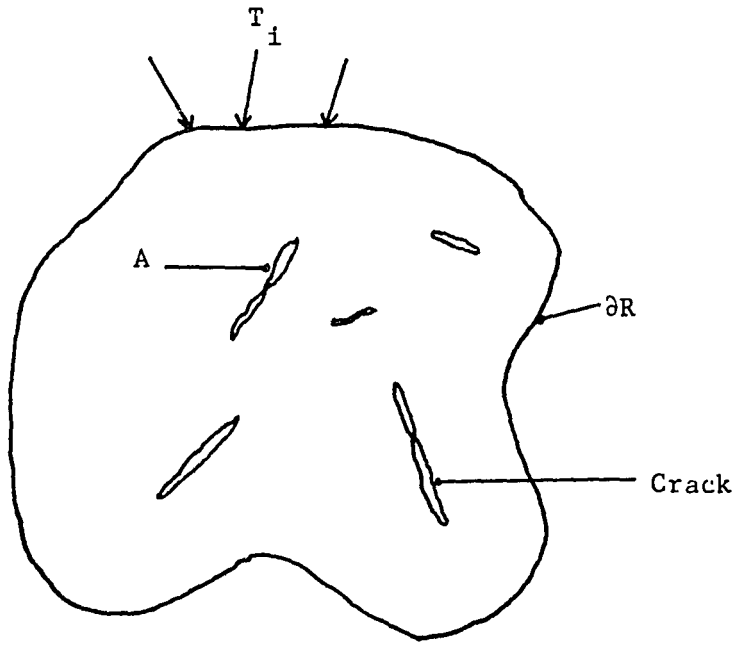

Fig. 6.9 Schematic of Elastoplastic Body Containing Cracks

unit volume, $\frac{1}{2}\int_R \rho \frac{d}{dt}(\dot{u}_i \dot{u}_i)\, dV$ is the rate of kinetic energy, and by following Griffith, we can write crack surface energy rate per unit area, $\dot{\Gamma}$, as

$$\dot{\Gamma} = \gamma \dot{A} \tag{6.38}$$

where γ is the crack surface energy per unit area. The internal energy density is decomposed in two parts; namely,

$$\dot{E} = \dot{E}_e + \dot{D} \tag{6.39.1}$$

$$\dot{E}_e = \sigma_{ij} \dot{\varepsilon}^e_{ij} \tag{6.39.2}$$

$$\dot{D} = \sigma_{ij} \dot{\varepsilon}^p_{ij} \tag{6.39.3}$$

where $\dot{E}_e$ is the elastic energy rate per unit volume, $\dot{D}$ is the dissipated energy rate per unit volume, and the usual decomposition of strain rate hold. It is noteworthy that if the body is considered as elastic and total strains are employed, Eq. (6.37) reduces to the energy balance equation of Griffith.

6.5.1.2 Two-Component Damaged Body. Now, we consider the mixture of two components or fractions damaged body as described in the previous sections. Let R', $\partial R'$ denote its volume and boundaries, respectively, and T'_i, F'_i surface tractions and body forces, respectively. Let $\dot{E}'$ denote the rate of work of the external forces which act on an element ΔV of the material, then

A: Potential Crack Extension Sites

B: Unlikely Zone for Crack Extension

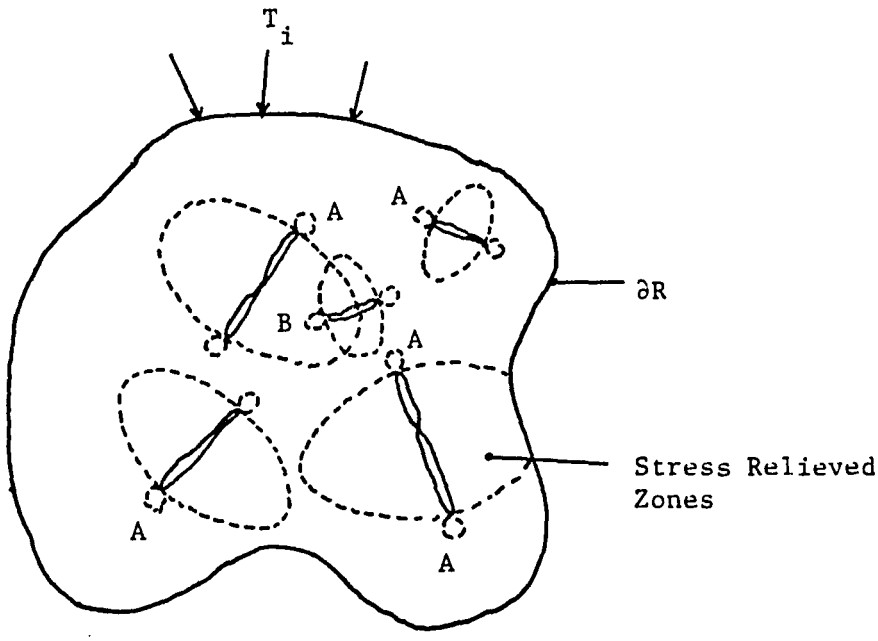

Fig. 6.10 Schematic of Damaged Body with Development of Damaged Zones (Van Mier, 1984)

$$\dot{E}' = \frac{1}{\Delta V} \int_{\Delta V} \sigma_{ij} \dot{\varepsilon}_{ij} \, dV \tag{6.40}$$

Part of this work will be stored as elastic energy and part of it will be dissipated due to the plastic deformations

$$\dot{E}' = \frac{1}{\Delta V} \left[\int_{\Delta V} \sigma_{ij} \dot{\varepsilon}^{e}_{ij} \, dV + \int_{\Delta V} \sigma_{ij} \dot{\varepsilon}^{p}_{ij} \, dV \right] + \dot{Q} \tag{6.41}$$

where $\dot{Q}$ represents the rate of dissipated work in order to transform topical (undamaged) volume into damaged volume. It can be expressed as

$$\dot{Q} = q \dot{V}_o \tag{6.42}$$

where $\dot{V}_o$ is the rate of change V_o; thus, it represents the rate of change of topical volume to damaged volume, and q is the transformation energy per unit volume. The above considerations allow us to conclude that an equation similar to Eq. (6.37) is valid for the damaged body with the following distinguishing differences:

- Instead of $\dot{\Gamma}$ we have $\dot{Q}$
- The internal elastic and plastic rate of energy is the summation of the energies involved in the topical and the damaged part; thus,

$$\dot{E}^{e} = \int_{\Delta V} \sigma_{ij} \dot{\varepsilon}^{e}_{ij} \, dV = \int_{\Delta V_t} \sigma^{t}_{ij} \dot{\varepsilon}^{e}_{ij} \, dV + \int_{\Delta V_o} \sigma_{ij} \dot{\varepsilon}^{e}_{ij} \, dV \tag{6.43.1}$$

$$\dot{D} = \int_{\Delta V} \sigma_{ij} \dot{\varepsilon}^{p}_{ij} \, dV = \int_{\Delta V_t} \sigma^{t}_{ij} \dot{\varepsilon}^{p}_{ij} \, dV + \int_{\Delta V_o} \sigma^{o}_{ij} \dot{\varepsilon}^{p}_{ij} \, dV \tag{6.43.2}$$

6.5.2 Stability of Damage Growth

Following the concepts of fracture mechanics (Davis and Sih, (1965), we consider two cases. Under "fixed grip" conditions, it is assumed that the outer boundary is fixed during damage growth. If, in addition, the body force distribution is ignored, the rate of energy of the applied forces vanishes, and from Eqs. (6.37) and (6.41), we obtain

$$\int_R \dot{E} \, dV + \int_R \dot{D} \, dV + \dot{Q} = 0 \tag{6.44}$$

Here, quasi-static loading are assumed; hence, the rate of kinetic energy is neglected.

Now, by setting

$$\dot{U} = \int_R \dot{E}^{e} \, dV \tag{6.45}$$

$$\dot{H} = \int_{\partial R} T_i \dot{u}_i \, dS + \int_R \rho f_k \dot{u}_k \, dV \tag{6.46}$$

and considering the total potential energy

$$\Pi = U + H \tag{6.47}$$

it follows from Eqs. (6.43) to (6.47) that

$$-\frac{\partial \Pi}{\partial V_o} = \frac{\partial D}{\partial V_o} + \frac{\partial Q}{\partial V_o} = -\frac{\partial U}{\partial V_o} = G \tag{6.48}$$

Here, G is referred to as the strain energy transformation rate. It represents the energy required to transform topical volume to damaged one.

Under "fixed force" (dead load) conditions, the load is kept constant, while the boundary is free to move. For such a case, the work done by the unchanging boundary loads (neglecting body forces) is twice the increase of elastic strain energy, Spooner and Dougill (1975), Bazant and Kim (1979), Eftis and Liebowitz (1975) and Goodier (1968)

$$\frac{\partial H}{\partial V_o} = 2\frac{\partial U}{\partial V_o} \tag{6.49}$$

It follows from Eqs. (6.37), (6.45) and (6.49) that for the fixed force case (quasi-static loading conditions)

$$-\frac{\partial \Pi}{\partial V_o} = \frac{\partial D}{\partial V_o} + \frac{\partial Q}{\partial V_o} = \frac{\partial U}{\partial V_o} = G \tag{6.50}$$

Equation (6.48) or (6.50) are fulfilled during the damage growth. As the damage growth is assumed to be quasi-static,

$$\frac{\partial K}{\partial V_o} = 0 \tag{6.51}$$

and K is the total kinetic energy. If the damage growth occurs, then the kinetic energy is increased so that

$$\frac{\partial^2 K}{\partial V_o^2} > 0 \tag{6.52}$$

and the condition for unstable damage growth reduces to

$$-\frac{\partial^2 \Pi}{\partial (V_o)^2} - \frac{\partial^2 D}{\partial (V_o)^2} - \frac{\partial^2 Q}{\partial (V_o)^2} > 0 \tag{6.53}$$

The above relation represents an analytical criterion similar to the one proposed according to Griffith's theory. Its physical interpretation is similar to the interpretation of unstable crack growth in Griffith's sense.

6.5.3 Discussion

The rate of energy balance for a medium with cracks and for a two-component material were considered. Mathematical similarities in the energy balance equations for the two bodies exist if the following substitutions are made:

$$\dot{\Gamma} \leftrightarrow \dot{Q}$$

$$\dot{A}(t) \leftrightarrow \dot{V}_o\ (t) \tag{6.54}$$

$$\gamma \leftrightarrow q$$

This shows that the phenomenological approach to the crack initiation and growth can be equivalent to a "pure" fracture mechanics approach as far as energy balance is concerned. Also, the damage model captures

other effects of crack initiation and propagation such as degradation of strength, degradation of elastic properties and induced anisotropy. These attributes were discussed previously.

6.6 Multiaxial Stress Paths

In this section, the question of the effect of damage of the stress-strain response is examined with emphasis on the failure behavior. As damage accumulates, the topical volume transforms into damaged volume. Because of this transformation and the increase in the damaged volume, the (remaining) topical volume cannot resist stress and strain as it would have if there were no damage. As a consequence, after damage initiates, the topical volume experiences increased deformations and approaches failure at a faster rate compared to those experienced if no damage occurred.

Let us now consider a material element (specimen). Let a number of cracks exist in the element; thus, damage has already accumulated to a (small) extent. Let this element be subjected to a small increment of deformation. Part of this deformation will be stored in the element as elastic straining. Another part will deform the topical and damaged part plastically. Part of the topical volume will be unable to sustain the increased deformation and the cracks associated with it will extend and/or new cracks will be initiated. Under this extension or formation of cracks, the stresses in the element will be redistributed until the element reaches equilibrium. On the other hand, the increased deformation may be such that an equilibrium state cannot be reached. This will

happen if the stresses in the topical part have reached or are very close to the ultimate yield surface associated with the topical part resulting in failure of the element.

In order to verify the model and illustrate the above failure considerations, the material parameters were determined from available test data for a concrete, given by Van Mier (1984). Next, we consider a uniaxial compression test such that $\sigma_{11} = \sigma$ (compression positive), the other components of σ_{ij} being zero. For these values, Eq. (3.2) yields

$$\sigma_{22}^t = \sigma_{33}^t = -\frac{r}{3\ (1-r)}\sigma \tag{6.55}$$

which indicates that the radial stresses in the topical zone are tensile. This is consistent with experimental observations that show formation of cracks parallel to the loading axis in a uniaxial compression test (e.g., Van Mier, 1984). This phenomenon is usually termed slabbing or bursting.

Figure 6.11 compares the predicted curves for the average and topical responses for a test such that $\sigma_1/\sigma_2 = 1/0.33$ and $\sigma_1/\sigma_3 = 1/0.05$. It is seen that although the response is softening, the topical response is hardening. Figure 6.12 shows the topical and average stress paths in J_1 vs. $\sqrt{J_{2D}}$ space. Point A corresponds to the peak value of the average stress. In the prepeak region, the average stress follows oath OA. In the post peak (softening) region, the average path follows path AB. Because of damage accumulation, the topical stress path,

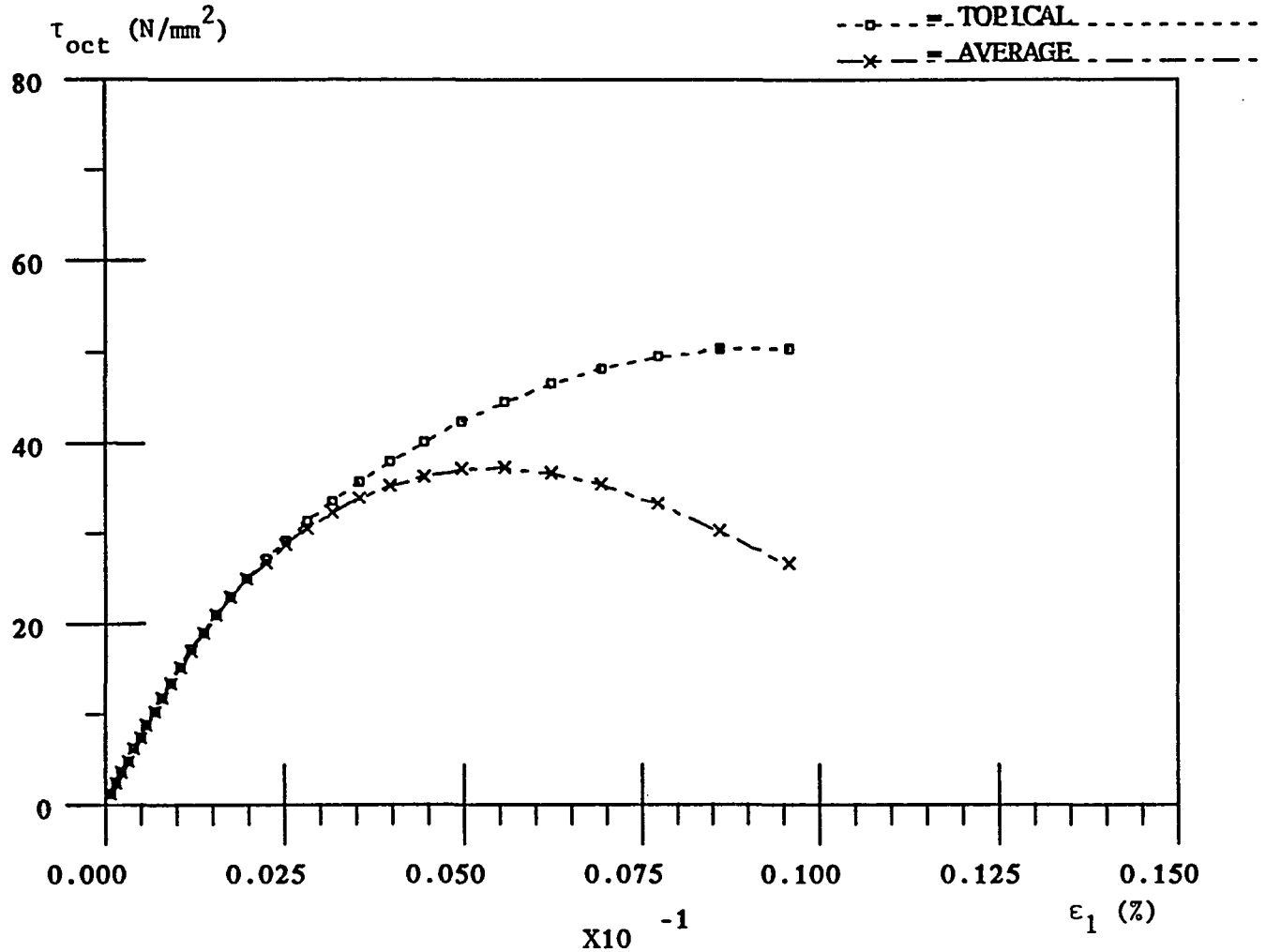

Fig. 6.11 Comparison of Topical and Average Responses

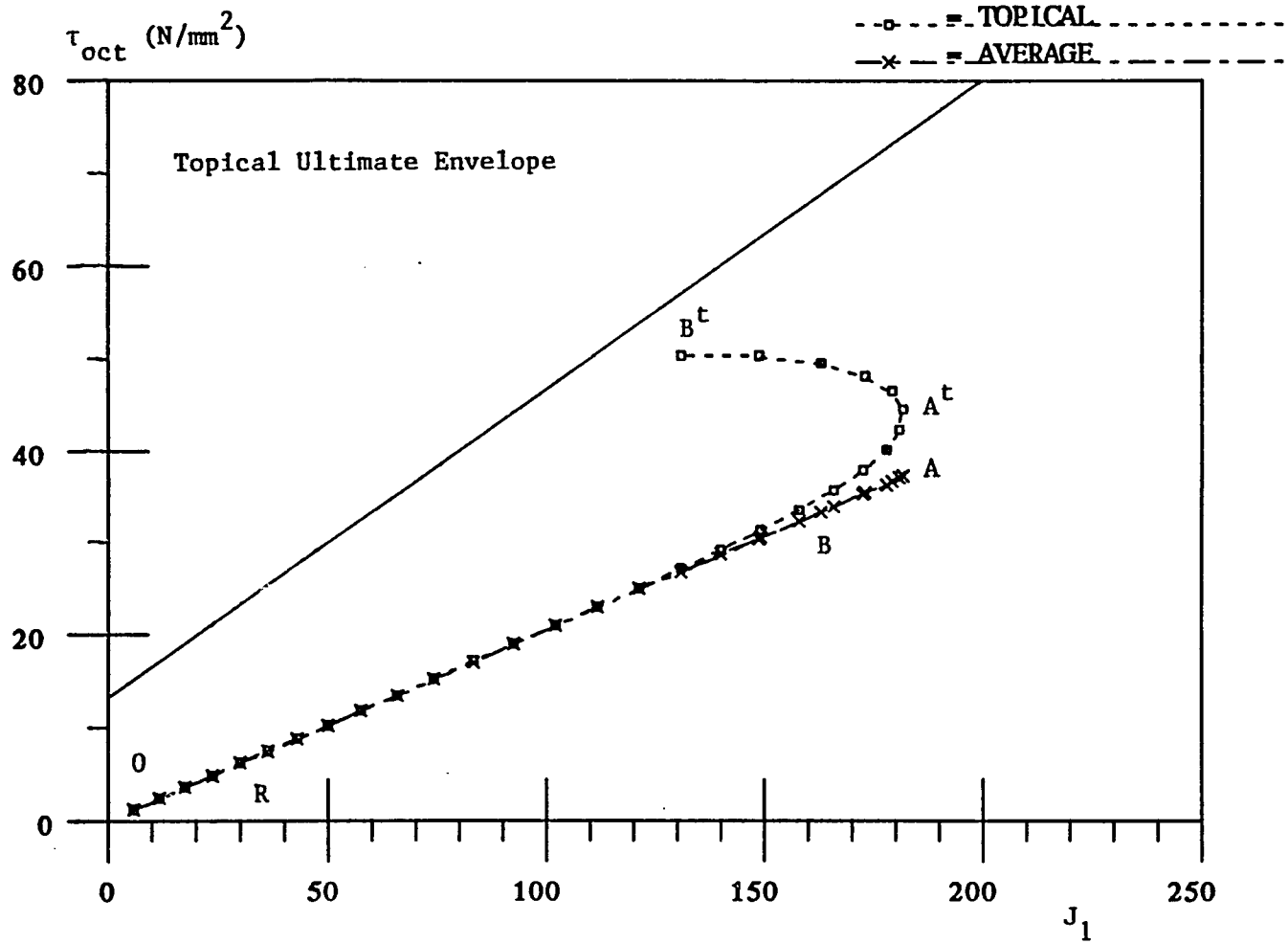

Fig. 6.12 Comparison of Topical and Average Stress Paths

$OA^t\ B^t$, is different than that of the average stress path, OAB; the hydrostatic part of the topical stress is decreasing after the peak. The rate at which the topical response approaches the ultimate conditions (Fig. 6.12) increases with increasing damage accumulation. Also, the damage accumulates faster in the post peak region than in the pre-peak region. Note that in the absence of damage, the topical and average stress path would be identical following line OA, and after point A is reached, the response would continue to be hardening (not softening); thus, the stress would extend beyond point A along line OA. Damage; that is, $r \geq 0$, initiates at point R, at which the shear stress is about 30% of the stress at peak. This is consistent with experimental observations, Van Mier (1984).

CHAPTER 7

VERIFICATION OF THE MODEL

7.1 Integration of the Constitutive Relations

The constitutive relations derived previously can be written in incremental form; matrix notation is used herein

$$\{d\sigma\} = [L]\{d\varepsilon\} - dr\{S\} \tag{7.1}$$

This equation describes a set of nonlinear differential equations involving stress and strain. Integration of Eq. (7.1) along a loading path yields the total stress and strains.

A computer procedure is developed (using Fortran) for the numerical integration of Eq. (7.1). This routine is similar to an integration routine for elastoplastic incremental equations. Important features of the integration of elastoplastic incremental equations are discussed in detail by Faruque (1983) and Faruque and Desai (1985). In a numerical scheme such as the finite element method, the increments of strain $\{d\varepsilon\}$ are obtained. From this increment of strain, the increment in topical stress is calculated through Eq. (3.3), and subsequently the elastic strains are computed from Eq. (3.4). Through Eq. (4.13) the increment of plastic strains is obtained and subsequently the increment dr is calculated from Eq. (3.23). Finally, the increments of stress $\{d\sigma\}$ are calculated from Eq. (7.1).

The increments of strain, $\{d\varepsilon\}$, obtained from a numerical scheme such as the finite element method, may not be small enough, such that convergence is assured. Thus, the computed stresses may be far from being accurate. There are a number of techniques available to correct the stresses within an increment; for example, subincrementation techniques (Faruque, 1983).

7.2 Laboratory Test Data

Here a description of the materials used for verification of the model is given. The constants for these materials were described in Chapter 5. Verification with respect to joints as well as description of the materials used are given in Chapter 8.

7.2.1. Concrete

Cubical concrete specimens were tested by Van Mier (1984). The size of the cubes was 100 x 100 x 100mm. For all the tests, the same concrete mix was used. The maximum aggregate size was 16mm. The ratio between cube size used and maximum aggregate was equal to 6 ~ 7. The cement content was 320 kg/m^3, the type of cement being an ordinary Portland cement (type A). The water cement (W/C) ratio was 0.50. The specimens were cast in stiff molds and during casting the specimens were vibrated on a vibrating table for 180 seconds. Approximately one hour after casting, the specimens were vibrated again for 120 seconds. The casting surfaces were finished and the specimens were placed under a plastic cap to avoid drying out. After 28 days, the prisms were sawn.

After grinding them, the specimens were sealed in plastic bags and placed in a room with constant temperature at 20°C. During sawing and grinding, care was taken that the specimens were always in a wet condition.

A truly triaxial servo-controlled machine was used for testing of the cubical specimens. The three loading axes are not connected to each other and can be independent. Forces were measured by means of calibrated load cells. Deformations were measured using three different methods, depending upon the type of test. Details of the concrete and the testing devices used are given by Van Mier (1984).

Figure 7.1 shows the comparison of the prediction and the observation for a loading test such that $\sigma_1/\sigma_2 = 10$ and $\sigma_2 = \sigma_3$. In Fig. 7.1a, the curve for major strain ε_1 vs. τ_{oct} is plotted, while in Fig. 7.1b, the plot of minor strain $\varepsilon_2 = \varepsilon_3$ vs. τ_{oct} is shown. Finally, in Fig. 7.1c, the comparison between prediction and observation of volume changes during loading is shown. It is seen from Fig. 5.3 that a good agreement is achieved between prediction and observation.

Figure 7.2 shows the stress-strain response curves for a uniaxial compression test. It is noted that in the softening regime, the volume changes are negative (dilation). The predictions here compare well with the experimental results.

Figure 7.3 shows the comparison of the stress-strain and volumetric responses for a test such that $\sigma_1/\sigma_2 = 1.0/0.33$ and $\sigma_1/\sigma_3 = 1.0/0.05$. The initial confining pressure is 0.0 kpa.

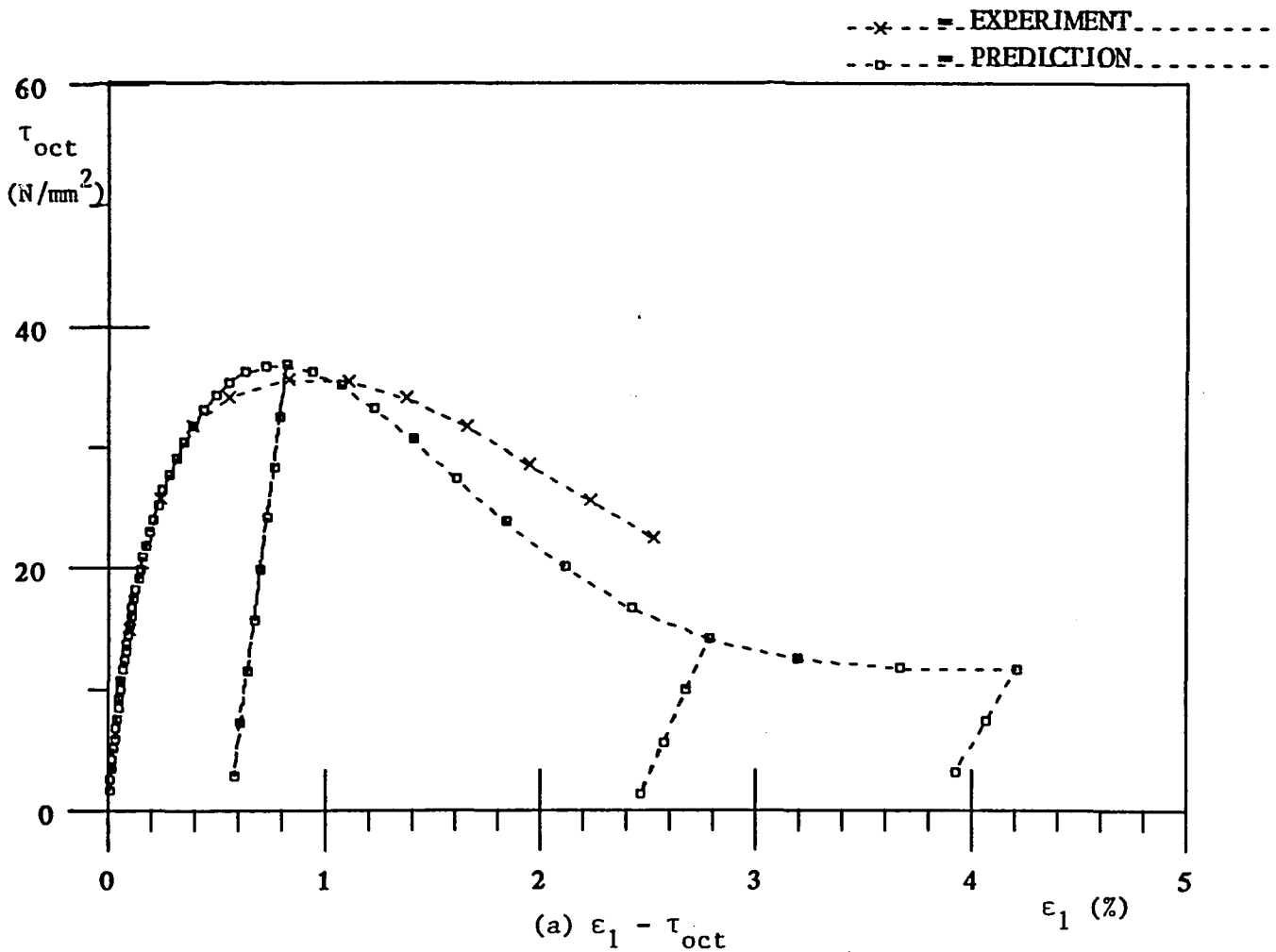

Fig. 7.1 Comparison for Triaxial Constant Stress Ratio, Concrete Test $\sigma_1/\sigma_2 = \sigma_1\ \sigma_3 = 1.0/0.1$

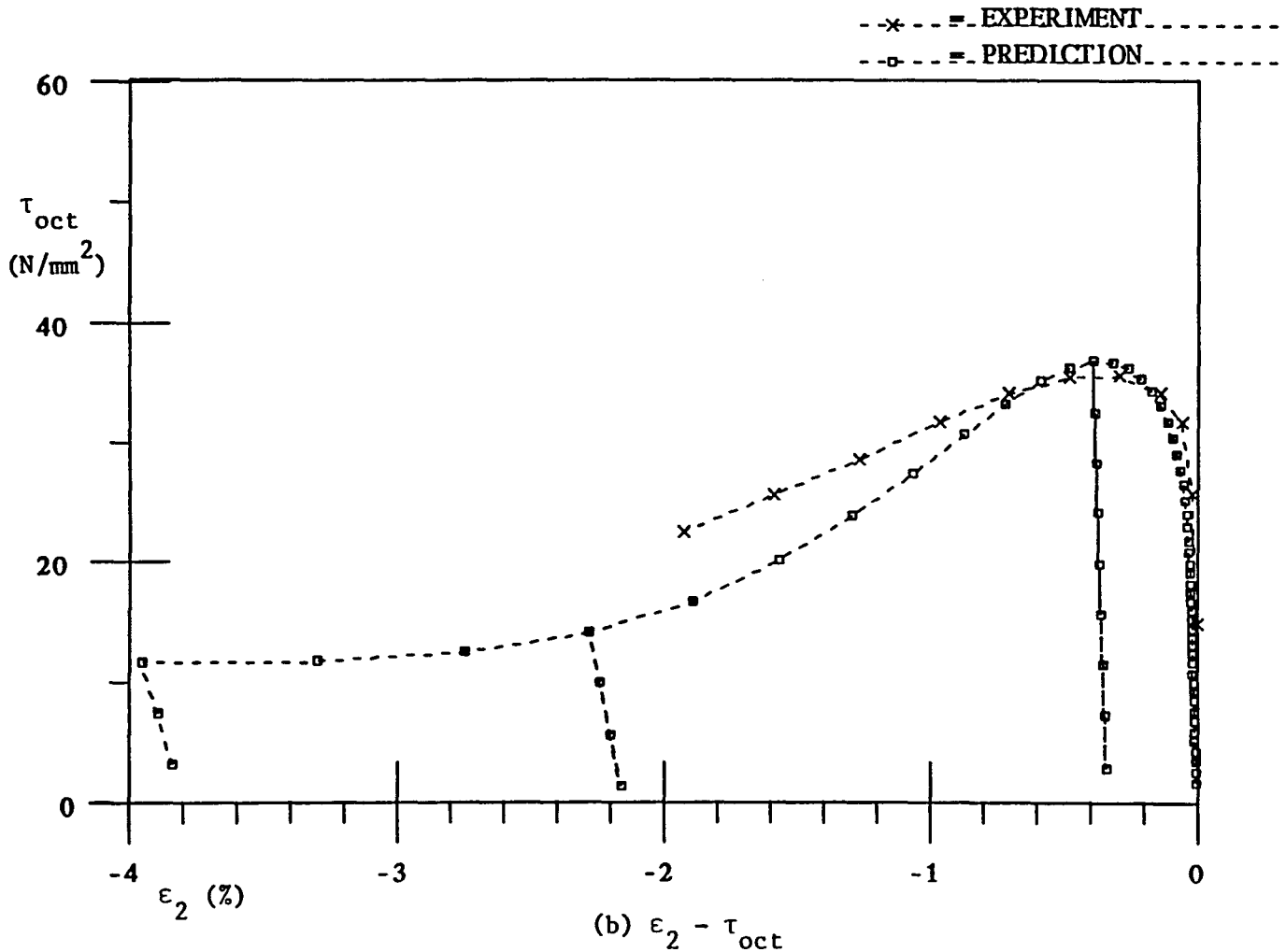

Fig. 7.1 (Continued)

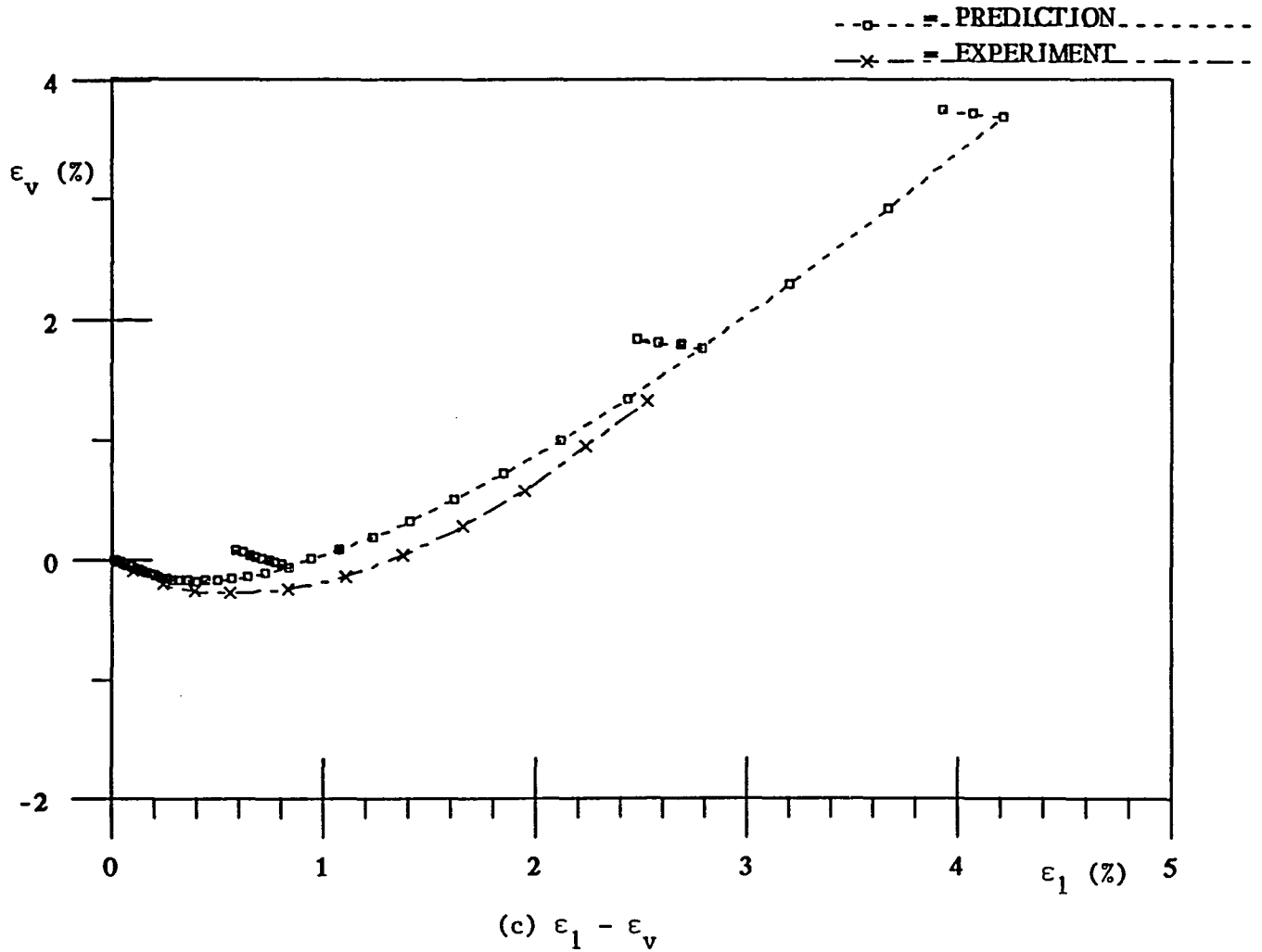

(c) $\varepsilon_1 - \varepsilon_v$

Fig. 7.1 (Continued)

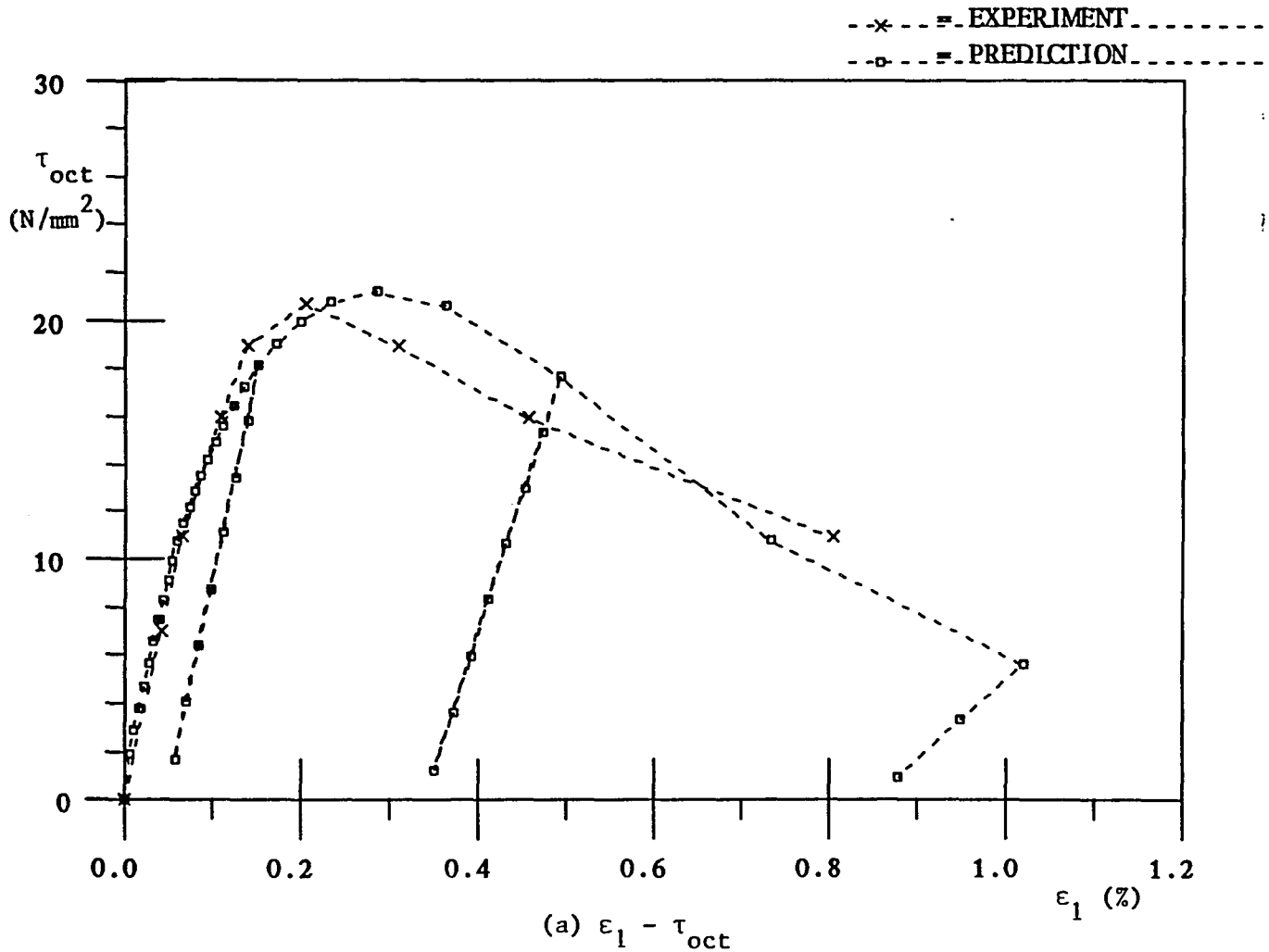

Fig. 7.2 Comparison for Uniaxial Compression Test, Concrete

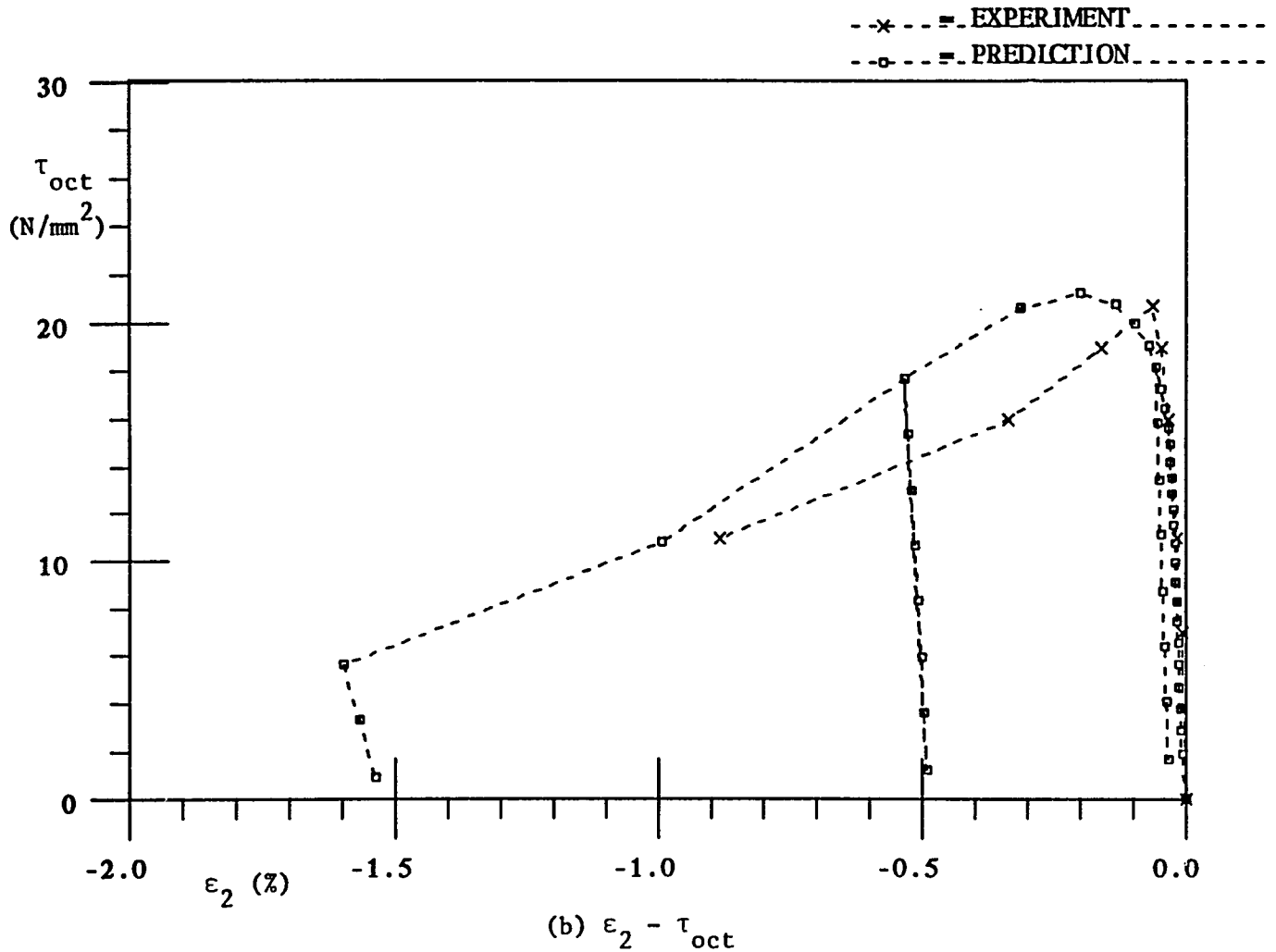

(b) $\varepsilon_2 - \tau_{oct}$

Fig. 7.2 (Continued)

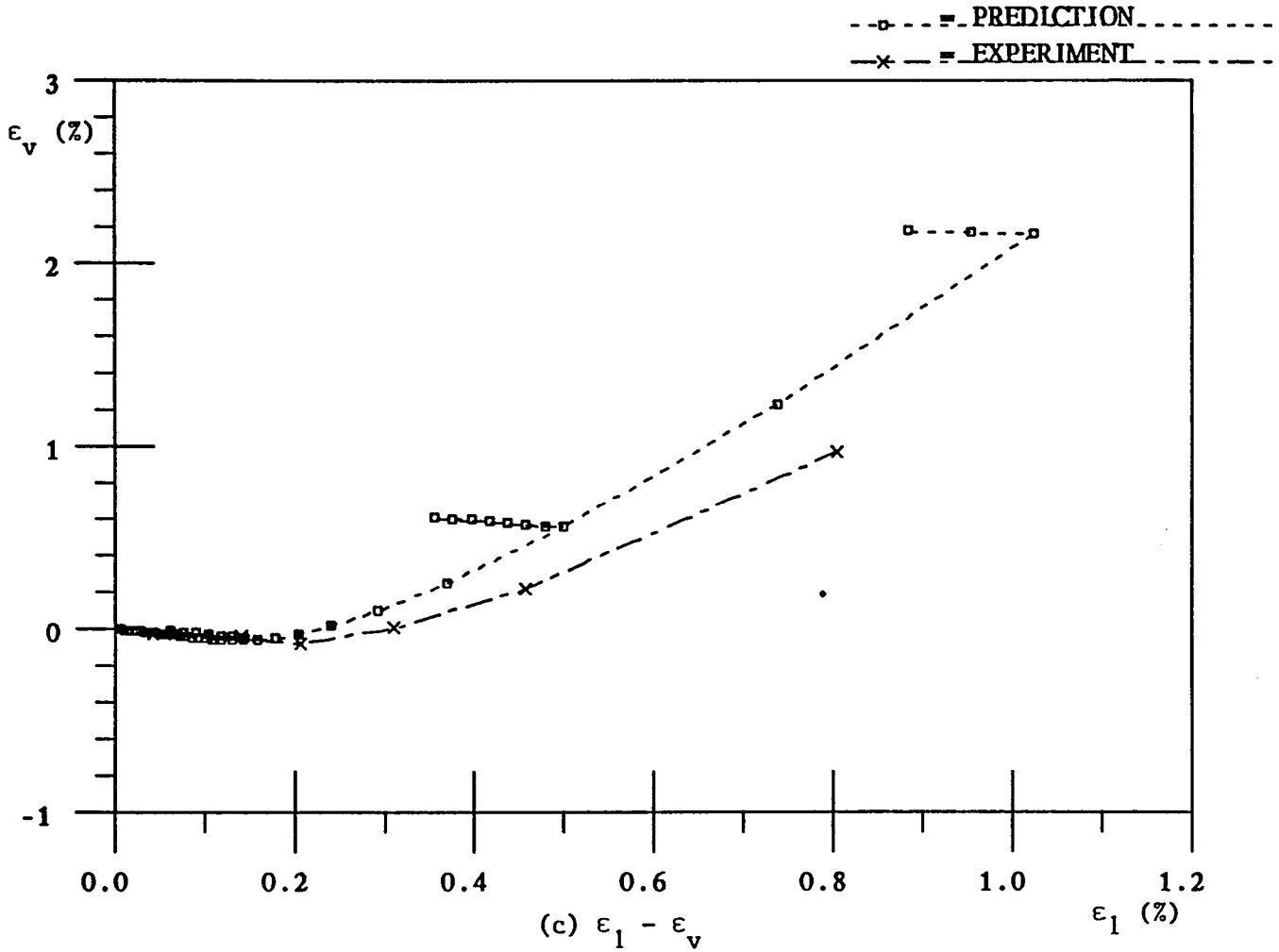

Fig. 7.2 (Continued)

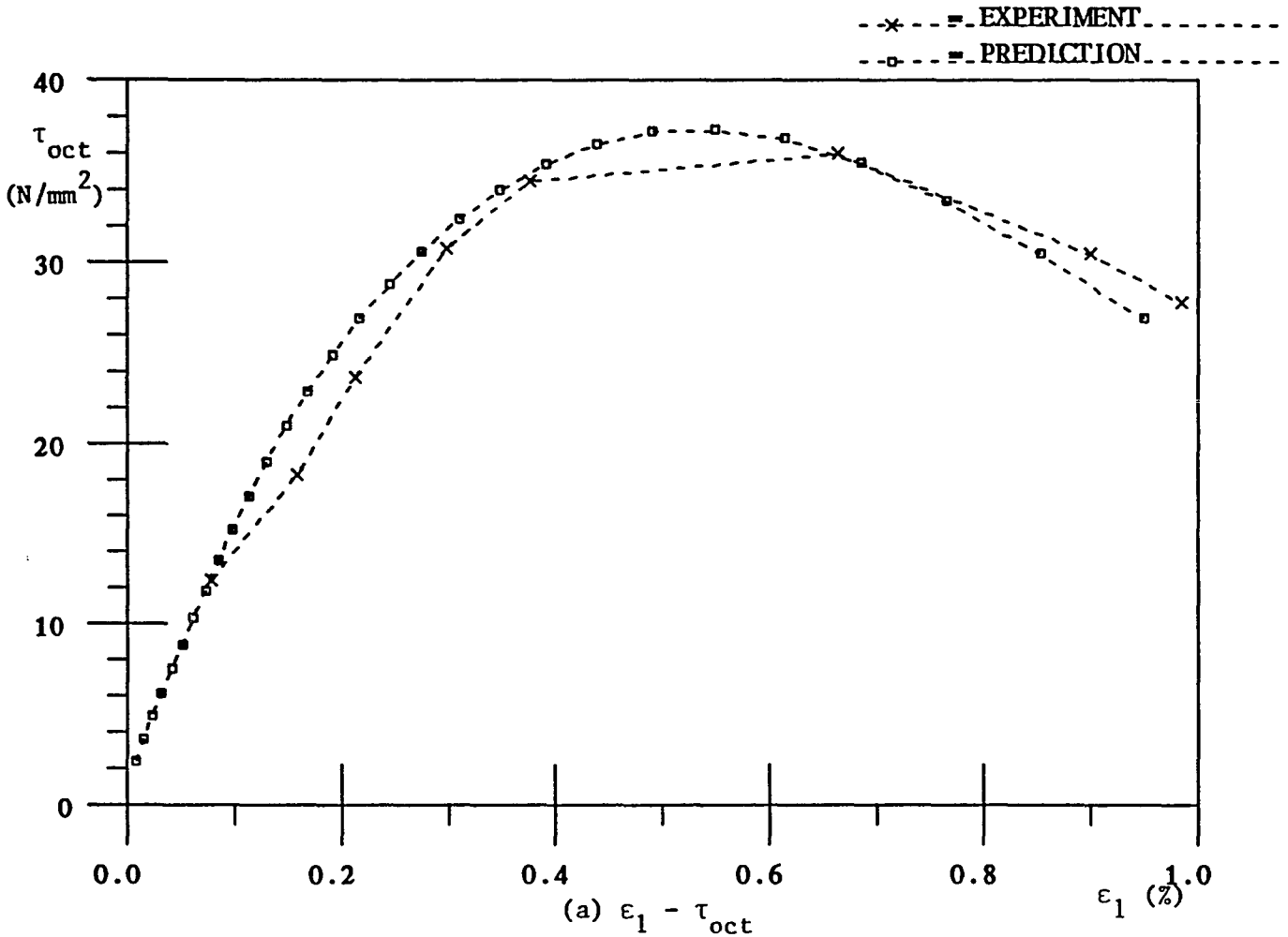

(a) $\varepsilon_1 - \tau_{oct}$

Fig. 7.3 Comparison for Triaxial Constant Stress Ratio Test, Concrete, $\sigma_1/\sigma_2 = 1/0.33$, $\sigma_1/\sigma_3 = 1/0.05$

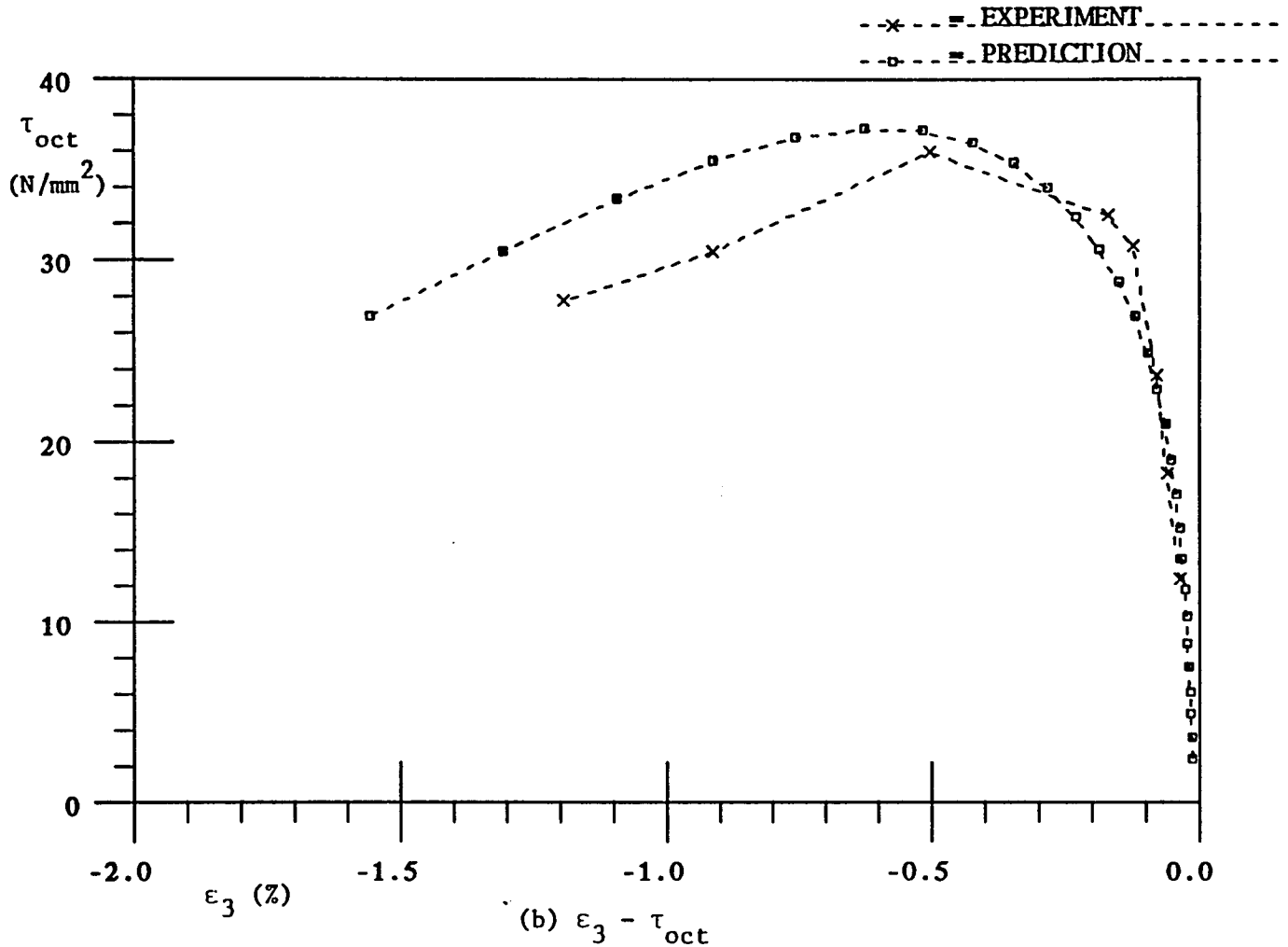

Fig. 7.3 (Continued)

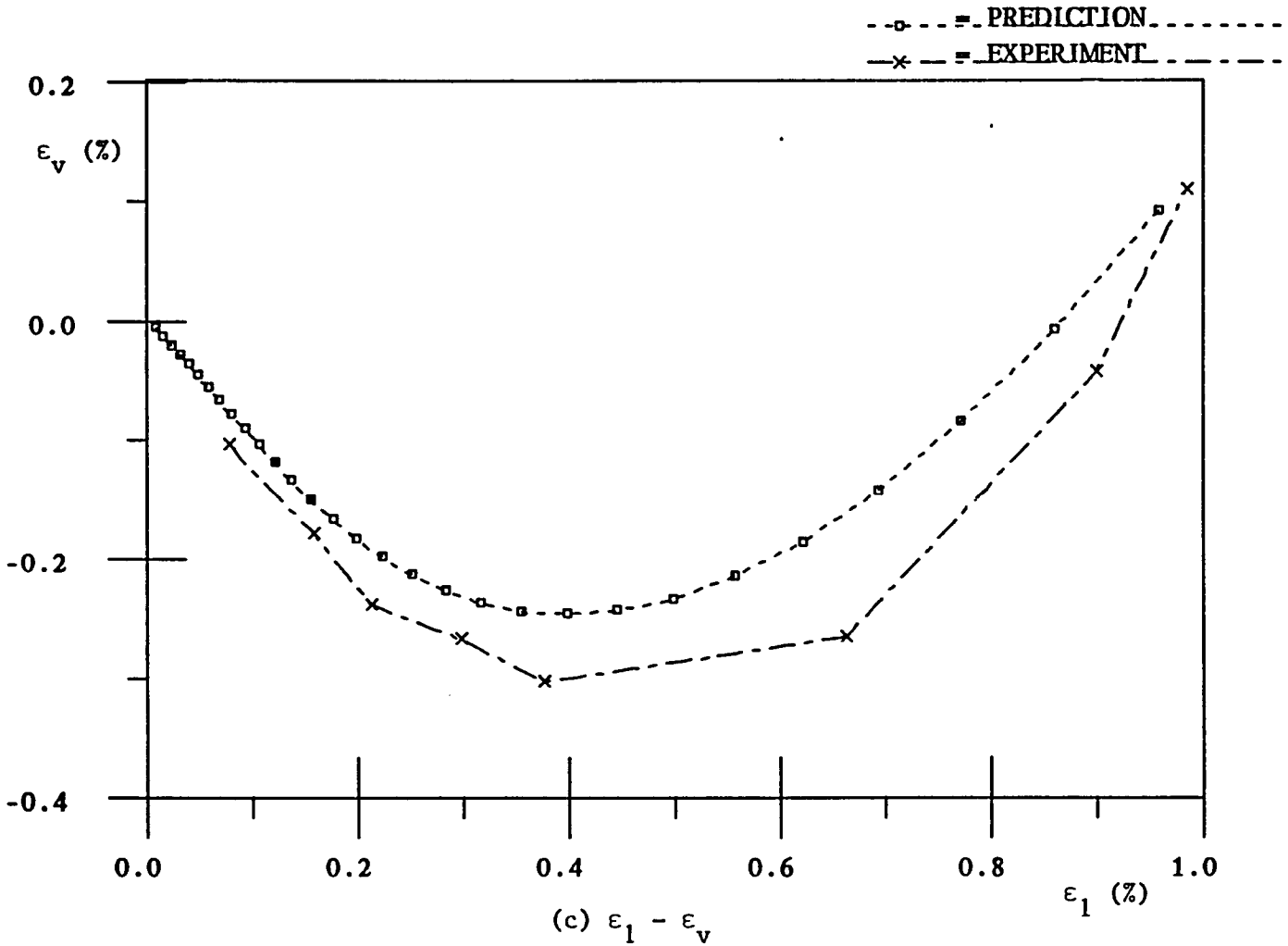

Fig. 7.3 (Continued)

Figure 7.4 shows the comparisons for a nonproportional loading test. This test was performed such that the ratio between the applied displacements remained constant such that $u_1/u_2 = 1.0/0.1$ and $u_1/u_3 = 1.0/0.1$. It is evident from these figures that the predictions from the model compare well with the experimental results. Aspects related to failure and topical prefailure stress paths for the above tests were discussed in Chapter 6.

7.2.2. Cohesionless Soil

The material constants for this soil were given in Chapter 5. The test results were reported by Lee and Seed (1967). The soil used was a fine uniform sand from the Sacramento River. The specific gravity and limiting void ratios were $G_s = 2.68$, $e_{min} = 0.61$ and $e_{max} = 1.03$. For the dense samples, the initial density $e_i = 0.61$; the above being the maximum obtainable density.

All tests were performed in a triaxial compression chamber on specimens which were initially 1.40 in (3.56 cm) in diameter and 3.4 in (8.64 cm) high. The sides of the mold were vibrated sufficiently to densify the sand to the desired condition. The axial strain of a number of samples was measured when compressed under equal all-round confining pressure and compared to the volumetric strain measured with the burette. Details of the soil and experimental devices used are given by Lee and Seed (1967).

Figure 7.5 shows the comparison between the predicted and observed stress-strain responses for a test with initial confining

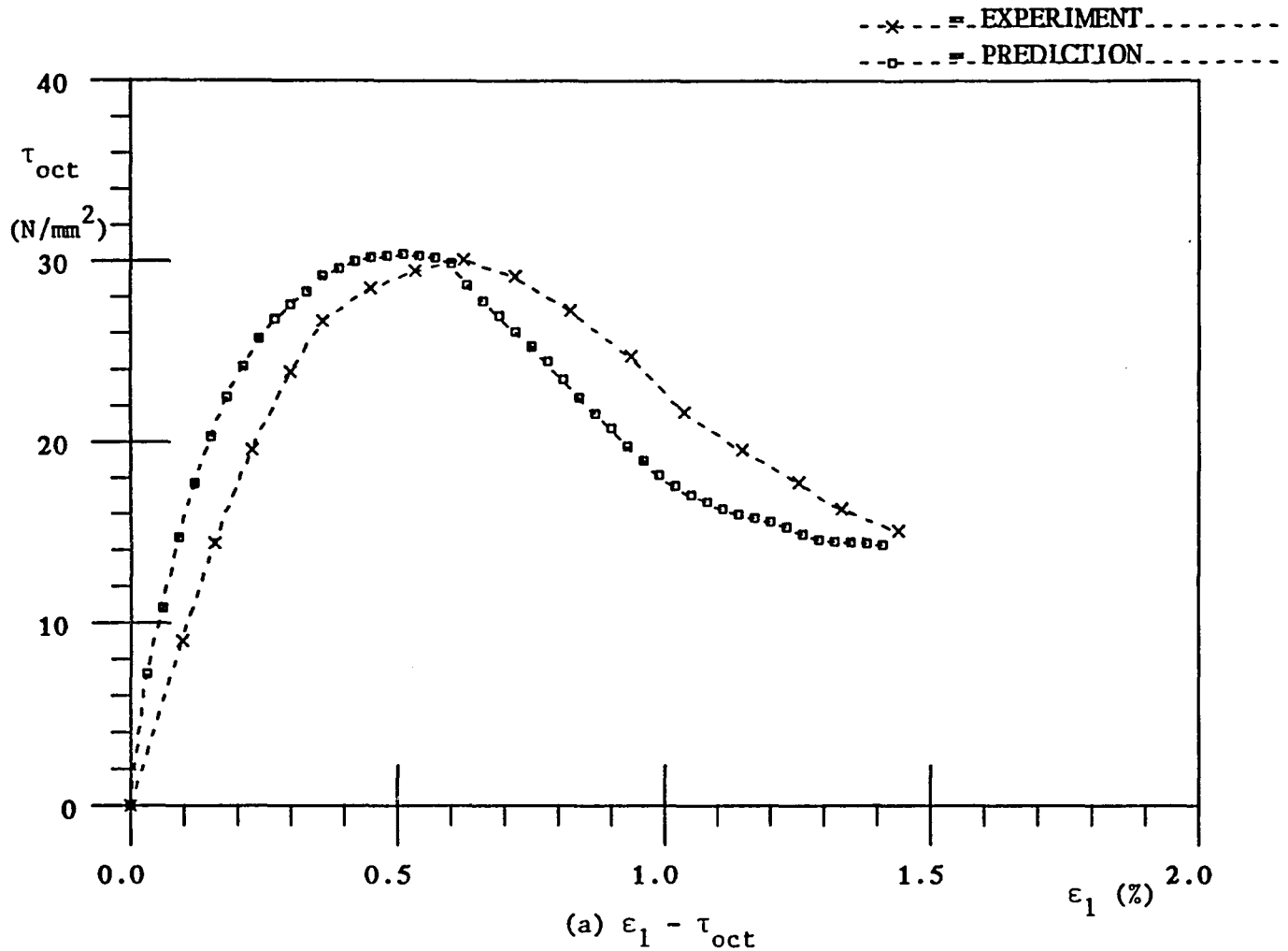

Fig. 7.4 Comparison for a Test Such That σ_1/σ_2 = 0.1/1.0, σ_3/σ_1 = 0.05, Concrete

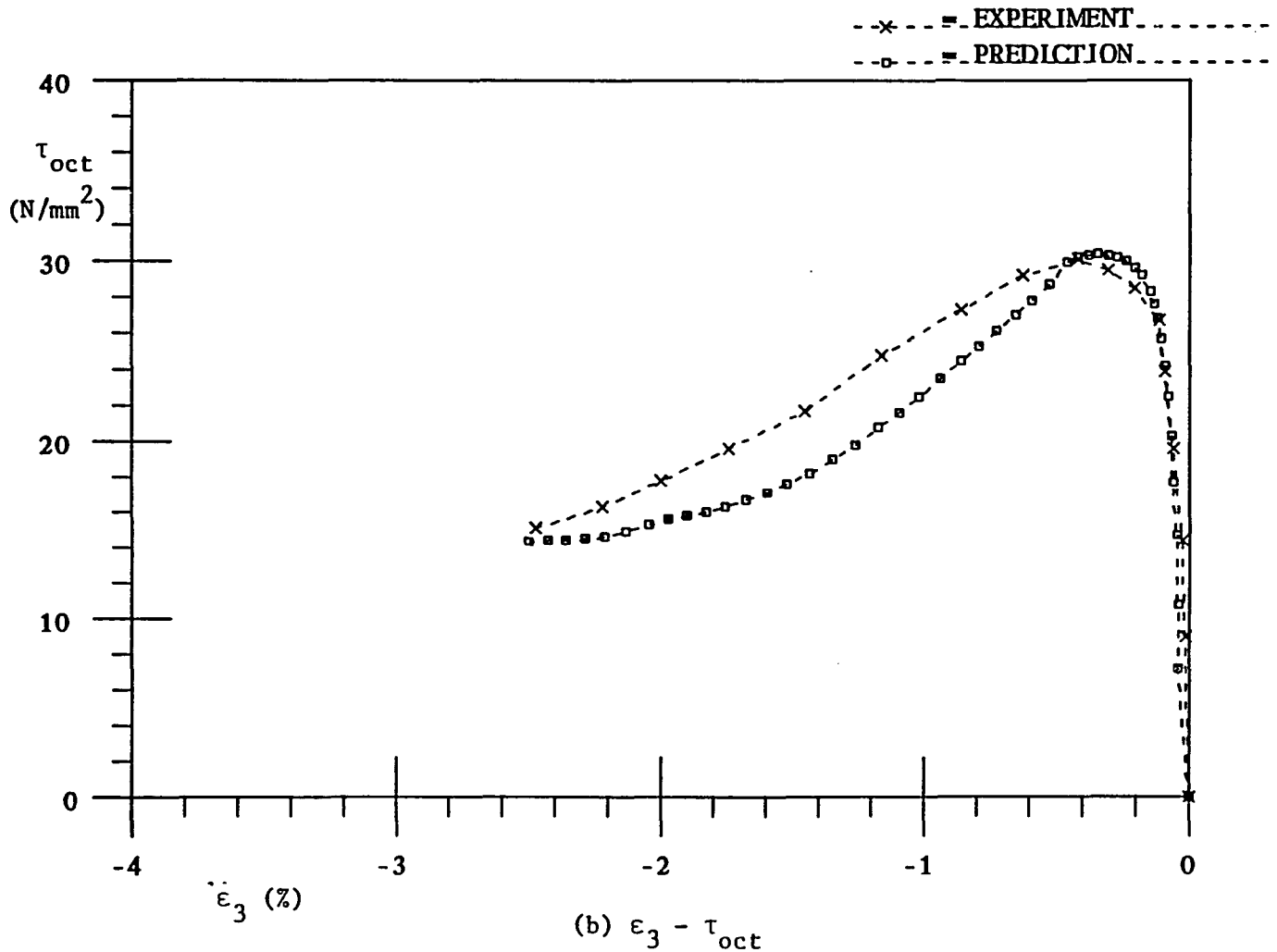

(b) ε_3 - τ_{oct}

Fig. 7.4 (Continued)

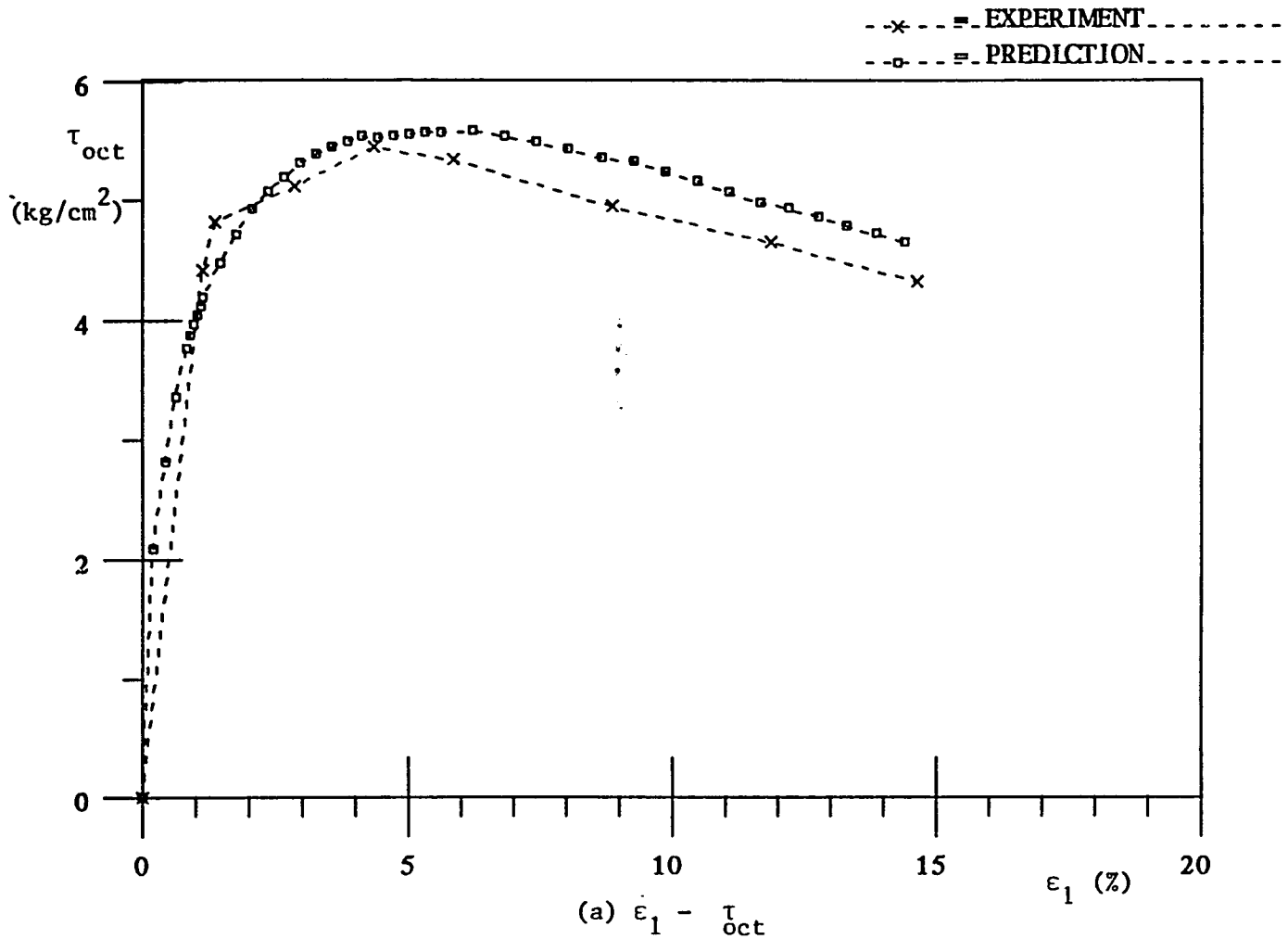

Fig. 7.5 Comparison for Drained Triaxial Compression Test, Soil, σ_o = 3 kg/cm^2

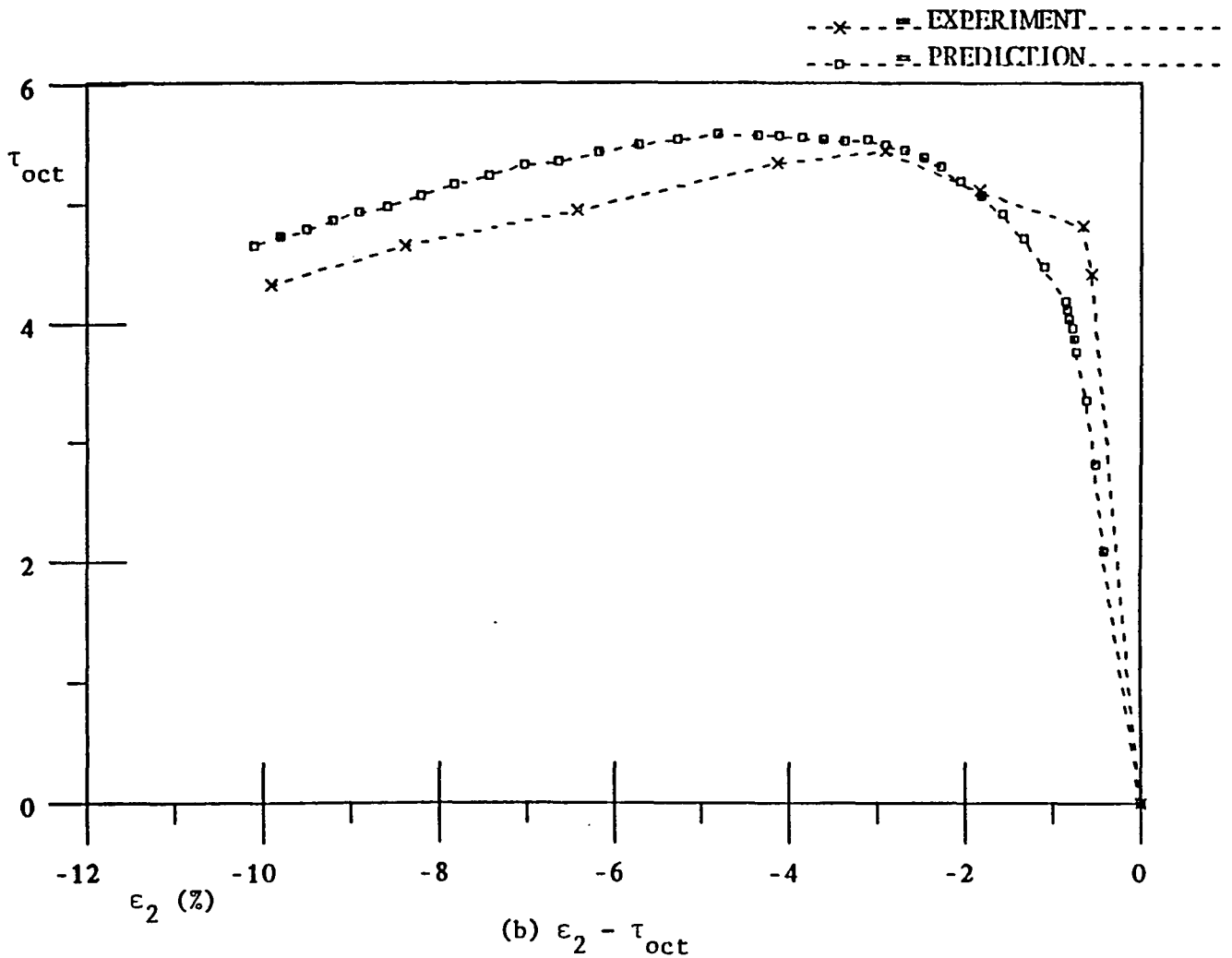

(b) $\varepsilon_2 - \tau_{oct}$

Fig. 7.5 (Continued)

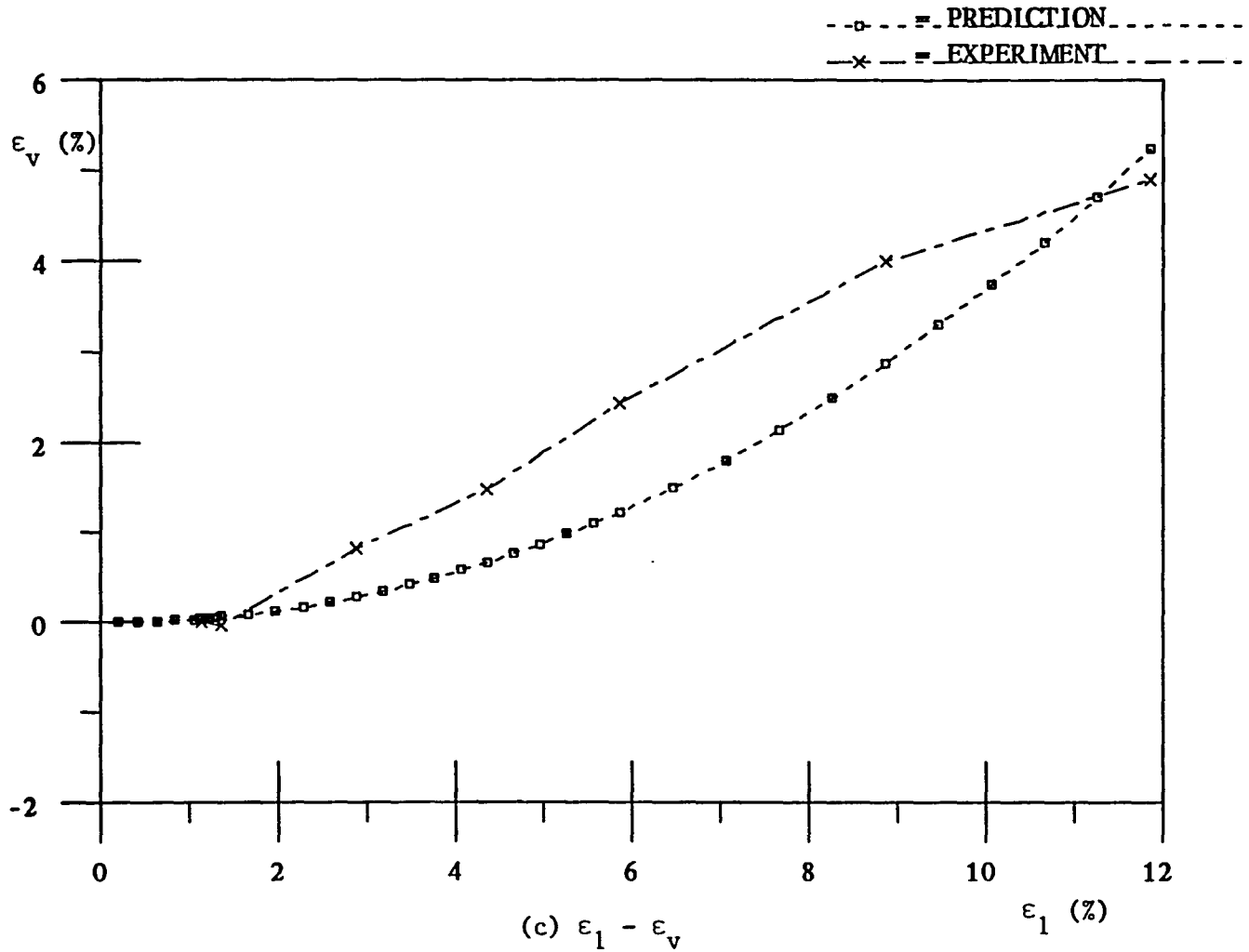

(c) $\varepsilon_1 - \varepsilon_v$

Fig. 7.5 (Continued)

pressure σ_o = 3 kg/cm^2. The comparison of stress-strain and volumetric response is good. Figures 7.6 through 7.8 show the stress-strain and volumetric response curves for conventional triaxial compression (CTC) tests at initial confining pressure of 6 kg/cm^2, 10.5 kg/cm^2 and 20 kg/cm^2, respectively. It is evident from the above figures that the predicted stress-strain and volumetric responses are in agreement with the experimental results.

7.2.3. Comments

In the above comparisons for concrete and soil, the material constants were determined from the first two tests presented. These constants were then used for back prediction of other tests that were not used for finding the constants.

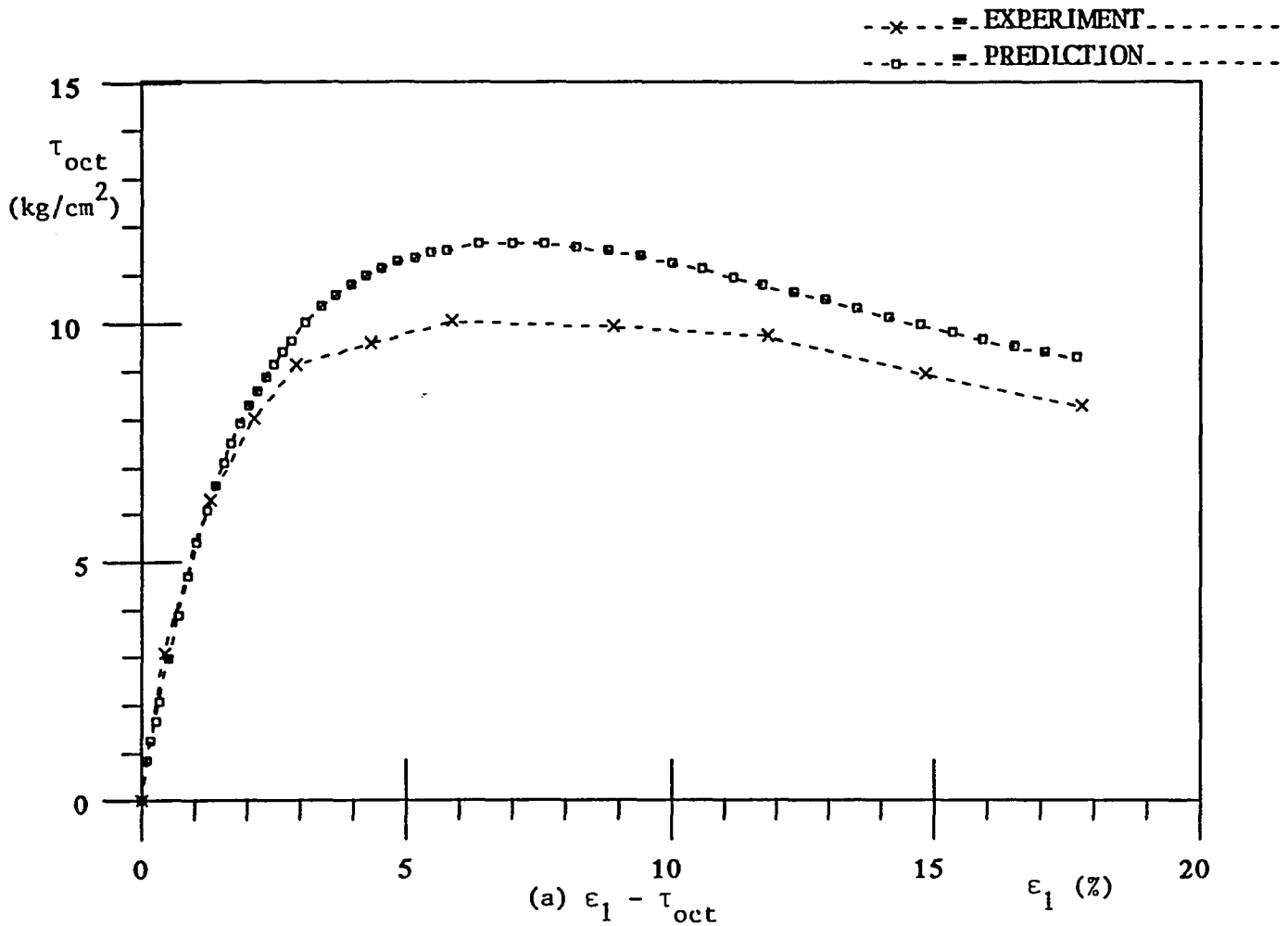

Fig. 7.6 Comparison for Drained Triaxial Compression Test, Soil, σ_o = 6 kg/cm^2

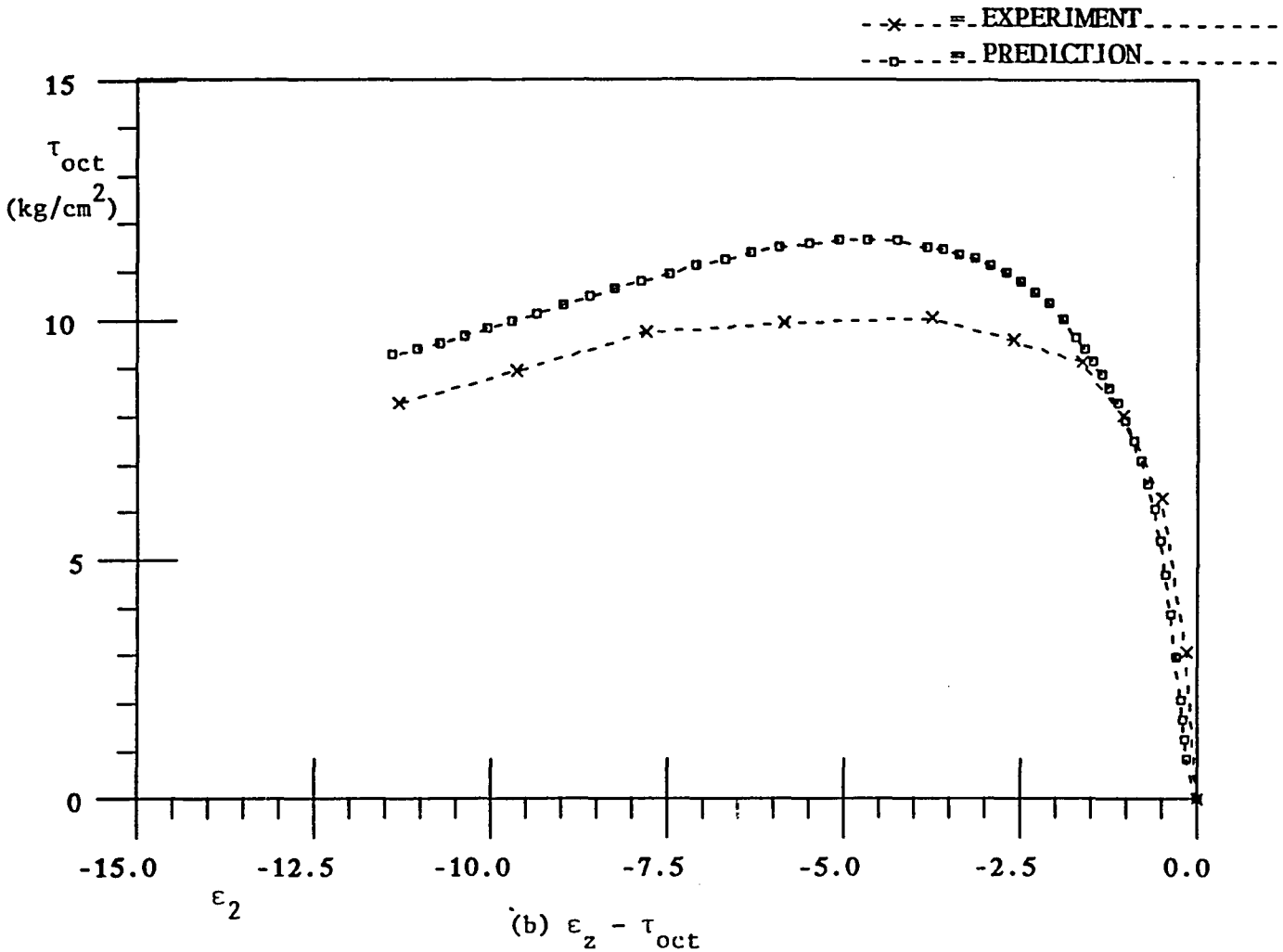

Fig. 7.6 (Continued)

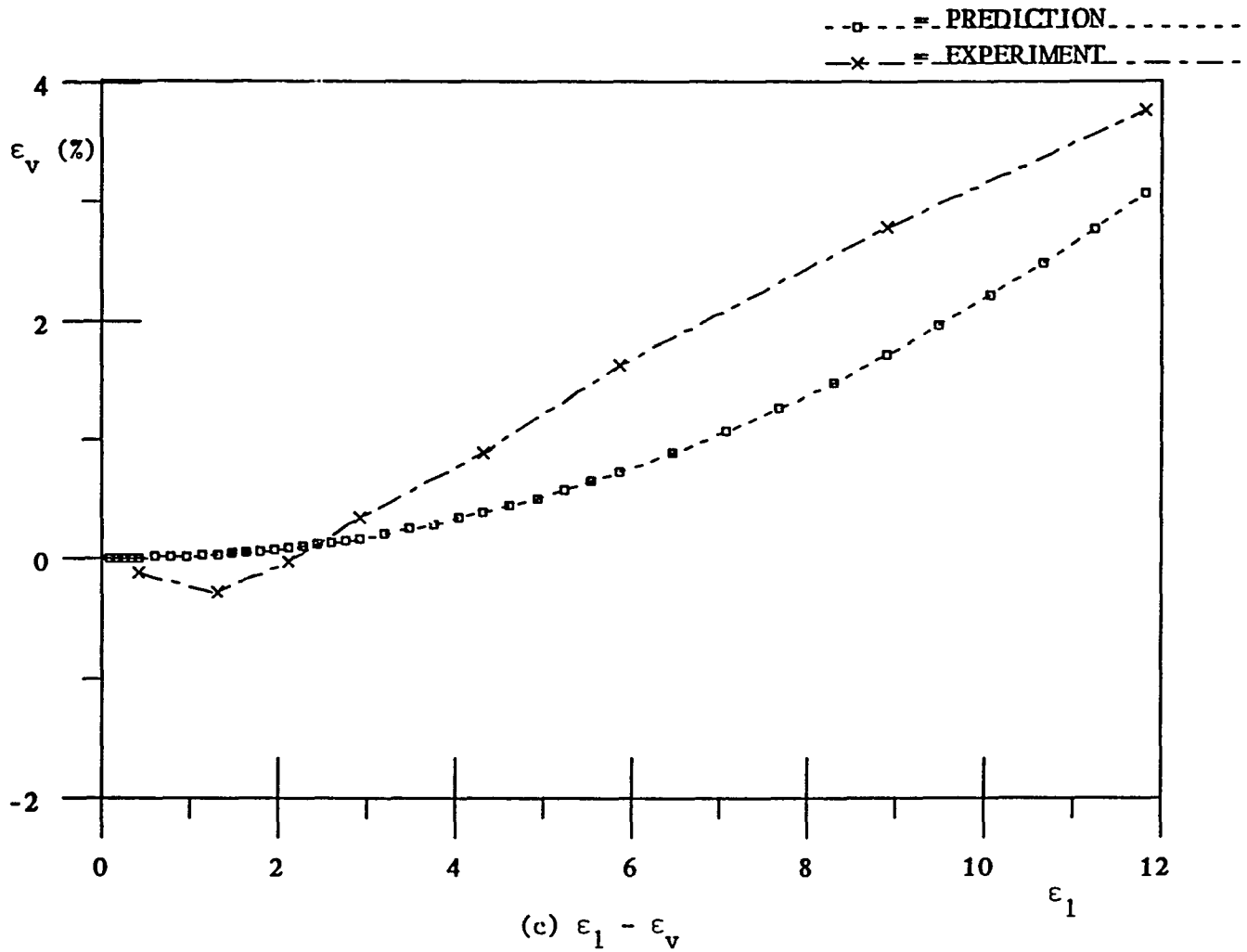

(c) $\varepsilon_l - \varepsilon_v$

Fig. 7.6 (Continued)

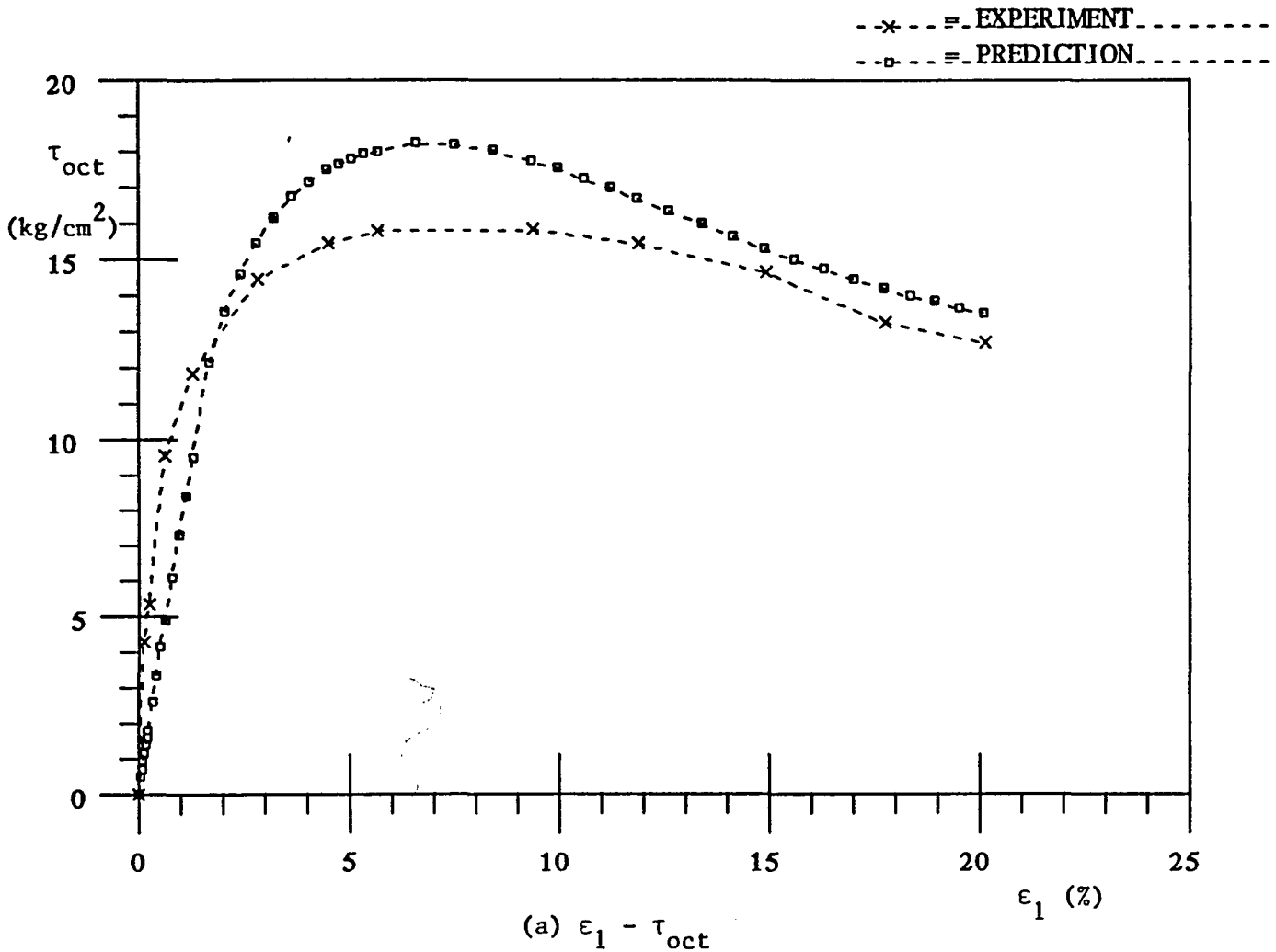

(a) $\varepsilon_1 - \tau_{oct}$

Fig. 7.7 Comparison for Drained Triaxial Compression Test, Soil, σ_o = 10.5 kg/cm^2

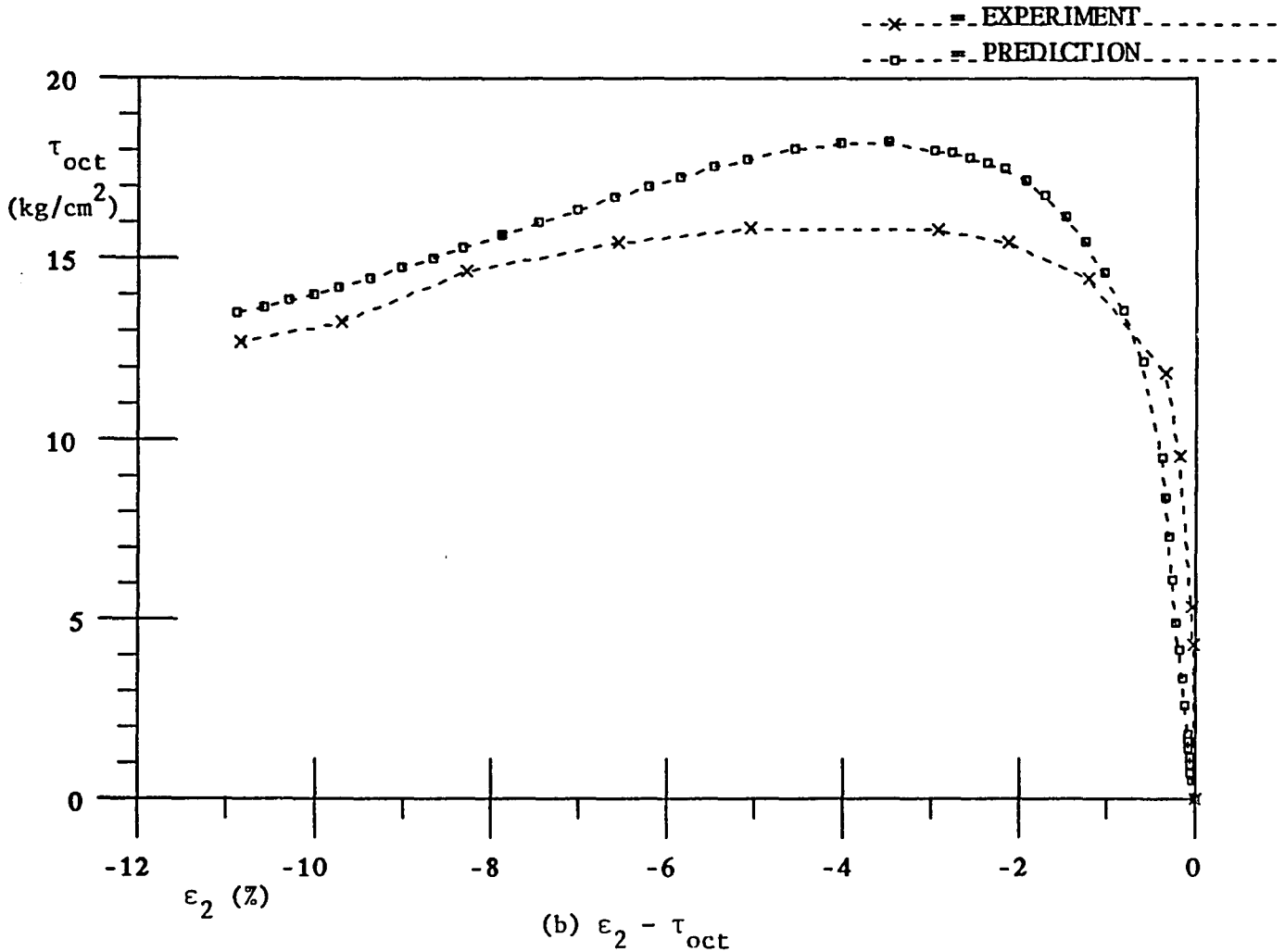

(b) ε_2 - τ_{oct}

Fig. 7.7 (Continued)

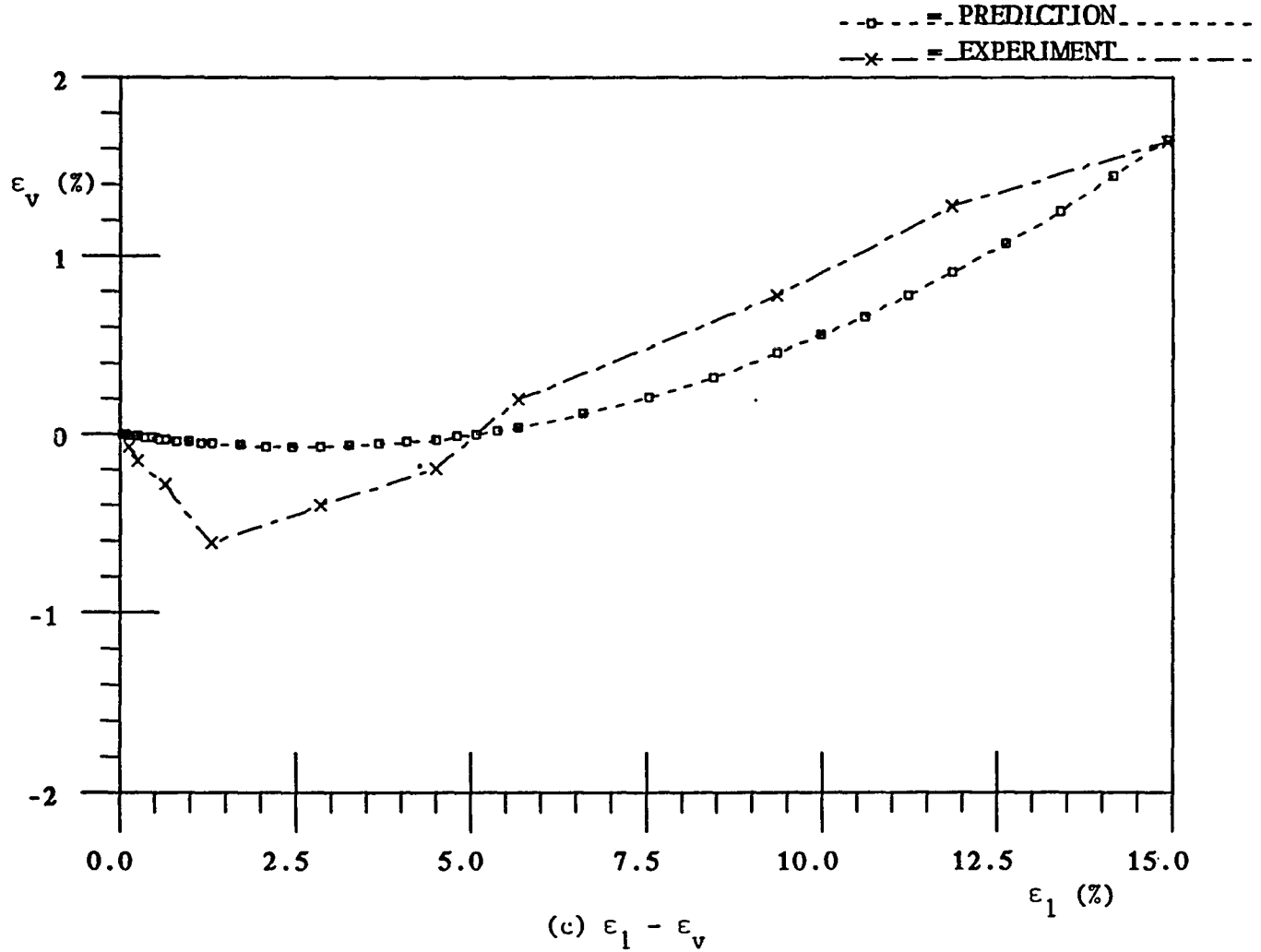

(c) $\varepsilon_1 - \varepsilon_v$

Fig. 7.7 (Continued)

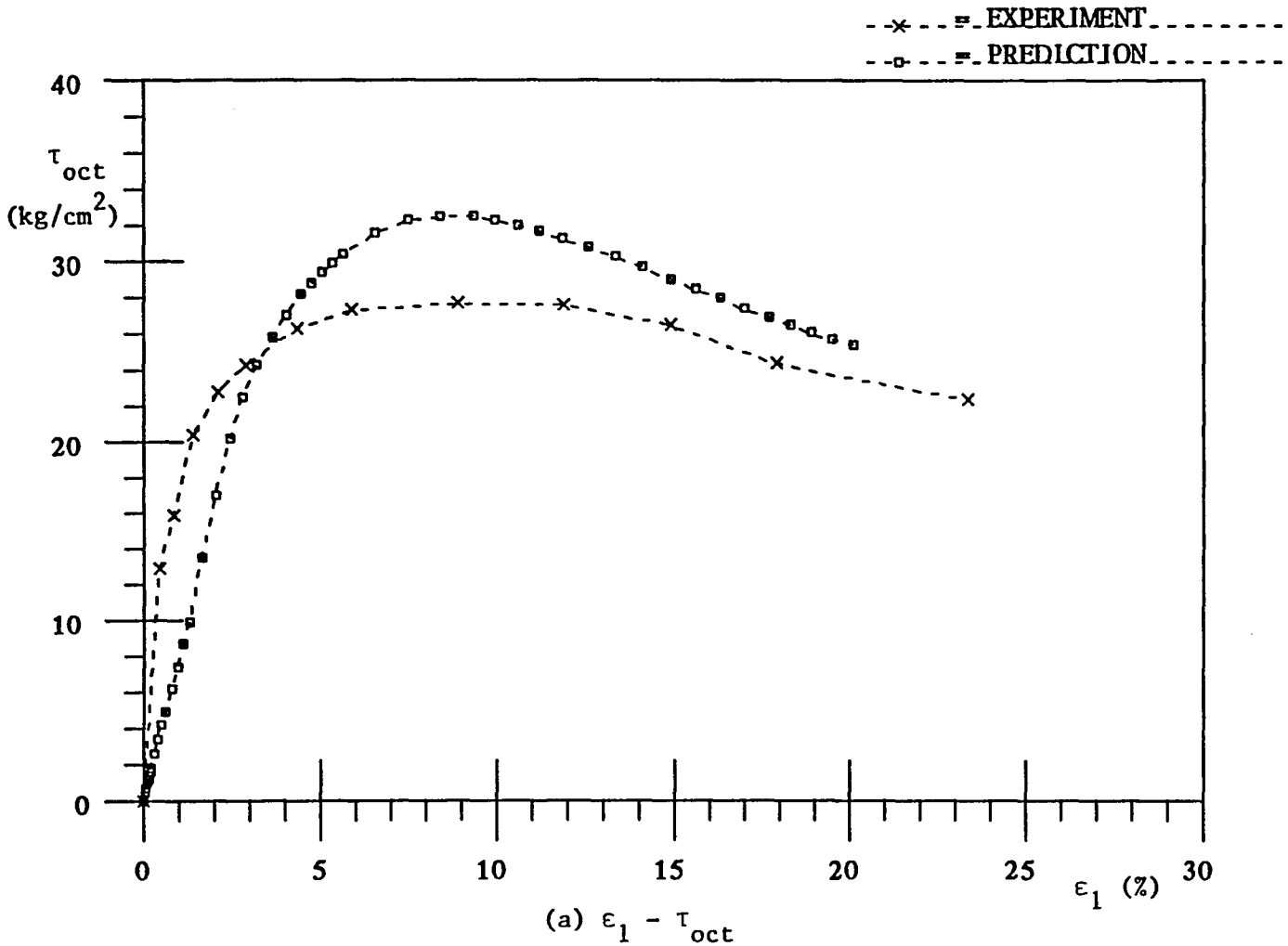

Fig. 7.8 Comparison for Drained Triaxial Compression Test, Soil, σ_o = 20 kg/cm^2

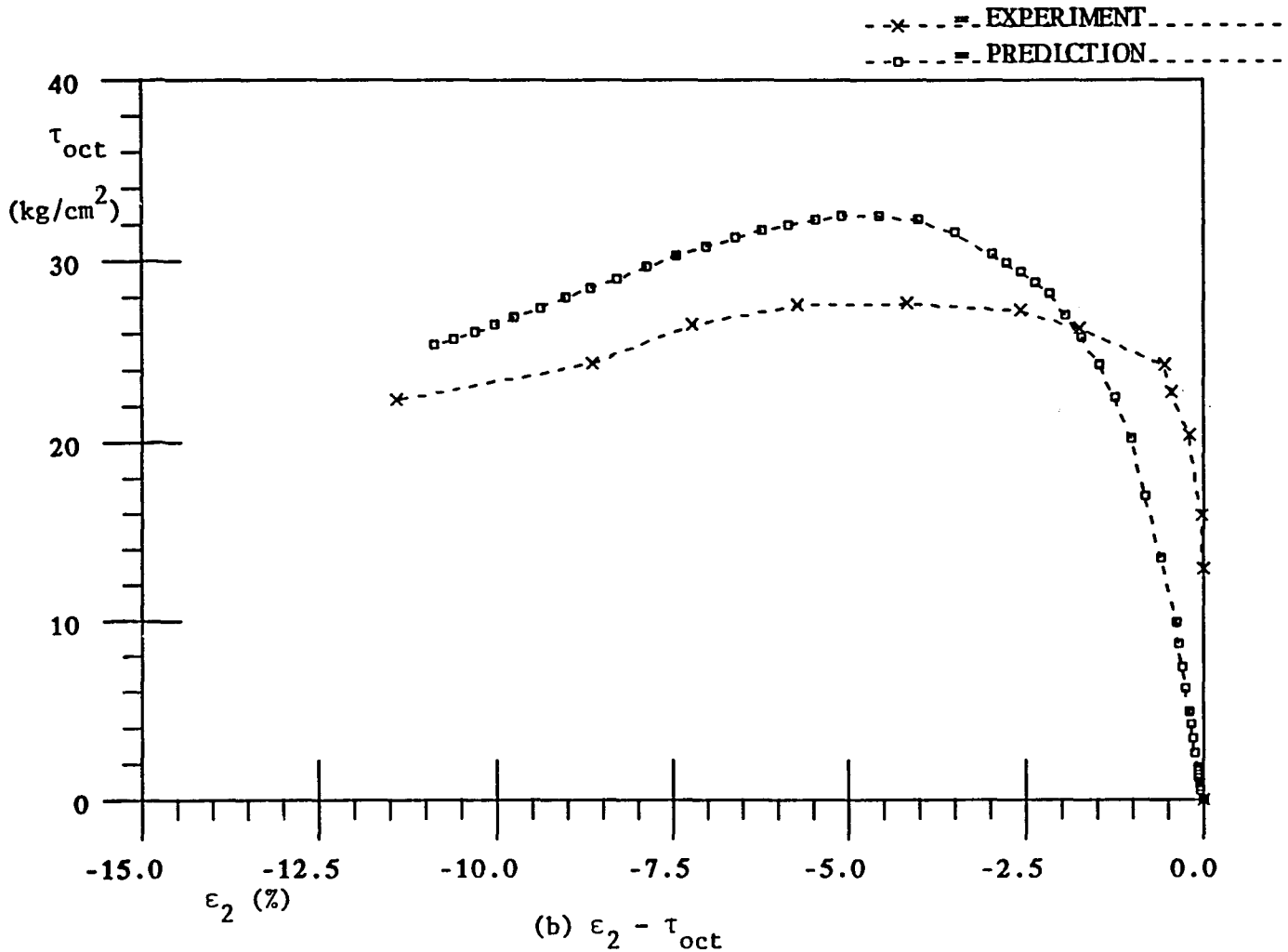

(b) $\varepsilon_2 - \tau_{oct}$

Fig. 7.8 (Continued)

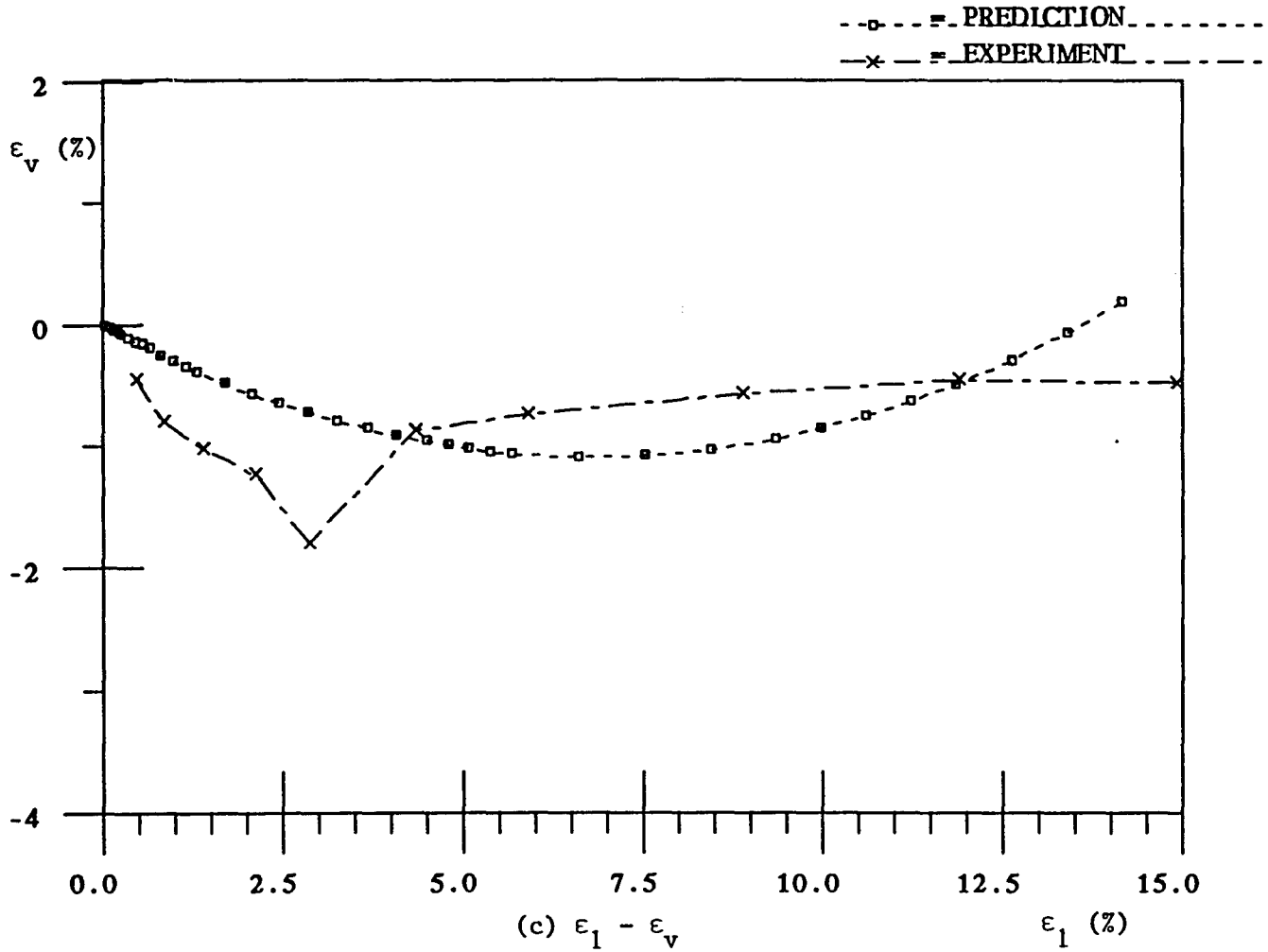

Fig. 7.8 (Continued)

CHAPTER 8

EXTENSION TO JOINT MODELLING

The aim of this chapter is to extend the proposed theory to modelling of interfaces and joints; whatever mathematical formulation is used to idealize the behavior of interfaces, the related constants are to be determined from laboratory testing. A review of existing devices for joint testing is out of the scope of this dissertation. The device developed by Desai (1980) was used for a series of tests on joints in concrete. The purpose of these tests was to obtain information on the softening part of the shear force - shear displacement curve. An extension of the damage theory is proposed for the constitutive behavior of joints.

8.1 Interface Testing

Desai (1980) has developed a device called Cyclic Multi Degree of Freedom (CYMDOF) for testing of interfaces and joints under both static and dynamic (cyclic) loading conditions for simulation of translational, torsional and rocking modes of deformation. The details of design, development and construction of the device are given by Desai (1980). For convenient reference, a brief description of the device is presented herein. The translational part of the CYMDOF shear

device consists of a large shear box. The bottom half of the box is fixed to a frame which is designed to withstand a (vertical or horizontal) load up to 30 tons (2.72×10^4 kg) and the top box is loaded by a horizontal actuator of approximately 7 tons (6.35×10^3 kg) capacity. Normal load is applied through a vertical actuator of the same capacity as the horizontal one. The bottom part of the box is 16 x 16 x 9 inches (40 x 40 x 23 cm) and the top part is 12 x 12 x 9 (30.5 x 30.5 x 23 cm). The horizontal hydraulic cylinder is fixed to one of the vertical members of the loading frame. The vertical hydraulic cylinder is fixed to the junction point of upper diagonal members of the frame through a pin joint. A hydraulic pump of 3000 psi (2.07×10^4 kPa) supplies the required pressure input. Load cells, to monitor horizontal and vertical loads, and Linear Variable Differential Transformers (LVDT), to record horizontal and vertical displacements, are controlled by MTS electronic control units. A function generator allows load application in a variety of forms.

8.1.1. Artificial Rock Joint Tests

In this study, CYMDOF shear device is utilized to test the behavior of rock joints. Concrete blocks are used as artificial rock since the purpose here is not to determine the properties of actual rock joints but to verify the model developed for joints of brittle, rock like materials. The concrete blocks used (Fig. 8.1) for the tests are made from a mix of aggregate, sand and cement. The W/C ratio of the mix is approximately 0.5 while the unconfined compression strength of the

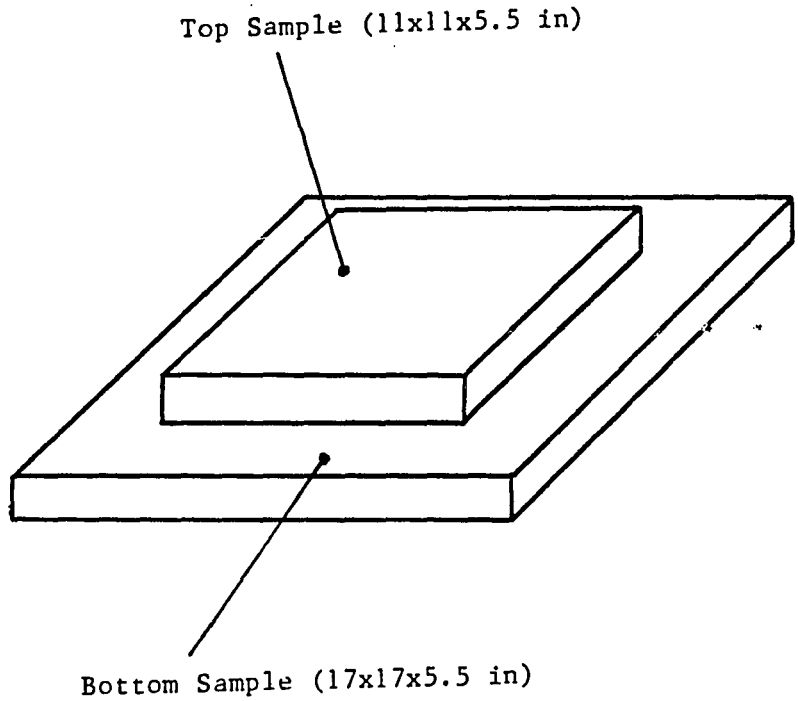

Fig. 8.1 Concrete Blocks Used for Joint Testing (1 in = 2.54 cm)

concrete at the interface is approximately f'_c = 5000 psi (34450 kPa). Mechanical concrete mixer is used for mixing and wooden molds are used for casting. Asperities of various angle θ (Fig. 8.2) are created through metallic (steel) forms. Details on the sample preparation and testing procedure and development of the plasticity model (for joints are given by Fishman (1986). Also, an extensive and rather complete series of tests on artificial rock (concrete) were performed by Fishman (1986); thus, the present testing program is a part of this work.

8.1.2. Testing Program

In the present study, concrete-concrete interfaces are tested for static shear (translational) mode. First, the bottom box is placed, centered and oriented so that the edges of the block remain parallel with the edges of the steel box. Second, the top box is placed in position and centered properly. The initial position of the top and bottom box is such that the asperities are as of Fig. 8.2. After all the electrical connections are restored and checked, the hydraulic pump is turned on (it needs approximately 10 minutes to warm up) and the data acquisition system is activated. The type of the test; e.g., static, type of control; e.g., displacement control, etc., are set by adjusting appropriate knobs on the MTS control units and on the connected function generator.

In the present tests, the normal load (stress) is kept constant and it is applied first by connecting the vertical actuator to the top sample. At this point, the initial readings of the LVDT's are recorded.

The type of horizontal load is adjusted for proper loading rate, maximum amplitude, etc. The interactive computer code developed for data acquisition is run on the computer and the horizontal mode is applied. The computer (MINC) reads LVDT and load cell channels and stores the load-displacement histories as voltage at selected time intervals. The data (voltage) recorded are reduced to load and displacement so that the complete load displacement curve can be plotted.

8.1.3. Tests

For the purpose of the present study a limited series of static tests were performed. A complete series of tests with varying asperity construction, normal loads, rate of loading, etc., were performed by Fishman (1986). The asperity angle θ (Fig. 8.2) considered here is $\theta = 15°$. The maximum amplitude of displacement was 0.5 inch (1.27 cm). During the test, normal load, shear load, horizontal displacement and vertical displacement were measured. The corresponding results to a normal stress of 50 psi are shown in Fig. 8.3. The loading rate for this test was 0.05 in/minute (0.127 cm/minute). As shown in Fig. 8.3, during increasing shearing displacement, the shear stress initially reaches a peak value and subsequently a reduction in shear stress is noted. Note that slightly before the maximum shear displacements are reached, the top sample asperities override the ones of the bottom sample. The effect of this is clearly depicted as a (sharp) decrease in shear stress during the second part of the test which is decreasing the displacement from its maximum to zero.

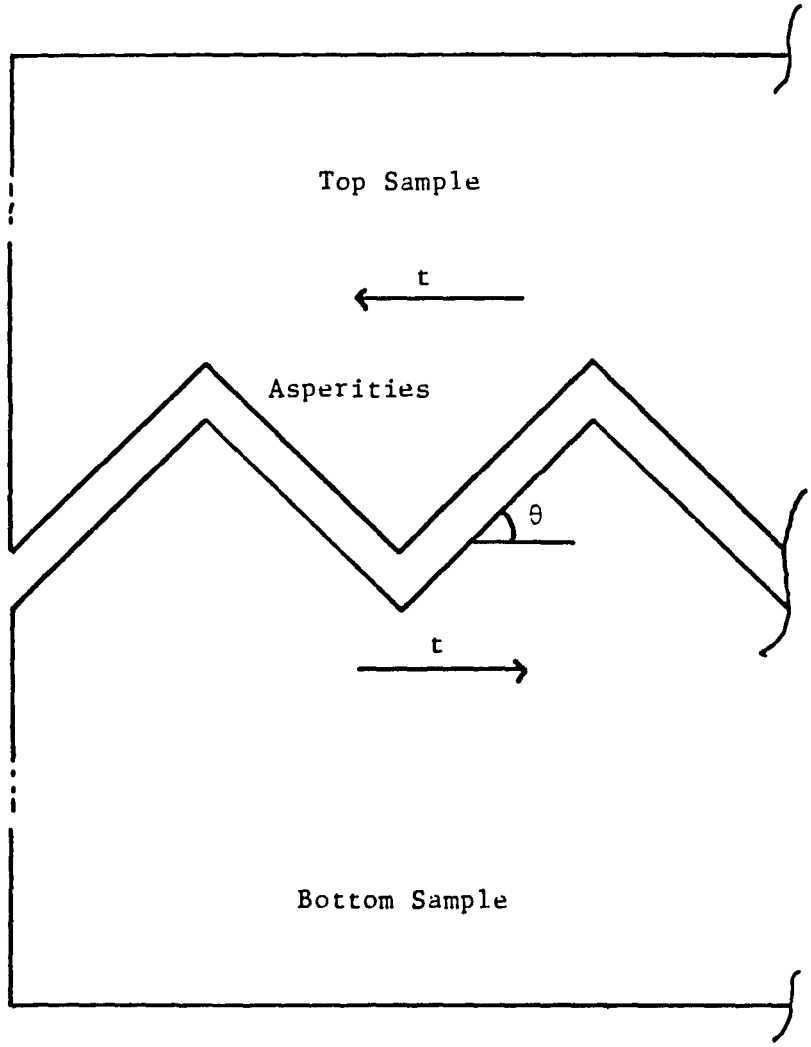

Fig. 8.2 Joint Profile Indicating Asperity Angle θ

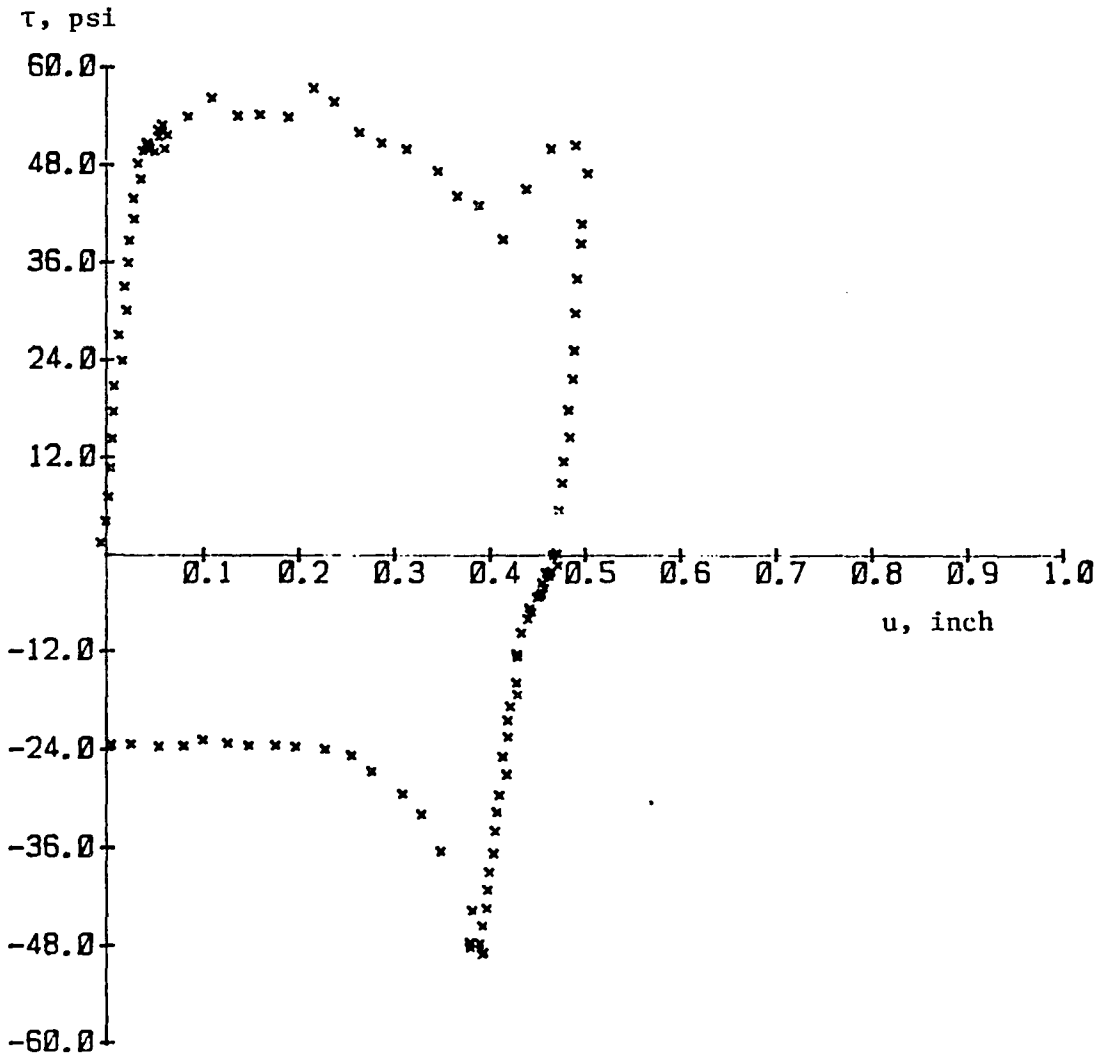

Fig. 8.3(a) Shear Stress Versus Displacement Static Test, 0 = 15°, Normal Stress 50 psi (1.0 inch = 2.54 cm, 1 psi = 6.89 kPa)

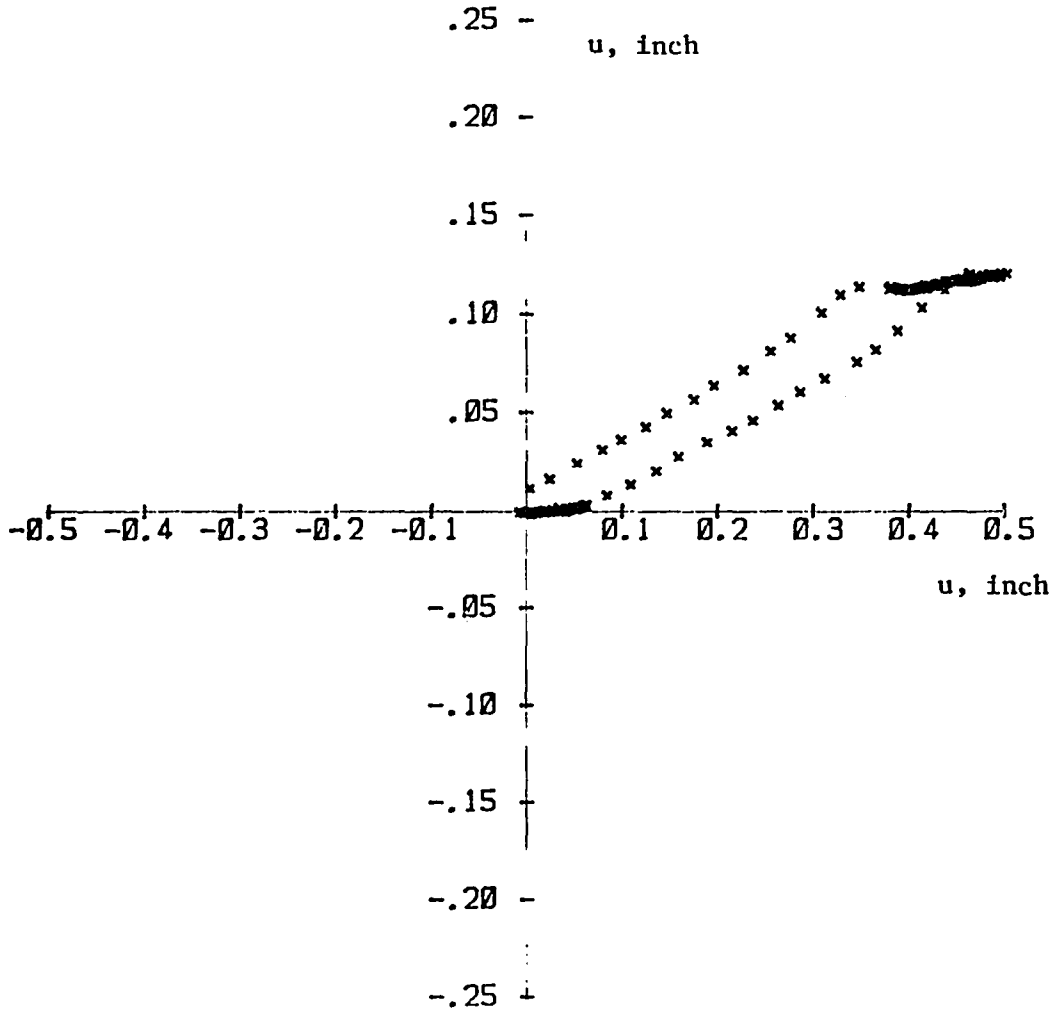

Fig. 8.3(b) Vertical Displacement Versus Horizontal Displacement, Front LVDT Measurements (1 inch = 2.54 cm)

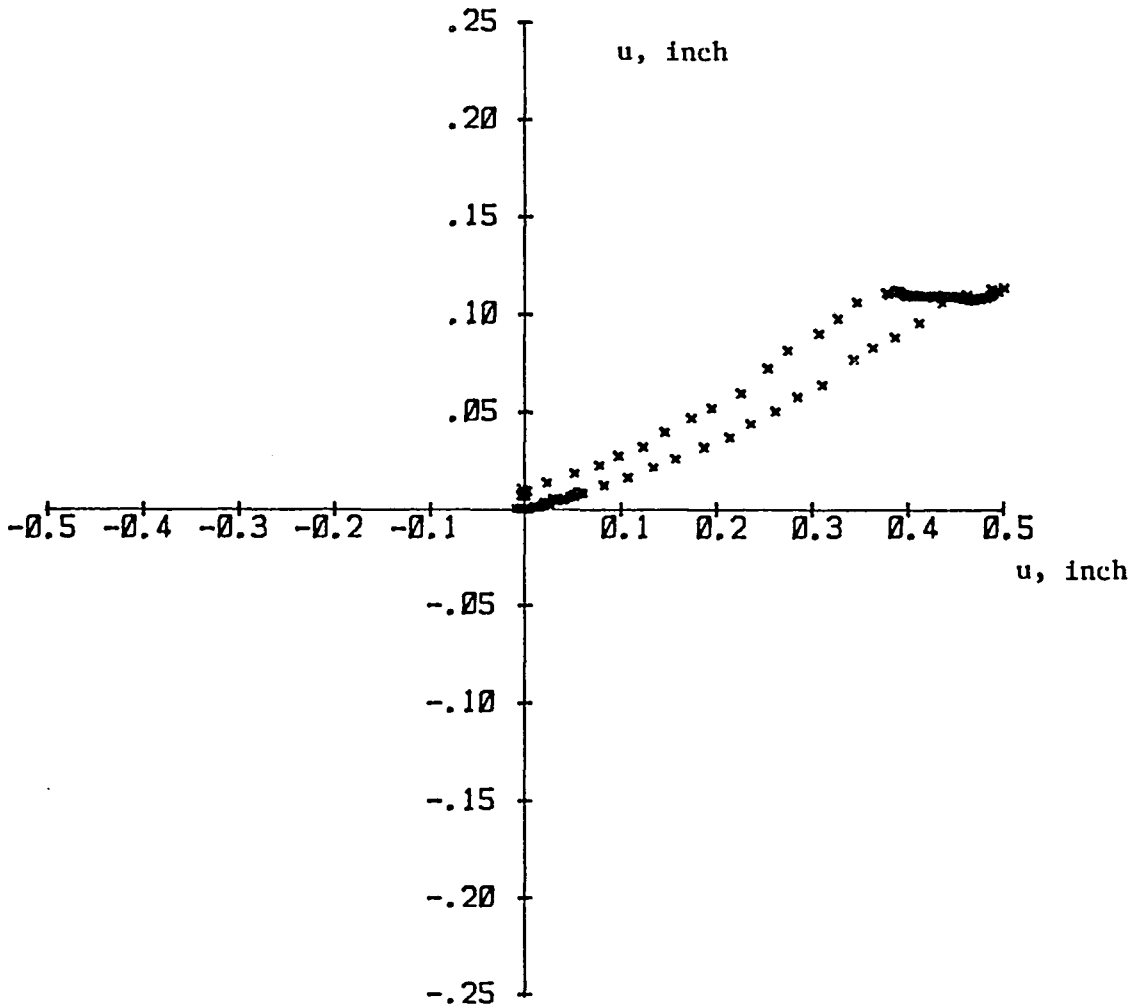

Fig. 8.3(c) Vertical Displacement Versus Horizontal Displacement, Back LVDT Measurements (1 inch = 2.54 cm)

As far as the vertical (normal) displacements are concerned, there is an initial, relatively small compaction followed by dilation (Fig. 8.3b, c). For clarity, results from two different sets of LVDT's are presented in Fig. 8.3. Figure 8.4 shows the recorded shear stress-horizontal displacement response for a test with 50 psi (345 kPa) normal stress. Here, the maximum horizontal displacement was 0.25 inches (0.64 cm). The above tests are typical of a series for different normal loads.

8.2 Interface Modelling

The deformational properties of interfaces and joints are, in general, different than the deformational properties of a material undergoing general three-dimensional deformation. This implies that although a constitutive model may be valid for general "continuum" behavior, its validity may need analysis and investigation when specialized to joint behavior. For example, characterization of damage in a joint may be different than characterization of damage in a body undergoing general deformation. In the following, experimental observations inspire recommendations for damage representation in joints. A theory is proposed to describe the force-displacement behavior of softening joints.

Consider a joint subjected to a shear force T. The joint is, in general, rough (not perfectly smooth). Part of the applied shear force will be resisted by interlocking of the asperities. Another part will be resisted by friction along the surfaces of contact between the upper and lower part of the joint. In a phenomenological approach, we can write

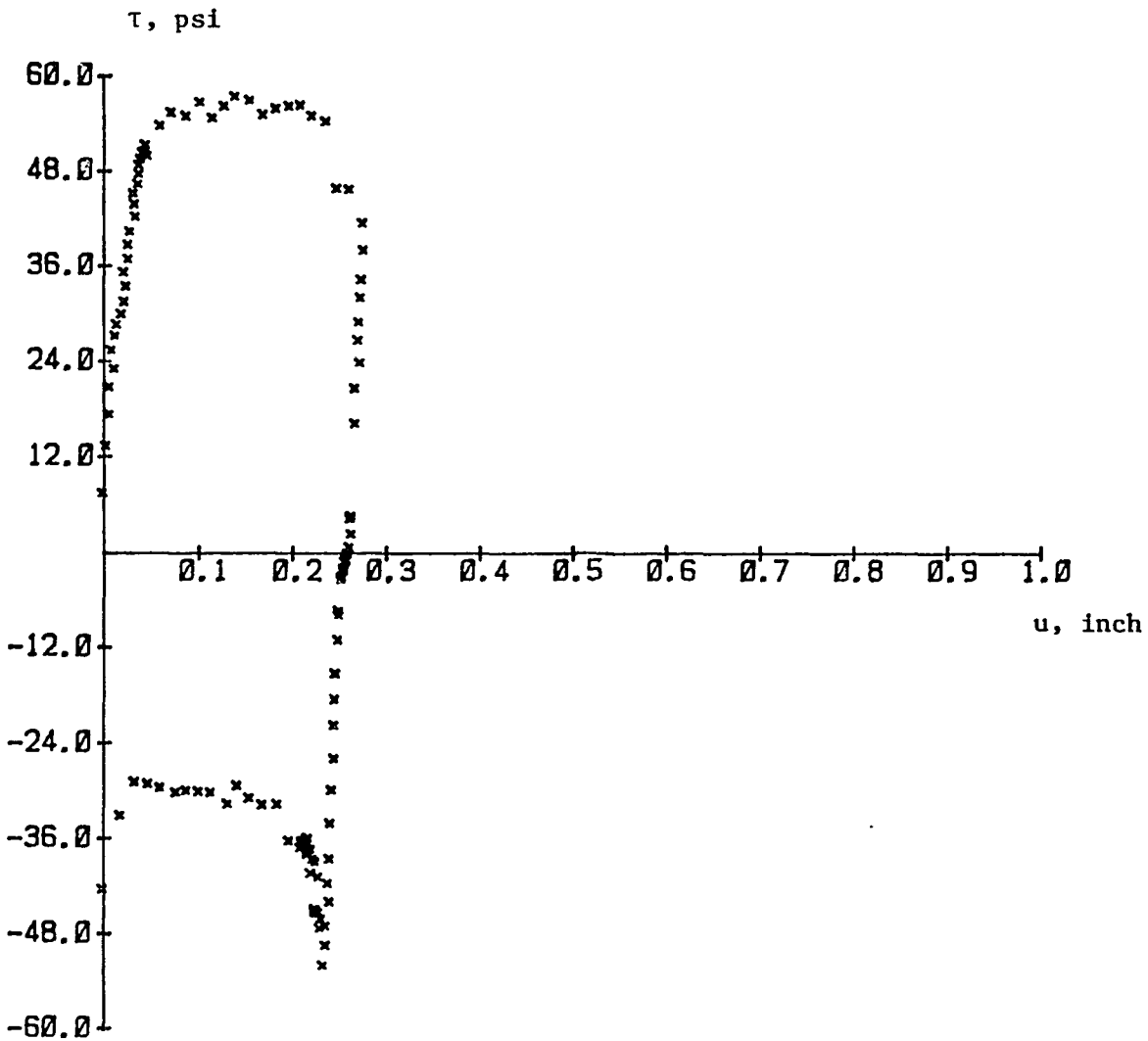

Fig. 8.4 Shear Stress Versus Displacement Static Test, 0 = 15°, Normal Stress 50 psi (1 inch = 2.54 cm, 1 psi = 6.89 kPa)

$$T = T_f + T_r \tag{8.1}$$

where T_f indicates shear force resisted by friction and T_r is shear force resisted from interlocking of asperities. In the case of a smooth joint, $T_r = 0$. Associated with each force is an area such that the corresponding stresses are defined..

$$T_f = \tau_f A_f \tag{8.2}$$

and

$$T_r = \tau_r A_r \tag{8.3}$$

where A_f, A_r denote areas and τ_f and τ_r are shear stresses. The overall shear stress, τ, is defined such that

$$T = \tau A \tag{8.4}$$

and

$$A = A_f + A_r \tag{8.5}$$

In order to derive the overall (homogenized) stress deformation relations, we consider a unit area; namely, $A = 1$. The ratio of A_f to A is defined such that

$$r = \frac{A_f}{A} = A_f \tag{8.6}$$

since A = 1.

From Eqs. (8.1) through (8.6), we obtain

$$T = r\,\tau_f + (1-r)\,\tau_r \tag{8.7}$$

A Coulomb-type law will be assumed for the friction shear stress τ_f thus

$$\tau_f = \mu_f\, N \tag{8.8}$$

where N is the applied normal load and μ_f the corresponding coefficient of friction. From Eqs. (8.7) and (8.8), we obtain

$$T = r\,\mu_f\, N + (1-r)\,\tau_r \tag{8.9}$$

Setting $r\,\mu_f = \tan\phi$ and $(1-r)\,\tau_r = C$. Equation (8.9) can we written as

$$T = \tan\phi\, N + c \tag{8.10}$$

where ϕ here has a meaning of generalized friction angle while c represents cohesion. Thus, roughness can be represented as similar to cohesion. Also, under general loading, r will not remain constant since r depends on damage accumulation in the asperities. For the case of a smooth joint, Eq. (8.9) or (8.10) reduce to the classical Coulomb friction equations. Differentiating Eq. (8.9) with respect to time, we obtain

$$dT = dr\,(\tau_f - \tau_r) + (1-r)\,d\tau_r + r\,d\tau_f \tag{8.11}$$

So far, only static variables were considered. It is an experimental fact that during deformation of joints, only part of the relative displacements are recovered. In general,

$$du = du^e + du^p \tag{8.12}$$

$$dv = dv^e + dv^p \tag{8.13}$$

where u denotes the relative shear displacement, v denotes the relative normal displacement, a superscript e denotes elastic and p plastic, and d denotes an (infinitesimal) increment. The following elasticity relations hold:

$$d\tau_r = G\, du^e \tag{8.14}$$

$$dN = K\, dv^e \tag{8.15}$$

where K, G are the elasticity parameters. Also, for the friction part, the following holds:

$$d\tau_f = \mu_f\, dN \tag{8.16}$$

Also, the total (average) shear stress increment $d\tau$ is related to du^e through

$$d\tau = G'\, du^e \tag{8.17}$$

where G' is the elastic shear modulus corresponding to the total (average) response. In order that the formulation is complete, the evolution law for the damage parameter r must be specified. Since damage growth is irreversible, we can, without loss in generality, write

$$dr = R\, du^p \tag{8.18}$$

A specific functional expression for R is not studied herein. It is the micromechanics of joint behavior that decide and control such a functional representation for R. Finally, the so-called plastic dilatancy ratio D is defined such that

$$-dv^p = D\, du^p \tag{8.19}$$

Thus, Eq. (8.13) can be written as

$$dv = \frac{1}{K} dN - D\, du^p \tag{8.20}$$

where K denotes the elastic bulk modulus for the joint. From the above equations, we derive the final force-relative displacement equations. From Eqs. (8.11), (8.14-8.20), it follows that

$$dT = (\tau_f - \tau_r)\, R\, du^p + (1-r)\, G\, du^e + r\, \mu_f\, dN \tag{8.21}$$

From Eqs. (8.12), (8.13) and (8.21), we obtain

$$dT = (\tau_f - \tau_r)\, R\, du - (\tau_f - \tau_r)\, R \frac{dT}{G'} + (1-r) \frac{G}{G'} dT + r\, \mu_f\, dN \tag{8.22}$$

Also, from Eqs. (8.12) and (8.20),

$$dv = \frac{dN}{K} - D\ du + D\ \frac{dT}{G'} \tag{8.23}$$

Rearranging Eqs. (8.22) and (8.23) results in

$$dT = A\ du + B\ dv \tag{8.24.1}$$

$$A = \frac{(\tau_f - \tau_r)\ R + r\ \mu_f\ K\ D}{1 + (\tau_f - \tau_r)\ \frac{R}{G'} - (1-r)\ \frac{G}{G'} + r\ \mu_f\ K\ \frac{D}{G'}} \tag{8.24.2}$$

$$B = \frac{r\ \mu_f\ K}{1 + (\tau_f - \tau_r)\ \frac{R}{G'} - (1-r)\ \frac{G}{G'} + r\ \mu_f\ K\ \frac{D}{G'}} \tag{8.24.3}$$

$$dN = (K - \frac{A}{G'})\ (D\ du + (K - \frac{D}{G'}\ B)\ dv \tag{8.25}$$

Equations (8.24) and (8.25) can we written in matrix form as

$$\begin{matrix} dT \\ dN \end{matrix} = \begin{matrix} A & B \\ (K - \frac{A}{G'})\ D & (K - \frac{D}{G'}\ B) \end{matrix} \begin{matrix} du \\ dv \end{matrix} \tag{8.26}$$

Equations (8.26) are the final force-relative displacement equations. The first noteworthy fact is that the off-diagonal terms in the constitutive matrix (2 x 2) are, in general, non zero. This implies that the proposed constitutive equations capture the effect of coupling between the shear and normal responses of the joint.

The proposed theory is not elastic since irreversible deformations are present. Also, the theory is not elastoplastic since the general theory of plasticity involving yield surfaces, plastic potentials, etc., was not employed. The theory accounts for inealstic deformations, damage progression, and coupling of shear and normal behavior.

In order that the theory be implementable for the response of real materials, the following parameters are needed:

- Elasticity parameters: K, G

The above are assumed constant and can be identified from experimental measurements of the reversible part of the deformation.

- Friction parameter: μ_f

As mentioned earlier, when the theory is specialized for smooth joints it reduces to the classical Coulomb friction theory. Thus, μ_f can be identified from the conditions at "yield" of a smooth joint.

- Evolution law for the damage functional R (further details are given below.

Finally,

- Evolution law for the plastic dilatancy factor, D.

The experiment (micromechanics) is the major deciding factor for the evolution law of R and D. It is possible though to theoretically restrict the above evolution laws. If an initial value or r, r_I is established, depending on the initial roughness, then for $u^p = 0$, the value of r should be equal to r_I. Also, when the residual conditions are reached, r reaches an ultimate value close to unity. Thus,

$$u^p = 0 \rightarrow r = r_I$$

$$u^p = u^p_{res} \rightarrow r \cong 1$$

Further, since, in general, dilation is suppressed at the residual conditions, we have

$$r \cong 1 \rightarrow D\ (r) = 0$$

Also

$$r = r_I \rightarrow D\ (r) = \text{maximum}$$

In order that the above formulation is complete, a comprehensive series of tests with measurements at the micromechanics level is needed. These measurements will be the key factor in establishing an evolution law for R and D. Proposing and/or verifying such evolution laws is out of the scope of this dissertation.

CHAPTER 9

SUMMARY AND CONCLUSIONS

In this study, first, the experimental and theoretical observations on the deformational characteristics of brittle geomaterials was reviewed and discussed. A basic conclusion is that special features such as strain softening can not be considered as a true material (continuum) property. These conclusions created a renewed emphasis on the constitutive modelling of such materials. Under the inspiration of the pioneer work of Kachanov (1958), a model that accounts for structural changes in such materials is developed. These effects are incorporated in the theory through a tensor form of a damage variable. It is shown subsequently that formation of damage is responsible for the softening in strength observed in experiments, for the degradation of the elastic shear modulus, and for induced anisotropy. A generalized model is incorporated for the so-called topical or continuum part of the behavior, whereas the damage part is represented by the so-called stress-relieved behavior.

The question of uniqueness in the strain-softening regime is examined. It is shown that the constitutive equations lead to a unique solution for the case of rate dependent as well as rate independent formulation. Its implementation in finite element analysis shows mesh site insensitivity in the hardening and softening regimes.

The general theory of bifurcation of differential equations is employed in order to study the effect of damage accumulation on formation of narrow, so-called shear bands. It is shown that as damage is accumulated, the material approaches localization of deformation.

The theory of mixtures is employed for a further theoretical establishment of the model. Energy considerations show the equivalence of the two-component damage body to an elastoplastic body containing cracks; the equivalence considered in the Griffith sense. The mechanisms of failure are considered and discussed with respect to multiaxial stress paths. An explanation of failure, at the microlevel, is given.

A number of material constants are involved in the theory. Strictly speaking, the constants can be rigorously evaluated through microstructural analysis rather than phenomenological procedures. Experimental techniques such as X-ray and radiographic that give light to important measurements of structural changes during deformation are not readily available. Thus, the material constants are evaluated approximately from available "stress-strain" data.

From a philosophical point of view, it may be that the present investigation creates further questions as far as understanding of material behavior and its mathematical modelling are concerned. The need and feel for further experimental and theoretical studies is rigorous though it is believed that the proposed conept can provide a general yet simplified approach for characterizing behavior of (geologic) materials undergoing microcracking and fracture leading to loss of strength and strength softening.

APPENDIX A

The flow rule of associated plasticity is expressed as

$$\dot{\varepsilon}^{p}_{ij} = \lambda \frac{\partial F}{\partial \sigma_{ij}} \tag{A.1}$$

where F is the yield surface. The coefficient λ is expressed as

$$\lambda = \frac{\frac{\partial F}{\partial \sigma_{ij}} C^{e}_{ijk\ell} \dot{\varepsilon}_{k\ell}}{\frac{\partial F}{\partial \sigma_{rs}} C^{e}_{rspq} \frac{\partial F}{\partial \sigma_{pq}} - H} \tag{A.2}$$

where $H = \left(\frac{\partial F}{\partial \sigma_{k\ell}} \frac{\partial F}{\partial \sigma_{k\ell}}\right)^{1/2} \frac{\partial F}{\partial \xi}$ and ξ is the trajectory of plastic strains $= \int (\dot{\varepsilon}_{ij} \dot{\varepsilon}_{ij})^{1/2}$. From (A.1) and (A.2), we obtain

$$\lambda = \frac{1}{h'} \frac{\partial F}{\partial \sigma_{k\ell}} \dot{\sigma}_{k\ell} \tag{A.3}$$

where $h' = - \left(\frac{\partial F}{\partial \sigma_{k\ell}} \frac{\partial F}{\partial \sigma_{k\ell}}\right)^{1/2} \frac{\partial F}{\partial \xi}$. Now, from the flow rule (A.1) and (A.3), we have

$$\dot{\varepsilon}^{p}_{ij} = \frac{1}{h'} \frac{\partial F}{\partial \sigma_{ij}} \frac{\partial F}{\partial \sigma_{k\ell}} \dot{\sigma}_{k\ell} \tag{A.4}$$

The yield function F is expressed as

$$F = J_{2D} + \alpha J_1^{\,n} + \gamma J_1^{\,2} = 0 \tag{A.5}$$

where J_{2D} is the second invariant of the deviator stress tensor and J_1 the first invariant of the stress tensor. For convenience, only a truncated form of the general function is adopted herein; however, the derivation can be made for the general case also. It follows from (A.4) and (A.5) that

$$\dot{E}_{ij} = \frac{\dot{S}_{ij}}{2G} + \frac{S_{ij}}{h'} \left[\frac{\partial F}{\partial J_1} \dot{\sigma}_{kk} + S_{k\ell} \dot{\sigma}_{k\ell}\right] \tag{A.6.1}$$

$$\dot{\varepsilon}_{kk} = \frac{\dot{\sigma}_{kk}}{3K} + \frac{1}{h'} \left[3 \left(\frac{\partial F}{\partial J_1}\right)^2 \dot{\sigma}_{kk} + 3 \frac{\partial F}{\partial J_1} S_{k\ell} \dot{\sigma}_{k\ell}\right] \tag{A.6.2}$$

From (A.6) and the relations involving μ and β, Rudnicki and Rice (1975), the following relations are obtained:

$$\frac{1}{h'} = \frac{1}{h} \frac{1}{4\tau^2} \tag{A.7.1}$$

$$\mu = \beta = \frac{3}{2} \frac{1}{\tau} \frac{\partial F}{\partial J_1} \tag{A.7.2}$$

In the yield function expressed in (A.5), α is the hardening parameter such that $\alpha = \alpha_1 / \xi^{\eta_1}$ are the hardening constants.

APPENDIX B

VALUES OF (h/G) AT LOCALIZATION AND SHEAR BAND INCLINATION ANGLE θ_o FOR VARIOUS VALUES OF DAMAGE ACCUMULATION. SOLUTION CORRESPONDS TO PURE SHEAR (N = 0) AND ν = 0.3

μ	β	$(h/G)_{cr}$	θ_o (degrees)
(a) r = 0.5			
0.0	0.0	0.0	45.0
0.3	0.0	0.004	46.9
0.3	0.15	-0.007	49.0
0.3	0.3	-0.009	51.0
0.6	0.0	0.016	49.0
0.6	0.15	-0.01	51.0
0.6	0.3	-0.028	53.1
0.6	0.45	-0.038	55.2
0.6	0.6	-0.04	57.4
0.9	0.0	0.036	51.0
0.9	0.15	-0.05	53.1
0.9	0.3	-0.038	55.2
0.9	0.45	-0.06	57.4
0.9	0.6	-0.08	59.6
(b) r = 0.75			
0.0	0.0	0.0	45.0
0.3	0.0	0.001	46.0
0.3	0.15	-0.002	48.1
0.3	0.3	0.003	50.2
0.6	0.0	0.005	47.1
0.6	0.15	-0.007	49.2
0.6	0.3	-0.009	51.3
0.6	0.45	-0.003	53.4
0.6	0.6	0.013	55.6
0.9	0.0	0.011	48.1
0.9	0.15	-0.009	50.2
0.9	0.3	-0.020	52.3
0.9	0.45	-0.022	54.5
0.9	0.6	-0.014	56.7

μ	β	$(h/G_{cr}$	θ_o (degrees)
(c) r = 0.9			
0.0	0.0	0.0	45.0
0.3	0.0	0.0002	45.4
0.3	0.15	0.0018	47.5
0.3	0.3	0.014	49.7
0.6	0.0	0.0008	45.8
0.6	0.15	-0.001	47.9
0.6	0.3	0.007	50.1
0.6	0.45	0.026	52.3
0.6	0.6	0.056	54.5
0.9	0.0	0.0018	46.3
0.9	0.15	-0.0036	48.4
0.9	0.3	0.0014	50.5
0.9	0.45	0.0167	52.7
0.9	0.6	0.0426	54.9
(d) r = 0.99			
0.0	0.0	0.0	45.0
0.3	0.0	0.2×10^{-9}	45.0
0.3	0.15	0.0056	47.1
0.3	0.3	0.022	49.3
0.6	0.0	0.9×10^{-9}	45.0
0.6	0.15	0.0056	47.15
0.6	0.3	0.023	49.3
0.6	0.45	0.051	51.5
0.6	0.6	0.0899	53.7
0.9	0.0	0.2×10^{-8}	45.0
0.9	0.15	0.0056	47.2
0.9	0.3	0.022	49.3
0.9	0.45	0.051	51.5
0.9	0.6	0.089	53.7

LIST OF REFERENCES

Baker, R. and Desai, C. S., "Induced Anisotropy During Plastic Straining," Intl. J. Num. Anal. Meth. in Geomechanics, 8, 167-185 (1984).

Barbee, T. W., Seaman, L., Crewdson, R. and Curran, D., "Dynamic Fracture Criteria for Ductile and Brittle Materials," J. Matls., 7, 393-401 (1972).

Bathe, K. J. and Ramaswamy, S., "On Three-Dimensional Analysis," Nucl. Engg. Design, 52, 385-409 (1979).

Bazant, Z. P., "Endochronic Inelasticity and Incremental Plasticity," Intl. J. Solids Structures, 7, 149-156 (1977).

Bazant, Z. P., "Work Inequality for Plastic Fracturing Materials," Int. J. Solids Structures, 16, 873-901 (1980).

Bazant, Z. P. and Kim, S. S., "Plastic Fracturing Theory for Concrete," J. Engr. Mech. Div., ASCE, 105, 407-478 (1979).

Betten, J., "Damage Tensors in Continuum Mechanics," J. de Mecanique Theorique et Appliquee, 2, 13-38 (1983).

Bowen, R. M., "Thermochemistry of Reacting Materials," J. Chem. Phys., 49, 1625-1637 (1969).

Bowen, R. M., "Thermochemistry of Reacting Materials," J. Chem. Phys., 50, 4601-4602 (1969).

Bowen, R. M., "Theory of Mixtures," in Continuum Physics (A. C. Eringen, Ed., Vol. 3, P. 1, Academic Press, New York (1975).

Brady, B. T., Duvall, W. I. and Horimo, F. G., "An Experimental Determination of the True Uniaxial Stress-Strain Behavior of Brittle Rock," Rock Mechanics, 5, 107-120 (1973).

Budianski, B. and O'Connell, R. T., "Elastic Moduli of a Cracked Solid," Intl. J. Solids Structures, 12, 81-97 (1976).

Carrasquillo, R. L., Nilson, A. H. and Slate, F. O., "Properties of High Strength Concrete Subject to Short Term Loads," Amer. Concr. Inst., 3, 171-178 (1981).

Carrasquillo, R. L., Slate, F. O. and Nilson, A. H., "Microcracking and Behavior of High Strength Concrete Subject to Short Term Loading," Amer. Concr. Inst., 3, 179-186 (1981).

Cedolin, L., Crutzen, V.R.J. and Dei Poli, S., "Triaxial Stress-Strain Relationship for Concrete," J. Engr. Mechs. Div. ASCE, 103, 423-439 (1977).

Cleary, M. P., "Elastic and Dynamic Response Regimes of Fluid Impregnated Solids with Diverse Microstructures," Intl. J. Solids Structures, 14, 795-819 (1978).

Cleary, M. P., Chen, I. W. and Lee, S. M., "Self Consistent Techniques for Heterogeneous Media," J. Engr. Mech. Div. ASCE, 106, 861-887 (1980).

Costin, L. S. and Holcomb, D. J., "A Continuum Model of Inelasticity Deformed Brittle Rock Based on Mechanics of Microcracks," Proc., Constitutive Laws for Engg. Matls., Univ. of Arizona, Tucson (1983).

Curran, D. R., Seaman, L. and Shockey, D. A., "Dynamic Failure in Solids," Physics Today, 30, 46-55 (1977).

Curran, D. R., Seaman, L. and Dein, J., "Constitutive Laws for Failing Materials," Mechanics of Engr. Materials, C. S. Desai and R. H. Gallagher (Eds.), John Wiley and Sons, Chichester, U. K., 139-152 (1984).

Dafalias, Y. F., "Modelling Cyclic Plasticity: Simplicity versus Sophistication," Mechanics of Engr. Materials, C. S. Desai and R. H. Gallagher (Eds.), John Wiley and Sons, Chichester, U. K., 153-178 (1984).

Davis, P. C. and Sih, G. C., "Stress Analysis of Cracks," Fracture Toughness and Its Applications, ASTM, STP 381, Philadelphia (1965).

Davison, L. and Stevens, A. L., "Thermomechanical Constitution of Spalling Elastic Bodies," J. Appl. Phys., 44, No. 2, 668-673 (1973).

Davison, L., Stevens, A. L. and Kipp, M. E., "Theory of Spall Damage Accumulation in Ductile Materials," J. Mech. Phys. Solids, 25, 11-28 (1977).

Dems, K. and Mroz, Z., "Stability Conditions for Brittle-Plastic Structures with Propagating Damage Surfaces," J. Struct. Mechs., 13, (1), 95-122 (1985).

Desai, C. S., "A Consistent Finite Element Technique for Work-Softening Behavior," Proc., Int. Conf. on Comp. Methods in Nonlinear Mechanics, J. T. Oden et al. (Eds.), Univ. of Texas, Austin, Texas (1974).

Desai, C. S., "A Dynamic Multi-Degree of Freedom Shear Device," Report, Dept. of Civil Engr., Virginia Tech, Blacksburg, Report No. 80-36 (1980).

Desai, C. S., "A General Basis for Yield, Failure and Potential Functions in Plasticity," Int. J. Num. Anal. Meth. in Geomechanics, 4, 361-375 (1980).

Desai, C. S. and Abel, J. F., Introduction to the Finite Element Method, Von Nostrand Reinhold, New York (1972).

Desai, C. S. and Faruque, M. O., "A Generalized Basis for Modelling Plastic Behavior of Materials," Proc., Int. Conf. on Const. Laws for Engng. Mat: Theory and Application, Univ. of Arizona, Tucson (1983).

Desai, C. S. and Faruque, M. O., "Constitutive Model for Geologic Materials," J. Eng. Mech. Div., ASCE, 110, 1391-1408 (1984).

Desai, C. S., Frantziskonis, G. and Somasundaram, S., "Constitutive Modelling for Geological Materials," Proc., 5th Intl. Conf. Num. Meth. in Geomech., Nagoya, Japan, April (1985).

Desai, C. S. and Siriwardane, H. J., "A Concept of Correction Functions to Account for Non-Associative Characteristics of Geologic Media," Int. J. Num. Anal. Meth. in Geomechanics, 4, 377-387 (1980).

Desai, C. S. and Siriwardane, H. J., Constitutive Laws for Engineering Materials, Prentice-Hall, Inc., Englewood Cliffs, N. J. (1983).

Desai, C. S., Somasundaram, S. and Frantziskonis, G., "A Hierarchical Approach for Constitutive Modelling of Geologic Materials," Int. J. Num. Anal. Meth. in Geomechanics, Vol. 10, No. 3 (1986).

Diaz, S. and Hilsdorf, H. K., "Fracture Mechanisms of Concrete Under Compressive Loads," Cement and Concr. Research, 3, 363-388 (1973).

DiMaggio, F. L. and Sandler, I. S., "Material Model for Granular Soils," J. Engr. Mechs. Div., ASCE, 97, EM3 (1971).

Dougill, J. W., "On Stable Progressively Fracturing Solids," ZAMP (Zeitschrift fur Angewandte Mathematik un Physik), 27, Fasc 4, 423-437 (1976).

Dougill, J. W. and Rida, M.A.M., "Further Consideration of Progressively Fracturing Solids," J. Engr. Mech. Div., ASCE, 106, 1021-1038 (1980).

Dragon, A. and Mroz, Z., "A Continuum Model for Plastic-Brittle Behavior of Rock and Concrete," Int. J. Engr. Science, 17, 121-137 (1979).

Drescher, A. and Vardoulakis, I., "Geometric Softening in Triaxial Tests on Granular Material," Geotechnique, 32, 291-303 (1982).

Drucker, D. C., "A Definition of Stable Inelastic Material," ASME Trans. 81, 101-106 (1959).

Drucker, D. C., "Some Classes of Inelastic Materials, Related Problems Basic to Future Technologies," Nucl. Engr. Design, 57, 309-322 (1980).

Eftis, J. and Liebowitz, H., "On Fracture Toughness Evaluation for Semi-Brittle Fracture," Engr. Fract. Mechs., 7, 101-135 (1975).

Fanella, D. and Krajcinovic, D., "Continuum Damage Mechanics of Fiber Reinforced Concrete," J. Engr. Mechs. Div., ASCE, 111, 995-1009 (1985).

Faruque, M. O., "Development of a Generalized Constitutive Model and Its Implementation in Soil-Structure Interaction," Ph.D. Dissertation, Univ. of Arizona, Tucson, AZ. (1983).

Faruque, M. O. and Desai, C. S., "Implementation of a General Constitutive Model for Geological Materials," Int. J. Num. Anal. Meth. in Geomechanics, 9 (1985).

Fishman, K. L., "Testing and Modelling for Interfaces and Joints," Ph.D. Dissertation, Univ. of Arizona (1986), under preparation.

Fonseka, G. I. and Krajcinovic, D., "The Continuous Damage Theory of Brittle Materials, Part 2: Uniaxial and Plane Response Modes," J. Appl. Mech., ASME, 48, 816-824 (1981).

Frantziskonis, G. and Desai, C. S., "Constitutive Model with Strain Softening," Int. J. Solids Structures, submitted.

Frantziskonis, G. and Desai, C. S., "Analysis of a Strain Softening Constitutive Law," Int. J. Solids Structures, submitted.

Frantziskonis, G. and Desai, C. ., "Elastoplastic Model with Damage for Strain Softening Geomaterials," Acta Mechanica, submitted.

Frantziskonis, G., Desai, C. S. and Somasundaram, S., "Constitutive Model for Nonassociative Behavior," J. Engr. Mech. Div., ASCE, in press.

Goodier, J. N., "Mathematical Theory of Equilibrium Cracks," in Fracture, (Ed. H. Liebowitz), Vol. 2, Academic Press, N. Y., (1968).

Green, A. E. and Naghdi, P. M., "A Dynamical Theory of Interacting Continua," Int. J. Engr. Sci., 3, 231-241 (1965).

Griffith, A. A., "The Phenomena of Rupture and Flow in Solids," Phil. Trans. Roy. Soc. London. Series A221, pp. 163-168 (1920).

Griffith, A. A., Proc. First Intl. Congress for Appl. Mechs., pp. 55-63, Delft (1924).

Hallbauer, D. K., Wagner, H. and Cook, N.G.W., "Some Observations Concerning the microscopic and Mechanical Behavior of Quartzite Specimens in Stiff, Triaxial Compression Tests," Int. J. Rock Mech. Min. Sci., 10, 713-718 (1973).

Hart, E. W., "A Phenomenological Theory for Plastic Deformation of Polycrystalline Metals," Acta Metallurgica, 18, 599-610 (1970).

Hashmi, Q., "Modelling for Nonassociative Behavior and Implementation," Ph.D. Dissertation, Univ. of Arizona (1986), under preparation.

Hayhurst, D. R., Dimmer, P. R. and Chernuka, M. W., "Estimates of the Creep Rupture Lifetime of Structures Using the Finite Element Method," J. Mech. Phys. Solids, 23, 335-355 (1975).

Hayhurst, D. R. and Leckie, F. A., "The Effect of Creep Constitutive and Damage Relationships Upon the Rupture Time of a Solid Circular Torsion Bar," J. Mech. Phys. Solids, 21, 431-446 (1973).

Hettler, A. and Vardoulakis, I., "Behavior of Dry Sand Tested With a Large Triaxial Apparatus," Geotechnique, 34, 183-198 (1984).

Hill, R., The Mathematical Theory of Plasticity, Oxford Univ. Press, Oxford, U. K. (1950).

Hill, R., "Acceleration Waves in Solids," J. Mech. Phys. Solids, 10, 1-6 (1962).

Hill, R. and Hutchinson, J. W., "Bifurcation Phenomena in the Plane Tension Test," J. Mech. Phys. Solids, 23, 239-264 (1975).

Hoeg, K., "Finite Element Analysis of Strain-Softening Clay," J. Soil Mech. Found. Div., 98, 43-58 (1972).

Hoenig, A., "The Behavior of a Flat Elliptical Crack in An Anisotropic Elastic Body," Intl. J. Solids Structures, 925-934 (1978).

Hoenig, A., "Elastic Moduli of a Non-Randomly Cracked Body," Int. J. Solids Structures, 15, 137-154 (1979).

Horii, H. and Nemat-Nasser, S., "Overall Moduli of Solids with Microcracks: Load Induced Anisotropy," J. Mech. Phys. Solids, 31, 155-168 (1983).

Hsu, T. T., Slate, F. O., Sturman, G. M. and Winter, G., "Microcracking of Plain Concrete and the Shape of the Stress-Strain Curve," J. Amer. Concrete Inst., 60, 209-222 (1963).

Hudson, J. A., Brown, E. T. and Fairhurst, C., "Shape of the Complete Stress-Strain Curve for Rock," Proc., 13th Symposium Rock Mechs., Univ. of Illinois, Urbana, Illinois (1971).

Hueckel,T., "On Plastic Flow Granular and Rock Like Materials With Variable Elasticity Moduli," Bull. Polish Acad. of Sci., Sec. Sci. Tech., 23, 405-414 (1975).

Hughes, B. P. and Chapman, G. P., "The Deformation of Concrete and Microconcrete in Compression and Tension With Particular Reference to Aggregate Size," Mag. Concrete Research, 18, 19-24 (1966).

Kachanov, L. M., The Theory of Creep, English Translation Ed. by A. J. Kennedy, Chs. IX, X, National Lending Library, Boston (1958).

Kawsan, I. K. and Jirsa, J. O., "Behavior of Concrete Under Compressive Loadings," J. Struct. Divis., ASCE, 95, 2543-2563 (1969).

Kotsovos, M. D. and Newman, J. B., "Generalized Stress-Strain Relations for Concrete," J. Engr. Mechs. Div., ASCE, 104, 845-856 (1978).

Krajcinovic, P. and Fonseka, G. K., "The Continuous Damage Theory of Brittle Materials, Part I: General Theory," J. Appl. Mech. ASME, 48, 809-815 (1981).

Krajcinovic, D. and Silva, M.A.G., "Statistical Aspects of the Continuous Damage Theory," Int. J. Solids Structures, 7, 551-562 (1982).

Lade, P. V., "Elastic-Plastic Stress Strain Theory for Cohesionless Soil With Curved Yield Surfaces," Int. J. Solids Structures, 13, 1019-1035 (1977).

Lee, K. L. and Seed, H. B., "Drained Strength Characteristics of Sand," J. Soil Mechs. & Found. Div., ASCE, 93, 117-141 (1967).

Lo, K. Y. and Lee, C. F. (1973), "Stress Analysis and Slope Stability in Strain Softening Materials," Geotechnique, 23, 1-7 (1973).

Loland, K. E., "Continuous Damage Model for Load Response Estimation of Concrete," Cement and Concrete Res., 10, 395-402 (1980).

Lotsberg, I., "Finite Element Analysis of Some Problems in Fracture Mechanics," Div. of Struct. Mech., The Norwegian Inst. of Technology Report No. 77, 5 (1977).

Maher, A. and Darwin, D., "Mortar Constituent of Concrete in Compression," J. Amer. Concrete Inst., 2, 100-111 (1982).

Maier, G., "Nonassociated and Coupled Flow Rules of Elastoplasticity for Geotechnical Media," Proc., Int. Conf. Soil Mech. and Found. Engr., Tokyo, Japan (1977).

Mandel, J., "Sur les Lignes de Glissement et le Calcul des Deplacements dans la Deformation Plastique," Comptes Rendus de l'Academie de Sciences, 275: 1272-1273 (1947).

Mandel, J., "Conditions de Stabilite et Postulat de Drucker," Proc., IUTAM Symp. Rheology Soil Mech., Grenoble, 1964, pp. 58-68 (1966).

Martin, J. R. and Leckie, F. A., "On the Creep Rupture of Structures," J. Mech. Phys. Solids, 20, 223-238 (1972).

Matsuoka, H. and Nakai, T., "Stress Deformation and Strength Characteristics of Soil Under Three Different Principal Stresses," Soils & Foundations, J. of Jap. Soc. of Soil Mech. & Found. Engg., 232, 59-70 (1974).

Mazars, J., "Mechanical Damage and Fracture of Concrete Structures," Advances in Fracture Research, 5th Int. Conf. Fracture. Cannes, 4, 1499-1506 (1981).

Mendelson, A., Plasticity: Theory and Applications, McMillan, New York (1968).

Molenkamp, F., "Comparison of Frictional Material Models With Respect to Shear Band Initiation," Geotechnique, 35, 127-143 (1985).

Mroz, Z., Norris, V. A. and Zienkiewicz, O. C., "An Anisotropic Hardening Model for Soils and Application to Cyclic Loading," Int. J. Num. Anal. Meth. in Geomechanics, 2, 203-221 (1978).

Nagaraj, B. K., "Modelling for Interfaces and Implementation," Doctoral Dissertation, Dept. of Civil Engg. and Engg. Mech., Univ. of Arizona, Tucson (1986).

Nemat-Nasser, S., Iwakuma, T. and Hejazi, M., "On Composites With Periodic Structure," Mechs. of Matls., 1, 239-250 (1982).

Nemat-Nasser, S. and Taya, M., "On Effective Moduli of an Elastic Body Containing Periodically Distributed Voids," Quart. Appl. Math., 39, 43-54 (1981).

Nayak, G. C. and Zienkiewicz, O. C., "Elastoplastic Stress Analysis. A Generalization for Various Constitutive Relations Including Strain Softening," Int. J. Num. Meth. Engg., 5, 113-135 (1972).

Nelson, I., Baron, M. L. and Sandler, I., "Mathematical Models for Geological Materials for Wave Propagation Studies," Shock Waves and the Mechanical Properties of Solids, Syracuse Univ. Press, N. Y. (1971).

O'Connell, R. J. and Budiansky, B., "Seismic Velocities in Dry and Saturated Cracked Solids," J. Geophys. Res., 79, 5412-5426 (1974).

Ortiz, M., "A Constitutive Theory for the Inelastic Behavior of Concrete," Mechs. of Matls., 4, 67-93 (1985).

Paloniswamy, R. and Shah, S. P., "Fracture and Stress-Strain Relation of Concrete Under Triaxial Compression," J. Struct. Div., ASCE, 100, 901-916 (1974).

Parmar, A. and Mellor, P. B., "Growth of Voids in Biaxial Stress Field," Int. J. Mech. Sci., 22, 135-150 (1980).

Phillips, D. V. and Zienkiewicz, O. C., "Finite Element Nonlinear Analysis of Concrete Structures," Proc., The Institution of Civil Engrs., 61, 59-88 (1976).

Pietruszczak, St. and Mroz, Z., "Finite Element Analysis of Deformation of Strain-Softening Materials," Int. J. Num. Meths. Engr., 17, 327-334 (1981).

Prevost, J. H. and Hoeg, K., "Soil Mechanics and Plasticity Analysis of Strain Softening," Geotechnique, 25, 279-297 (1975).

Rabotnov, Y. N., Creep Problems in Structural Members, North-Holland (1969).

Read, H. E. and Hegemier, G. A., "Strain Softening of Rock, Soil and Concrete - A Review Article," Mechs. of Matls., 3, 271-294 (1984).

Rudnicki, J. W. and Rice, J. R., "Conditions for the Localization of Deformation in Pressure-Sensitive Dilatant Materials," J. Mech. Phys. Solids, 23, 371-394 (1975).

Salami, M. R., "Constitutive Modelling of Concrete and Rocks Under Multiaxial Compressive Loadings," Doctoral Dissertation, Department of Civil Engr. & Engr. Mechs., Univ. of Arizona, Tucson (1986).

Sandler, J. S., "Strain Softening for Static and Dynamic Problems," ASME Winter Annual Meeting, Symposium on Constitutive Equations: Micro, Macro and Computational Aspects, CEQ, New Orleans, December (1984).

Schofield, A. N. and Wroth, C. P., Critical State Soil Mechanics, McGraw-Hill, London (1968).

Shah, S. P. and Chandra, S., "Fracture of Concrete Subjected to Cyclic and Sustained Loading," ACI-Journal, October, 861-825 (1970).

Shah, S. P. and Slate, F. O., "Internal Microcracking, Mortar-Aggregate Bond and the Stress-Strain Curve of Concrete," Proc., Intl. Conf. on the Structure of Concrete and Its Behavior Under Load, London, September (1965).

Shockey, D. R., Curran, L., Seaman, J. T., Rosenberg, J. T. and Petersen, C. F., "Fragmentation of Rock Under Dynamic Loads," Int. J. Rock Mechs., 11, 303-317 (1974).

Slate, F. O. and Olsefski, S., "X-rays for Study of Internal Structure and Microcracking of Concrete," J. of Amer. Concr. Inst., 575-588 (1963).

Spooner, O. C. and Dougill, J. W., "A Quantitative Assessment of Damage Sustained in Concrete During Compressive Loading," Mag. Concrete Res., 27, 151-160 (1975).

Spooner, D. C., Pomeroy, C. D, and Dougill, J. W., "Damage and Energy Dissipation in Cement Pastes in Compression," Mag. Concr. Research, 28, 21-29 (1976).

Stroeven, P., "Geometric Porbability Approach to the Examination of Microcracking in Plain Concrete," J. of Matls. Scie., 14, 1141-1151 (1979).

Sture, S., "Stress Analysis of Strain-Softening Materials," in W. Wittke (Ed.), Proc., 3rd Int. Conf. Num. Meth. in Geomech., Aachen, W. Germany (1979).

Sture, S. and Ko, H. Y., "Strain-Softening of Brittle Geologic Materials," Int. J. Num. Anal. Meth. Geomechanics, 3, 237-253 (1978).

Suaris, W. and Shah, S. P., "Rate-Sensitive Damage Theory for Brittle Solids," J. Engr. Mechs. Div., ASCE, 110, 985-997 (1984).

Valanis, K. C., "A Theory of Viscoplasticity Without a Yield Surface, Part I, General Theory," Archives of Mechs., 23, 517-534 (1971).

Valanis, K. C., "A Theory of Viscoplasticity Without a Yield Surface, Part II, Application to Mechanical Behavior of Metals," Archives of Mechs., 23, 535-551 (1971).

Valanis, K. C., "On the Uniqueness of Solution of the Initial Value Problem in Softening Materials," J. Appl. Mechs., ASME, 29, 1-5 (1985).

Van Eekelen, H.A.M., "Isotropic Yield Surfaces in Three Dimensions for Use in Soil Mechanics," Int. J. Num. Anal. Meth. Geomechs., 4, 89-101 (1980).

Van Mier, J.G.M., "Strain Softening of Concrete Under Multiaxial Loading Conditions," Doctoral Dissertation, Eindoven, Univ. of Technology, The Netherlands (1984).

Vardoulakis, I., "Shear Band Inclination and Shear Modulus of Sand in Biaxial Tests," Int. J. Num. Anal. Meth. Geomechs., 4, 103-119 (1980).

Vermeer, P. A., "A Double Hardening Model for Sand," Geotechnique, 28, 413-433 (1978).

Wawersik, W. R. and Fairhurst, C., "A Study of Brittle Rock Fracture in Laboratory Compression Experiments," Int. J. Rock Mech. Min. Sci., 7, 561-575 (1970).

Whitman, L., "Visco-Damage Tension Model for Rocks in Ground-Shock Applications," Int. J. Num. Anal. Meth. Geomech., 9, 71-89 (1985).

Wilde, P., "Two Invariant Depending Models of Granular Media," Arch. Mech., 29, 799-809 (1977).

Wittmann, F. H., "Creep and Shrinkage Mechanisms," in Creep and Shrinkage in Concrete Structures, Ed. by Z. P. Bazant and F. H. Wittmann, Wiley (1982).

Wu, F. H. and Freund, L. B., "Deformation Trapping Due to a Thermo-plastic Instability in One-Dimensional Wave Propagation," J. Mech. Phys. Solids, 32, 119-132 (1984).

Young Bing-Lin, Dafalias, Y. F. and Herrmann, L. R., "A Bounding Surface Plasticity Model for Concrete," J. Eng. Mech. Div., ASCE, 111, 359-380 (1985).

Zaman, M. M., Desai, C. S. and Drumm, E. C., "Interface Model for Dynamic Soil-Structure Interaction," J. Geotech. Eng., ASCE, 110, 1257-1273 (1983).